

**Synthesis of β -Cyclodextrin
Functionalized Cellulose Nanocrystals and
Their Interactions with Amphiphilic Compounds**

by

Feifei Zhang

A thesis
presented to the University of Waterloo
in fulfillment of the
thesis requirement for the degree of
Master of Applied Science
in
Chemical Engineering
(Nanotechnology)

Waterloo, Ontario, Canada, 2014

© Feifei Zhang 2014

Author's Declaration

I hereby declare that I am the sole author of this thesis. This is a true copy of the thesis, including any required final revisions, as accepted by my examiners.

I understand that my thesis may be made electronically available to the public.

Abstract

Cellulose nanocrystal (CNC) obtained from acid hydrolysis of cellulose fibres has attracted enormous interests due to its large surface area, high negative surface charge density, potential functionalities from modifications of surface hydroxyl groups and high aspect ratio. The special physical and chemical properties made CNC an excellent candidate for various applications, such as drug delivery, antimicrobials, water treatment, personal care products, etc. Upon grafting CNC with β -Cyclodextrin (β -CD), the hybrid system forms inclusion complex with water insoluble molecules or hydrophobic segments of amphiphilic polymers, hence novel functionalities can be introduced to CNC, such as the delivery of various active ingredients, constructing macromolecular structures with enhanced mechanical strength and modifying rheological property of solutions. In this thesis, the surface modification of CNC and CNC derivatives by β -CD and their characterization were reported and discussed. Due to the fact that β -CD forms inclusion complex with amphiphilic molecules, such as surfactants which are among the most important components in personal care formulations. Thus, the behaviors of CNC and CNC derivatives with grafted β -CD in the solution of amphiphilic molecules are of great importance for personal care applications and thus were investigated in detail. In order to have a better understanding on the surfactant behaviors in the presence of impurities, the influence of alcohol in surfactant solutions was also studied.

β -CD functionalized CNC was prepared using cyanuric chloride as the cross-linking reagent. (MCT- β -CD) was synthesized by firstly hydrolyzing one chlorine atom in aqueous solution at 0°C then substituting the second chlorine atom by β -CD at room temperature in alkaline solutions. Then it was grafted by reacting the third chlorine atom with hydroxyl groups on the surface of CNC in aqueous solution. The grafting of β -CD was confirmed by UV-vis and FTIR spectroscopy. Grafting ratio was found to be 24.8 $\mu\text{mol/g}$ for CNC-CD using phenolphthalein (PHTH) inclusion method. Briefly, the UV absorbance of PHTH solution decreases with increasing β -CD concentration upon the formation of inclusion complex. By measuring the absorbance of equilibrated CNC-CD and PHTH mixture, grafting ratio of β -CD can be determined from the calibration. The reaction conditions including water content, temperature and alkali concentration were investigated and the main limiting factor in using cyanuric chloride as the cross-linking reagent was found to be the hydrolysis of reactive chlorines. With the optimized reaction conditions, the grafting ratio was enhanced compared to previous reported studies using the same cross-linking reagent. The interaction between CNC-CD and various charged amphiphilic molecules were studied by isothermal titration calorimetry (ITC), tensiometry, zeta potential, turbidity and conductivity. The behavior of CNC was altered upon the grafting β -CD due to the host-guest interactions between β -CD and amphiphilic molecules. Shielded hydrophobicity of amphiphilic molecules, CNC-CD induced micellization, inclusion complex induced aggregation and transition of aggregation structures were

observed and analyzed. Furthermore, preliminary research study to investigate the CNC-CD's ability to modify the viscosity of amphiphilic polymer solutions was conducted. The results indicated the potential application of CNC-CD as viscosity modifier in personal care formulations.

CNC was desulfated then cationized (dcCNC) by hydrolysis of sulfate groups and modification with glycidyl ammonium chloride (GTMAC). Then, β -CD was grafted using cyanuric chloride as the cross-linking reagent. Characterizations of dcCNC-CD were carried out using similar methods as described earlier. It was observed that due to the inverse of surface charge on CNC, the behaviors of dcCNC and dcCNC-CD in solutions of cationic and anionic surfactants were significantly different from those of pristine CNC. It was suggested that unlike CNC-CD, host-guest interactions between β -CD and amphiphilic molecules facilitated the re-dispersion of dcCNC-CD and enhanced the stability of the solutions by host-guest interaction and inclusion complex induced micellization. The influence of temperature and ionic strength on the interactions was studied using ITC. The dcCNC-CD has potential applications in conditioning formulations due to its affinity towards negatively charged hair/skin surfaces and the ability to deliver the benefits of nutrition, active or protective compounds.

In order to gain a better insight on the surfactants' interfacial and bulk behaviors for understanding polymer/surfactant interactions, the influence of impurities on the surface activity, pre-micellar aggregation and critical micelle concentration (cmc) were studied using mixtures of sodium dodecyl sulfate (SDS) and 1-dodecanol. Tensiometry indicated a significantly enhanced surface activity with increasing molar ratio of 1-dodecanol and decreasing temperature. The pre-micellar aggregation of dodecanol and SDS and solubilization of pre-micellar aggregates upon micellization were confirmed by light scattering and ITC. Increasing the 1-dodecanol fraction facilitated the aggregation and cmc of SDS and reduced the percentage of bound counter ion (f), and the influence of ionic strength on the cmc and f were discussed.

As a result of above studies, knowledge on the surface modification of CNC, cyanuric chloride chemistry, interface and bulk solution behaviors of amphiphilic molecules were advanced. The studies of interactions between amphiphilic molecules and β -CD grafted CNC and CNC derivatives provided in-depth understanding on the system, which will be critical for applications in personal care products.

Acknowledgement

I would like to express my sincere gratitude to my supervisor, Dr. Michael K.C. Tam for his guidance, inspiration and support during my MASc study and in writing of this thesis. His patience and enthusiasm also encouraged me and helped me come across the difficulties in my research. I deeply appreciate the opportunity to study and work under his supervision.

I would also like to thank my committee members Dr. Leonardo Simon and Dr. Boxin Zhao for their insightful comments, questions and encouragement.

I would like to extend my gratitude to all my labmates for their helpful suggestions, discussion and supports during my study. Special thanks are given to the visiting scholar, César Brinatti, for his advice, enlightening discussion and assistance in ITC experiments.

Last but not the least, I would like to express my heartfelt gratefulness to my parents, G. Zhang and F. Nan, for their immense love, constant support, guidance and encouragement throughout out my life.

Table of Contents

List of Figures	ix
List of Tables	xiii
List of Schemes	xiv
1 Introduction	1
1.1 Overview.....	1
1.2 Research Objectives.....	3
1.3 Thesis Outline.....	4
2 Literature Review	5
2.1 Polymers for Personal Care Applications.....	5
2.1.1 Polymers used as thickeners.....	5
2.1.2 Polymers used as delivery system.....	6
2.1.3 Polymers for conditioning.....	7
2.2 Polymer-Surfactant Systems.....	8
2.2.1 Surfactants and micellization.....	8
2.2.2 Mixed micelles.....	10
2.2.3 Polymer-surfactant interactions.....	12
2.3 Cellulose Nanocrystals (CNC).....	16
2.3.1 Cellulose.....	16
2.3.2 CNC synthesis.....	18
2.3.3 CNC properties.....	22
2.3.4 CNC modification.....	22
2.3.5 Interactions between cellulose, CNC, CNC derivatives and surfactants.....	25
2.4 Cyclodextrin and Cyclodextrin Polymers.....	29
2.4.1 Structure and properties.....	29
2.4.2 Inclusion complex formation and characterization.....	31
2.4.3 Interaction between cyclodextrin and surfactants.....	34
2.4.4 Cyclodextrin grafted polymers.....	38
2.4.5 Application of cyclodextrin in personal care products.....	39
3 β-Cyclodextrin-Functionalized Cellulose Nanocrystals and Their Interactions with	

Amphiphilic Molecules	43
3.1 Introduction	43
3.2 Experimental.....	45
3.2.1 Materials.....	45
3.2.2 Synthesis	45
3.2.3 Spectroscopy.....	46
3.2.4 Transmission electron microscopy (TEM)	46
3.2.5 Grafting ratio.....	46
3.2.6 Surface tensiometry	47
3.2.7 Isothermal titration calorimetry (ITC)	47
3.2.8 Zeta potential	47
3.2.9 Phase separation.....	47
3.2.10 Conductivity.....	47
3.3 Results and Discussion	48
3.3.1 UV-vis and FTIR	48
3.3.2 Grafting ratio of MCT- β -CD.....	49
3.3.3 Interactions with a non-ionic surfactant.....	51
3.3.4 Interactions with anionic surfactant	53
3.3.5 Interactions with a cationic surfactant	58
3.4 Conclusions	61
4 β-Cyclodextrin-functionalized Cellulose Nanocrystal Derivatives and Their Interactions with Amphiphilic Molecules	62
4.1 Introduction	62
4.2 Experimental section.....	64
4.2.1 Materials.....	64
4.2.2 Desulfation and cationization of CNC	64
4.2.3 Grafting of MCT- β -CD	65
4.2.4 Spectroscopy.....	65
4.2.5 Grafting ratio measurements.....	65
4.2.6 Surface tensiometry	66
4.2.7 Isothermal titration calorimetry	66
4.2.8 Zeta potential	66
4.2.9 Potentiometric titration	67

4.3	Results and discussion	67	
4.3.1	Characterization of dcCNC and dcCNC-CD	67	
4.3.2	UV-vis and FTIR of desulfated-cationic-CNC (dcCNC).....	69	
4.3.3	Grafting ratio of MCT- β -CD	71	
4.3.4	Interactions between dcCNC, dcCNC-CD and cationic surfactants	71	
4.3.5	Interactions between dcCNC, dcCNC-CD and anionic surfactants	77	
4.4	Conclusions	84	
5	Influence of 1-dodecanol on the Adsorption and Thermodynamic Properties of Sodium Dodecyl Sulfate Micellar Solution	85	
5.1	Introduction	85	
5.2	Experimental section.....	87	
5.2.1	Materials.....	87	
5.2.2	Surface tension	88	
5.2.3	Light scattering.....	88	
5.2.4	Isothermal titration calorimetry	89	
5.2.5	Conductivity titration	89	
5.3	Results and discussion.....	89	
5.3.1	Surface co-adsorption of 1-dodecanol/SDS (DDC/SDS) before micellization	90	
5.3.2	Light scattering and isothermal titration calorimetry (ITC).....	97	
5.3.3	Pre-micellar aggregation and micellization of SDS/1-dodecanol.....	101	
5.4	Conclusions	107	
6	Contributions and Recommendations	108	
6.1	General Contributions	108	
6.1.1	Synthesis, optimization and characterization of CNC-CD and its interaction with surfactants.....	108	
6.1.2	Synthesis and characterization of β -CD-functionalized cationic CNC and its interaction with surfactants.....	109	
6.1.3	Influence of 1-dodecanol on the adsorption and thermodynamic properties of sodium dodecyl sulfate micellar solution.....	109	
6.2	Recommendation for Future Studies.....	110	
	References.....	112	

List of Figures

Figure 2.1 (Left) Damaged hair, the cuticles are uplifted, light is diffused that causes an overall diminished shine of hair; (right) After treating with conditioner, the cuticles lay flat, light is reflected that causes hair to have a maximum shine.....	7
Figure 2.2 Surfactant self-assembly leads to a range of diverse structures. ²⁸	9
Figure 2.3 Schematic model of the binary surfactant system of TTAC and NP-15. Region I, no micelles in the mixed solution; region II, surfactants began to form aggregates; region III, TTAC-rich and NP-15-rich mixed micelles coexisted in the solution. ³⁵	11
Figure 2.4 Analytical ultracentrifuge of mixed surfactants: coexistence of two micelles. ³⁶	12
Figure 2.5 (a) Surface tension of SDS in the presence of varying concentrations of poly(vinyl pyrrolidone) (PVP). (b) A schematic plot of surface tension for individual surfactant and polymer-surfactant system. ³⁸	13
Figure 2.6 (a) ITC curve of 0.2M SDS titrating into water and 0.1wt% PEO (400 Da); (b) ITC curve of 0.2M SDS titrating into 0.1 wt% PEO (900 Da) and PEG (1450 Da); (c) ITC curve of 0.2M SDS titrating into 0.1 wt% PEO (3350 Da); (d) schematic of the dehydration and rehydration of non-ionic polymer interacting with surfactant. ⁴²	15
Figure 2.7 (a) Structure of single cellulose chain repeat unit, the direction of 1-4 linkage and intra-chain hydrogen bonding are shown; (b) Schematic of cellulose microfibrils with crystalline and amorphous regions; (c) Schematic of cellulose nanocrystals after amorphous regions are dissolved by acid hydrolysis. ⁴⁸	17
Figure 2.8 Schematics of two hydrogen bonding networks within cellulose fibre. Thin dotted lines are intra-chain bondings, thick dotted lines are inter-chain bondings. ⁵²	18
Figure 2.9 TEM images of dried dispersion of CNC derived from (a) tunicate (b) bacteria (c) ramie (d) sisal ^{63,75-77}	19
Figure 2.10 (a) Acid hydrolysis mechanism, (b) esterification of cellulose nanocrystal surface. ⁷⁶	21
Figure 2.11 Conductometric titration curves for H ₂ SO ₃ -hydrolyzed CNC (open circle), HCl-hydrolyzed CNC (open triangle), HCl-desulfated CNC-seventh step (solid circle), solvolytically desulfated CNC (solid triangle). ¹⁰²	23
Figure 2.12 Scheme of TEMPO-mediated oxidation of primary hydroxyl groups on the surface of CNC (left); suspension of HCl-hydrolyzed CNC suspension in the left tube and TEMPO-oxidized CNC in the right tube observed between crossed polarizers (right). ¹⁰⁸	24
Figure 2.13 Scheme of the phase diagram indicating the different regions with dense aggregates, loose aggregates, and precipitates in the case of DTAB-NaCMC mixed solutions. ¹²³	26
Figure 2.14 Mechanism of CNC-TTAB binding from ITC experiments. ¹²⁷	28
Figure 2.15 Calorimetric titration curves of SDS into CNC or M600-CNC suspensions (left); Calorimetric titration curves of DoTAB into CNC or M600-CNC suspensions (right). ¹²⁸	28

Figure 2.16 Chemical structure of α , β and γ cyclodextrins (left to right).....	30
Figure 2.17 Formation of inclusion complex.....	31
Figure 2.18 FTIR spectrum of cyclodextrin, orotic acid and their inclusion complex by kneading, co-precipitation and freeze-dried methods. ¹³⁷	33
Figure 2.19 X-ray diffraction spectrum of cyclodextrin, orotic acid and their inclusion complex by kneading, co-precipitation and freeze-dried methods. ¹³⁷	33
Figure 2.20 DSC spectrum of cyclodextrin, orotic acid and their inclusion complex by kneading, co-precipitation and freeze-dried methods. ¹³⁷	34
Figure 2.21 Surface tension result of SDS (a) and CPC (b) solutions containing 5.08 mM SDS and 2.00 mM CPC respectively upon addition of β -cyclodextrin. ¹⁴⁹	35
Figure 2.22 Integrated heat change per mole of injectant versus [cyclodextrin]/[SDS] molar ratio. Insert: concentration of free cyclodextrin (dashed thin line), free SDS (solid thin line), CD:SDS=1:1 complexes (dotted thin line), CD:SDS=2:1 complexes (solid thick line) as a function of [SDS]/[CD] ratio. ¹⁵¹	37
Figure 2.23 A) Cyclodextrin polymer with low cross-linking degree; B) Cyclodextrin polymer with high cross-linking degree	38
Figure 2.24 Polymerizable CD monomers. A) acrylamidomethyl-CD; B) maleic anhydride modified CD; C) methacryloyl-CD; D) mono-substituted vinyl CD. ¹⁶⁵	39
Figure 2.25 a) Effect of heat treatment at 50°C and 100°C on flavour content of tea tree oil; b) Effect of heat treatment at 50°C and 100°C on flavour content inclusion complex with β -cyclodextrin.....	40
Figure 2.26 a) Structure of β -cyclodextrin-retinol inclusion complex. b) Toxicity of pure retinol and β -cyclodextrin-retinol inclusion complex. ¹⁶⁸	41
Figure 2.27 Synthesis of the β -cyclodextrin-fullerene inclusion complex. ¹⁷⁰	41
Figure 3.1 UV-vis spectra of MCT- β -CD, CNC and CNC-CD.....	48
Figure 3.2 FTIR spectra of cyanuric chloride, MCT- β -CD, CNC-CDs synthesized in water and DMSO (top to bottom).....	49
Figure 3.3 UV absorbance of PHTH/ β -CD solutions with increasing β -CD concentrations (left). Calibration curve of absorbance and β -CD concentration (right).....	50
Figure 3.4 Phenolphthalein solutions with increasing β -CD concentration, where color faded from pink to colorless.....	50
Figure 3.5 Impact of reaction conditions on the grafting ratio of β -CD: CNC concentration (left), temperature and time (middle), NaCO_3 : CNC ratio (right).....	51
Figure 3.6 (A) Surface tension curves of water, 0.6 wt% CNC and 0.6 wt% CNC-CD suspensions with increasing TX-100 concentrations at 25°C.	52
Figure 3.7 Thermograms from titrating TX-100 into water, 0.18 mM β -CD, 0.6 wt% CNC and 0.6 wt% CNC-CD suspensions at 25°C (left). First-order differential curve of TX-100 to water ITC thermogram (right).....	53

Figure 3.8 (A) Surface tension curves of water, 0.6 wt% CNC and 0.6 wt% CNC-CD suspensions with increasing SDS concentrations at 25°C. (B) Thermograms from titrating SDS into water, 0.18 mM β -CD, 0.6 wt% CNC and 0.6 wt% CNC-CD suspensions at 25°C. The insert is an enlargement of the region at low SDS concentration.....	54
Figure 3.9 Comparison of ITC, transmittance and zeta potential results for CNC/SDS (A) and CNC-CD/SDS (B) samples.	56
Figure 3.10 Photos of 0.6 wt% SDS/CNC (A) and SDS/CNC-CD (B) samples with increasing SDS concentration.	56
Figure 3.11 Conductivity of 0.6 wt% CNC and CNC-CD suspensions with increasing SDS concentration at 25°C.	57
Figure 3.12 TEM images of 0.02 wt% of CNC (A) and CNC-CD (B) with 8.5 mM SDS.....	58
Figure 3.13 (A) Surface tension curves of water, 0.1 wt% CNC and 0.1 wt% CNC-CD suspensions with increasing CTAB concentrations at 28°C; (B) Thermograms of titrating SDS to water, 0.03 mM β -CD, 0.1 wt% CNC and 0.1 wt% CNC-CD suspensions at 28°C.	59
Figure 3.14 Conductivity of 0.1 wt% CNC and CNC-CD suspensions with increasing CTAB concentration at 28°C.	59
Figure 3.15 Comparison of ITC, transmittance and zeta potential results for CNC/CTAB (A) and CNC-CD/CTAB (B) samples.	60
Figure 3.16 Phase separation of 0.1 wt% CTAB/CNC (A) and CTAB/CNC-CD (B) samples with increasing CTAB concentration.	61
Figure 4.1 Zeta potential of desulfated CNC (dcCNC), desulfated-cationic CNC (dcCNC), CD grafted dcCNC synthesized in water (dcCNC-CD/H ₂ O) and in DMSO (dcCNC-CD/DMSO).	67
Figure 4.2 Conductometry titration of AgNO ₃ 2.5mM to dcCNC 40mg (A) and dcCNC-CD 42mg (B).	68
Figure 4.3 UV-vis spectra of MCT- β -CD, dcCNC, dcCNC-CD/water and dcCNC-CD/DMSO.	69
Figure 4.4 FTIR spectra of CNC, dcCNC, dcCNC-CD/water, dcCNC-CD/DMSO and MCT- β -CD.....	70
Figure 4.5 Surface tension of water, 0.35mM β -CD, 0.1 wt% dcCNC and 0.1 wt% dcCNC-CD with increasing CTAB concentration.	72
Figure 4.6 (A) Thermogram of CTAB titrations to water and dcCNC 0.1 wt%; (B) thermogram of CTAB titrations to water and dcCNC-CD 0.1 wt%; (C) enthalpy change of CTAB titrations to dcCNC 0.1 wt% and dcCNC-CD 0.1 wt% after subtracting CTAB dilution curve.....	73
Figure 4.7 Thermogram of CTAB titrations to dcCNC-CD 0.1 wt% at 28, 33 and 38 °C (A) and corresponding curves corrected for the heat effect of dilution (B).	74
Figure 4.8 Comparison of T%, zeta potential and conductivity results of CTAB to dcCNC 0.1 wt% (A) and dcCNC-CD 0.1 wt% (B).....	75
Figure 4.9 Image of dcCNC (A) and dcCNC-CD (B) suspensions with increasing CTAB concentration (mM).	76
Figure 4.10 Surface tension of water, 0.35mM β -CD, 0.1 wt% dcCNC and 0.1 wt% dcCNC-CD with increasing SDS concentrations.....	77

Figure 4.11 Thermograms of SDS titration to (A) water and dcCNC 0.1 wt%, (B) water and dcCNC-CD 0.1 wt%.	78
Figure 4.12 ITC curve for titrating 50 mM SDS into pure water and branched PEI solution (c) and (d) corresponding transmittance % curve. ¹⁹⁵	79
Figure 4.13 Phase separation of (A) dcCNC 0.1 wt% and (B) dcCNC-CD 0.1 wt% with increasing SDS concentrations in mM.	80
Figure 4.14 Comparison of ITC thermogram, transmittance%, zeta potential and conductivity measurements of (A) SDS/dcCNC and (B) SDS/dcCNC-CD with increasing SDS concentration. Concentration of dcCNC and dcCNC-CD was kept at 0.1 wt% in all the measurements.	82
Figure 4.15 Thermogram SDS titration to (A) dcCNC 0.1 wt% and (C) dcCNC-CD 0.1 wt% with 0, 0.01 M and 0.1 M of NaCl in solution. (B) and (D) are enthalpy curves in (A) and (C) corrected by subtracting corresponding SDS dilution curves respectively.	83
Figure 5.1 Surface tension of water upon titration of SDS, DDC/SDS of R=1:99 and 3:97 were plotted against logarithm of SDS concentration in mM at 15°C, 25°C and 35°C.	90
Figure 5.2 Surface activity of DDC at different temperature and DDC/SDS molar ratio.	93
Figure 5.3 Overall surface activity parameters of DDC/SDS with R=1:99 and 3:97 at 15°C, 25°C and 35°C.	94
Figure 5.4 Plot of surface tension vs. ln(SDS concentration) for pre-cmc concentrations with the percent surface coverage written above the points. ²³⁴	95
Figure 5.5 Plots of normalized Γ vs. SDS concentration showing the effects of temperature (at 15°C, 25°C and 35°C) on the surface concentration of R=1:99 and R=3:97.	96
Figure 5.6 Plots of Γ/Γ_m vs. SDS concentration. The effects of DDC/SDS molar ratio on degree of saturation at 15°C, 25°C and 35°C.	97
Figure 5.7 Light scattering of DDC/SDS mixture of various molar ratios at increasing SDS concentration.	98
Figure 5.8 (A) ITC isotherm of DDC/SDS mixture of various molar ratios at increasing SDS concentration at 25°C. The curves were corrected by subtracting the SDS dilution curve. (B) is the isotherm at lower SDS concentration, showing the minor change in DDC water-solubilization concentration.	99
Figure 5.9 Plots of I_R and ΔH vs. SDS concentration for DDC/SDS with various R. (e) shows the critical concentration and regions assigned in DDC/SDS with R of 5:95.	100
Figure 5.10 Aggregation composition (left axis) and micelle composition (right axis) of DDC with different R vs. SDS concentration.	106

List of Tables

Table 2.1 Sizes of CNC form various resources.....	20
Table 2.2 Properties of cyclodextrins.....	30
Table 2.3 Thermodynamic data for the formation of β -cyclodextrin-SDS inclusion complexes. ¹⁵¹	37
Table 4.1 Grafting ratio in wt% and $\mu\text{mol/g}$ of β -CD on dcCNC-CD comparing with that of CNC-CD.	71
Table 5.1 Minimum surface tension in the isotherms of SDS, R=1:99 and R=3:97 at 15, 25 and 35°C.....	91
Table 5.2 Characteristic adsorption parameters calculated by fitting experimental data to Equation 5.4.	92
Table 5.3 Surface coverage area per molecule A^0 of SDS, R=1:99, R=3:97 at 15°C, 25°C and 35°C.....	94
Table 5.4 DDC loading ratio of aggregate (q) and micelle (r) in DDC/SDS mixtures with increasing R.....	101
Table 5.5 Summarization of counterion binding % and cmc^* measured by conductivity titration of DDC/SDS mixtures with increasing R.	102
Table 5.6 Thermodynamic parameters of SDS micellization and DDC solubilization in DDC/SDS systems with increasing R.....	104
Table 5.7 Summarization of concentrations extracted from Figure 5.10 and ITC isotherm of DDC/SDS with various R (Figure 5.8A).....	107

List of Schemes

Scheme 2.1 Schematic illustration of a surfactant.	9
Scheme 2.2 Reaction scheme of cationization of CNC with GTMAC.....	24
Scheme 2.3 Chemical structure of β -cyclodextrin.	29
Scheme 3.1 Procedure for MCT- β -CD synthesis.	45
Scheme 3.3 Schematic diagrams describing the change in behavior of CNC-CD compared to CNC in differently charged surfactants. The concentration shown in the scheme is below the cmc for TX-100, and above the cmc for SDS and CTAB.....	55
Scheme 4.1 Reaction scheme of surface cationization of CNC with GTMAC in DMSO.	65
Scheme 5.1 Partitioning of DDC into aggregates and SDS micelles with the increasing mixture concentration.	103

1 Introduction

1.1 Overview

With the current development in nanotechnology, functional nanomaterials have attracted increasing interests due to their novel and tunable properties, as well as enhanced performances with further functionalization. Personal care, cosmetics and home care industry can take advantage of the various properties of these polymers to benefit their formulations. Broad spectrums of polymers with high performance are used in a wide range of products, such as detergents, emulsifiers, thickeners, rheology modifiers, protective barriers, active reagent carriers and so on. However, a large proportion of chemicals currently used to synthesize such nanomaterials are derived from petroleum-based sources and the synthetic procedures involve the use of toxic reagents that are potentially harmful to the environment. This situation raises concerns regarding the fast consumption of un-sustainable resources and the greenhouse effect and global warming. There is an urgent need to develop and use functionalized polymers derived from natural and renewable resources to replace the conventional materials used in many of today's products. There is a growing number of personal care products containing naturally derived polymers e.g. homo-polysaccharides (starch, cellulose) and hetero-polysaccharides (chitin, chitosan), as well as polypeptides that serve as viscosity modifiers.

Cellulose is one of the most abundant natural biomaterial that can be obtained from various renewable resources, such as wood, plant, tunicate, bacteria, etc. It is the primary constituent of cell walls and comprises of amorphous and crystalline domains. It's an effective water-based viscosity modifier and its derivatives are among the most widely used thickeners in many personal care products due to their special physical structure, ease of surface modification and good compatibility with wide a variety of personal care materials including non-ionic polymer, polyelectrolyte, cationic and anionic surfactants. The most common cellulosic derivatives are methylcellulose, hydroxypropylmethylcellulose and hydroxyethyl-cellulose. The main reason for the viscosity build-up with the addition of cellulosic polymers is their high molecular weights.¹ Cellulose derivatives are also used as additives in conditioning products, such as the quaternary ammonium salt that displays good affinity towards negatively charged hair and skin.

The acid hydrolysis of cellulose dissolves the amorphous domains releasing individual rod-like crystalline nanoparticles called Cellulose Nanocrystals (CNC). The hydrolysis with sulfuric acid introduces

negative charges on the surface of CNC particles in the form of sulfate ester groups. Due to electrostatic repulsion and nano-scale dimensions, CNC particles are homogeneously dispersed in aqueous solution and form suspensions that remain stable over months. CNC has a high aspect ratio (length/diameter) of 30 to 150 depending on its source. The rod-like structure has greater capacity to enhance the viscosity with increasing concentration. Studies on the rheological properties showed a concentration-dependent shear thinning behavior at low concentration and not so pronounced profile above a critical concentration,^{2,3} due to the alignment of nanocrystals under shear flow. Because of the crystallinity, CNC is considered to be stiffer than aluminum and steel. Potential applications as rheology modifiers and additives in gel or nanocomposites have been widely reported.⁴ The presence of abundant functional hydroxyl groups on the surface of CNC provides the opportunity for various modifications, such as esterification, TEMPO-media oxidation, cationization, fluorescent labeling as well as polymer grafting. Such modifications allow researchers to impart novel properties to CNC and explore the full potentials of this sustainable material.

Cyclodextrins are a family of cyclic oligosaccharides produced from enzymatic degradation of starch. Due to the location of hydroxyl groups on the molecule, the interior cavity of cyclodextrins is hydrophobic, whereas the external surface is hydrophilic. This unique property makes cyclodextrin molecules ideal hosts for entrapping un-polar molecules without formation of covalent bonding. The most common and commercially available system is β -cyclodextrin because of its relatively low water-solubility, ease of purification as well as its dimension. β -cyclodextrin has been intensively studied and utilized in various applications, such as foods, flavors, cosmetics, textiles, pharmaceuticals, personal care products and packaging materials.⁵ In personal care products, cyclodextrins are used to encapsulate insoluble, volatile and vulnerable active reagents such as essential oil, fragrance, antioxidant, antimicrobial, etc. The solubility, protective property and controlled release profile of β -cyclodextrin have found their applications in various personal care products such as toothpaste, skin creams, fabric softeners, deodorant, etc.⁶

Surfactants are among the most important components in all types of personal care products. The surface activity and ability to form micelles in aqueous solutions enable surfactants to be used as detergents, emulsifiers and solubilizers. Micellization of surfactants can be tuned by changing the chemical structure, counter ions and the presence of polymers. Interaction between surfactants and polymers are vital in the design of personal care formulations and many other applications, therefore they have been intensively studied in differently charged surfactant/polymer systems. It was reported that the presence of uncharged polymeric chains induced the formation of micelles at a concentration below the critical micelle concentration (cmc) of the surfactant due to hydrophobic interactions. The morphology,

solubility, dispersability and rheological behavior of polymer are also varied when interacting with different types of surfactants. In practical applications, controlling the phase behavior and interfacial properties, obtaining desirable rheology, reducing free surfactant molecule concentration and activity can be achieved by adjusting the interaction in polymer-surfactant system. The common techniques used to characterize the interactions are calorimetry, nuclear magnetic resonance (NMR), fluorescence, conductivity, rheometry, tensiometry, electromotive forces, etc.

1.2 Research Objectives

The present study focuses on harnessing the beneficial properties of CNC and β -cyclodextrin to develop novel functionalized CNC derivatives that can be used for viscosity control, film forming, conditioning and nutrient delivering in personal care products. Pristine CNC derived from sulfuric acid hydrolysis of cellulose possesses large amounts of negative charges on its surface. The highly negative zeta potential of \sim -50 mV ensures good dispersability of CNC particles in aqueous solutions at low pH and good film forming ability due to electrostatic repulsion.⁷ Cationically modified CNC is desirable for use as depositing polymers in conditioning formulations due to its affinity towards negatively charged hair and skin. With covalently bound β -cyclodextrin, CNC particles are able to deliver nutrients, active reagents, volatile fragrance molecules upon application, which can be protected and slowly release due to the unique property of β -cyclodextrin. Nevertheless, in order to apply β -cyclodextrin grafted CNC (CNC-CD) in practical applications, interactions between CNC-CD and other components, such surfactants, alcohols and other functioning polymers need to be fully understood to predict the behavior of CNC-CD in solution. Studies on such interactions would provide valuable information and knowledge that are critical for personal care formulations.

Therefore, based on a comprehensive review of previous studies, the objectives of this thesis are formulated:

- Synthesis, optimization of β -cyclodextrin grafting ratio, characterization of β -cyclodextrin functionalized CNC and its behavior in the presence of three types of amphiphiles in aqueous solutions.
- Synthesis and characterization of β -cyclodextrin functionalized cationic CNC and its behavior in the presence of similarly and oppositely charged amphiphiles in aqueous solutions and the effects of temperature and ionic strength.
- Investigating the effects of 1-dodecanol on the properties of sodium dodecyl sulfate solution with respect to surface activity, adsorption, light scattering and thermodynamic properties.

1.3 Thesis Outline

This thesis consists of 6 chapters. The research results and discussions of the projects are reported in Chapters 3 to 5. The layout of the sections is as follows: Chapter 1 briefly introduces the current concerns of personal care industries in connections to synthesis and application of sustainable materials. Unique properties of CNC and β -cyclodextrin and their potential applications in personal care products are discussed, followed by the development of research objectives. Chapter 2 is the literature review covering introductions to importance and relevance of polymers and surfactant in personal care products; behavior of surfactant in mixture systems; polymer-surfactant interactions in aqueous solutions, which provide the fundamental knowledge useful for analyzing behavior of CNC and β -cyclodextrin in solution in the presence of surfactants. Furthermore, physical and chemical properties, modifications and potential applications of CNC and β -cyclodextrin in personal care products are also reviewed. Chapter 3 and 4 introduce the synthesis and characterization of β -cyclodextrin grafted CNC and CNC derivative respectively. Interactions of functionalized CNC nanoparticles and three types of surfactants are investigated and analyzed. Chapter 5 reports studies on the surfactant mixture of sodium dodecyl sulfate and 1-dodecanol to analyze the influence of impurities on surfactant solutions. Chapter 6 summarizes the key conclusions of projects along with recommendations for further studies.

2 Literature Review

2.1 Polymers for Personal Care Applications

In personal care products polymers are always employed to enhance the viscosity, stability and consistency of the system, which at the same time affect the flow and delivery of the formulation. It has practical benefits to control the rheology of personal care products such as shower gels, shampoos and skin creams. Shear-thinning behavior is desirable due to the ease of distribution on skin or hair and thus is the key property for application. Such property can be obtained by properly adjust the selection and combination of polymers and surfactants in the formulations.

2.1.1 Polymers used as thickeners

Personal care and cosmetic industry have the greatest needs regarding the use and development of polymer thickeners. They are able to affect the rheological profile of the formulation along with the water sensitivity, formulation and their ability to deliver active compounds to the target site. For water-based systems, the viscosity is typically very low, thus both synthetic and natural polymers are used as thickeners to thicken and form a gel- or cream-like formulation. In order to impart a rigid structure of such polymers, polymers with one or more fatty components are preferred, such as natural or synthetic waxes, long-chain alcohols, lanolin, triglycerides etc. These structures are also beneficial to facilitate mold release due to the slight contraction upon cooling.

Synthetic waxes are widely used due to its relatively low cost. They are either mixtures of petroleum derived long chain hydrocarbons or directly synthesized from monomers (e.g., ethylene, vinyl pyrrolidone, vinyl acetate, dimethicones, etc.). Synthetic polymers based on acrylic acid, polyacrylamides and copolymers based on alkylene oxide are also commonly used. Natural polymers utilized as thickeners comprised of polysaccharides such as starch, guar gum, alginates, pectines, cellulose, gelatin, etc. Only small portion of thickeners used are modified natural polymers, mainly cellulose, such as hydroxyethylcellulose, methylcellulose and hydroxypropylcellulose.

Copolymers synthesized from acrylate and acid functional monomers alter the formulation viscosity by charged-induced chain entanglement and extension at varying pHs. Under high pH, electrostatic repulsion results in the hydration of polymer chain thereby increasing the viscosity. When acid groups on the copolymer are fully protonated at low pH, polymer chain collapses and form random coils resulting in a low viscosity solution. ⁸

Associated polymers are hydrophobically modified acid/acrylate copolymers with ethoxylated

hydrophobes. The most common polymers of this kind include hydrophobically modified ethylene oxide urethane (HEUR)^{9,10}, hydrophobically modified ethyl(hydroxyethyl)cellulose (HMEHEC)^{11,12}, hydrophobically modified hydroxyethyl cellulose (HMHEC)^{13,14} as well as the class of hydrophobic alkali-soluble emulsion (HASE)^{12,15}, which are polymers with hydrophobic groups attached to the backbone through ethylene-oxide side chains; behaving like a polyelectrolyte. These polymers build viscosity quickly by themselves or with suspension of particulates or pigments in aqueous solution. HEUR are nonionic polymers and the effect of viscosity modification is not impacted by changing pH or ionic strength of the solutions. Meanwhile, HASE polymers containing acid groups have good solubility in alkaline solutions and thicken the solution by the effect of charged induced polymer chain extension and association of hydrophobic side chains.¹⁶ However, pH decrease and an increase of ionic strength would eliminate their thickening effects. Despite the plausible viscosity enhancement, the limitations of hydrophobically modified polymers are the difficulty and complication of synthesis as well as the cost inefficiency due to the incompatibility between the water-soluble backbone and hydrophobic side chains.

2.1.2 Polymers used as delivery system

Currently, there are increasing numbers of formulations containing active ingredients to achieve better functionalities. One of the most practical applications is to increase shelf-life of products containing bioactive, photosensitive or oxygen-sensitive ingredients by protecting them from degradation by other components in the formulation, light or oxidants from the environment.¹⁷

For most of polymer delivery systems, active ingredients are physically entrapped in the matrix of polymers, which limits their application due to the facts of inefficient loading and uncontrollable ingredient release from polymeric matrix. Furthermore, some polymers used as matrix materials are potentially detrimental to the entrapped active ingredient, thereby reducing their efficacy of delivery.¹⁸

Different types of delivery of active reagents were reported. Anti-acne agents such as salicylic acid and vitamin A are emulsified and incorporated into polymer matrix for a better and complete release profile for the usage in skin care products.¹⁹ Antimicrobials can also be incorporated into the polymer matrix or covalently bound to polymer backbone as pendant groups. Triclosan is a broad-spectrum antimicrobial agent used in various personal care products. Its incorporation with polymers by melt-mixing impart persistent antimicrobial properties to the polymer.²⁰ Antimicrobials loaded in polymer matrix can be released upon degradation of polymer backbones. For example, poly(anhydride-esters) has been used to chemically incorporate salicylic acid (SA) for antibacterial purpose. Study showed they not only release SA when the polymers degrade, but fragments from degraded polymer backbones also have

antibacterial effect that further enhance their functionality.²¹ Another class of active agents commonly encountered in personal care products are antioxidants, such as Vitamin C (ascorbic acid), Vitamin E (retinol), butylated hydroxyanisole, butylhydroxyl toluene, etc. Most of the antioxidants are derived from natural sources such as cucumber extract, grape seed extract etc. Antioxidants defend skin against free radicals generated by UV light and pollutions in the atmosphere due to daily exposure, which contribute to the oxidation of skin and facilitate the aging process. The main drawbacks limiting their application are the poor water-solubility and instability in the presence of light and oxygen. Irritations and mild scaling are also reported upon direct application due to excessive exposure. To avoid these problems, antioxidants can be immobilized and stabilized by polymer to slow down their degradation by heat and light, reducing the occurrence of irritation, while neutralizing free radicals to help skin remained vital and healthy. ²²

2.1.3 Polymers for conditioning

Human hair is consistently damaged by various factors from the environment, such as air pollution, UV light, chlorinated water in swimming pool etc. as well as chemical treatments like ironing, coloring, styling etc. Other treatment to hair, e.g. brushing, blow drying and combing may also mechanically damage cuticles of hair.²³ The purpose of conditioning agents in hair conditioner or shampoo is to restore the lifted cuticle and protect hair from further damage as well as improve shine, strength and manageability of hair. Currently, almost all shampoos contain conditioning agents, which include fatty substances derived directly from natural sources such as vegetable oils, wax, lecithin and lanolin derivatives, but the more common ones are synthetic polymers such as quaternary ammonium compounds and silicones.

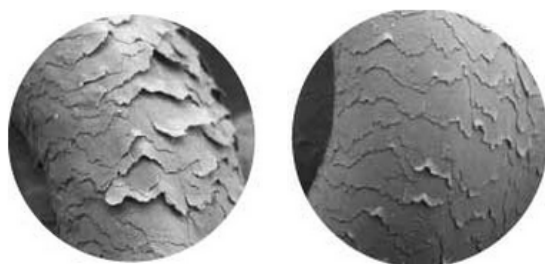


Figure 2.1 (Left) Damaged hair, the cuticles are uplifted, light is diffused that causes an overall diminished shine of hair; (right) After treating with conditioner, the cuticles lay flat, light is reflected that causes hair to have a maximum shine.

Silicones are a class of inorganic polymers derived from silicon dioxide. There are various

structures of silicone by modification with many different organic functional groups. They function as polymer surfactants to stabilize emulsions, and they, introduce mechanical strength and prolonged functioning to formulations, and form protecting films on hair as conditioning agents. The drawback in using silicone in shampoo is the extremely low deposition on the substrates due to the competitive interactions with surfactants and low affinity towards negatively charged hair. Loss of silicone is especially significant in 2-in-1 conditioning shampoo formulations. New formulations using cationic polymers to enhance deposition onto hair are attracting increasing attentions in application of hair conditioning.^{24,25}

Quaternary ammonium compounds such as polyquaternium-10, polyquaternium-16 and guar hydroxypropyltrimonium chloride have already been commercialized and applied in many types of hair care products. Cationic polymers adhere more strongly to the hair and have good film forming ability to generate coatings that make hair smooth, soft and better looking by altering the refractive index. They can also be incorporated in 2-in-1 shampoo formulations due to the strong electrostatic interactions. Upon dilution during rinsing, cationic polymers form complexes with both anionic and cationic surfactants and result in coacervation also known as “lockhead effect”. The coacervate contains high level of cationic charge, thus it has a strong affinity towards negatively charged hair, forming a clear coating. Due to its gel-like nature, it can also help with deposition of active agents with poor solubility.²⁶ Polymer molecular weight, charge density as well as viscosity play an important role when interacting with hair. However, it is known that excessive deposition on hair results in build-up and weigh-down the hair and makes it appears oily.²⁷ Thus, choosing the appropriate polymer and surfactant system is crucial for formulations aimed at providing additional benefits other than cleansing in order to predict and control the level of deposition and polymer accumulation.

2.2 Polymer-Surfactant Systems

2.2.1 Surfactants and micellization

Surfactants are a family of surface-active amphiphiles comprising of both lyophilic, (meaning soluble in a specific liquid), and lyophobic, (meaning insoluble) components (Scheme 2.1). When the liquid referred to is water, the two segments are classified as hydrophilic and hydrophobic respectively. Surfactants can be categorized by their hydrophilic component, such as nonionic, anionic or cationic surfactants. Hydrophobic parts are normally hydrocarbon chains.



Scheme 2.1 Schematic illustration of a surfactant.

As the name suggests, surfactants are surface active molecules that can adsorb onto surface or interface by driving forces, e.g. electrostatic, hydrophobic, hydrogen bonding and Van Der Waals interaction, etc. The surface activity of surfactants can be explained by the principles of free energy at the interface. At the interface, the free energy corresponds to the work needed to expand the area, which is also called surface tension. At the phase boundary, low free energy is the preferred state. When the interface is covered with surfactants, surface tension is reduced as well as the work required to expand the interface.²⁸ The reduction of surface tension is positively related to the surfactant concentration at the interface.

The types of surfactant structure may affect the adsorption at interfaces, and extensive studies to improve the understanding and design of surfactants with desired adsorption and salt tolerance have been reported²⁹. Such factors are:

- Increase of alkyl chain length increases the adsorption by orders of magnitude due to enhanced hydrophobicity.
- Presence of phenyl group in the surfactant increases the effective chain length thus also enhances the hydrophobicity and increases adsorption.
- Branching in surfactant hydrophobic chains largely effects adsorption due to the difficulties in surfactant packaging at interface.

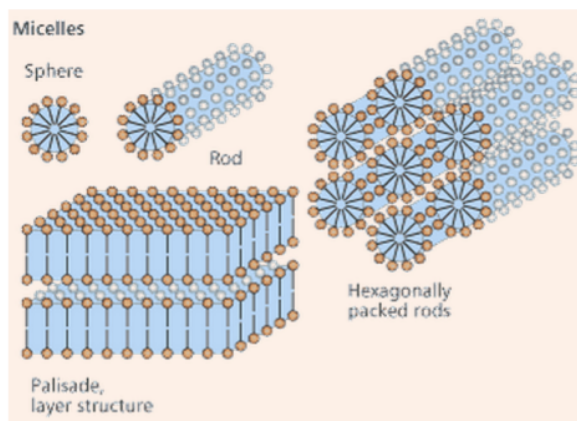


Figure 2.2 Surfactant self-assembly leads to a range of diverse structures. ³⁰

Aside from adsorption at interfaces, another characteristic property of surfactants is the ability of

forming micelles in bulk solutions at the critical micelle concentration (cmc). The difference between micellization from adsorption is that by partition to interface, hydrophobic groups of surfactant are removed from the water by exposing to nonpolar solvent or air, while micellization is the process when hydrophobic groups are repelled from water by hydrophobic and chain-chain interactions that form hydrophobic domains in the bulk. Upon micellization, the free energy of the whole system is reduced and the surfactant monomers behave in a very different manner from those in the bulk solution. Under specific temperature, pressure and ionic strength, micelles have unique packing parameters as well as cmc. However, micelles are not static once formed. They are in a dynamic equilibrium and continue to exchange monomers in the bulk and at the interface with those in the micelles. The exchange rate largely depends on the packing number, size and structure of the surfactant.³¹ To determine the cmc of a surfactant, techniques such as conductivity, fluorescence, self-diffusion, nuclear magnetic resonance (NMR), tensiometry and thermometry can be used. Furthermore, the morphology of micelles are also related to several aspects, such as surfactant concentration, aspect ratio of surfactant, size of hydrophilic groups, type and size of counter ions, etc. (Figure 2.2)³⁰

Currently, there are increasing concerns regarding utilizing and disposing of surfactants that raise important issues on toxicity to the ecological system. One biggest concern is on the biodegradability of surfactants. A review specifically focused on surfactant biodegradability points out that with the increase of linearity of hydrophobic group, biodegradability increases, while it decreases for isomeric materials, such as quaternary carbon terminated surfactants. In ethoxylated nonionic surfactants, the presence of oxypropylene or oxybutylene groups lowers their biodegradability.^{32,33} The toxicity of surfactants arise from their ability to penetrate cell membranes of organisms due to the similar amphiphilicity. Increase of hydrophobic groups and decrease of branching result in an increase in the surfactant toxicity. Other factors, such as shifting of phenyl group to central position in linear alkyl chains, decrease in the number of oxyethylene groups also influence the toxicity. It is noticed that certain changes in chemical structures promote degradability of surfactant, however it increases its toxicity or accumulative concentration in organisms. Thus, appropriate care should be taken in the synthesis and application of surfactants in order to reduce the potential damages.^{34,35}

2.2.2 Mixed micelles

In technical uses of surfactants, normally more than one species of surfactants are involved. Furthermore, lots of commercial surfactants are also inevitably mixtures of surfactants. Thus, mixed surfactants and micelles have received increasing attentions since the early 1980s.

Surfactant mixtures normally have improved solution and interfacial properties compared with those of individual surfactant. It was assumed that all the surfactant species are included in the mixed micelles produced in these mixed systems. The absorption of surfactant mixture systems can be either synergic or competitive, depending on various factors such as surfactant structure, pH, temperature, ionic strength, etc. Thus, it is desirable to be able to manipulate the system behavior for their use in practical applications.

It was reported that individual non-ionic surfactant octaethylene glycol mono n-dodecyl ($C_{12}EO_8$) does not adsorb on solid surfaces, but in the presence of anionic surfactant sodium dodecyl sulfate (SDS), synergic adsorption was observed and the adsorption of SDS on a similarly charged surface was facilitated. In such cases, the formation of micelles containing both surfactants is due to the driving force between hydrocarbon chains of the surfactants. Interestingly, in the mixture of SDS and $C_{12}EO_8$, a pH related co-adsorption behavior was also observed. At pH 5, the adsorption of $C_{12}EO_8$ was facilitated by addition of SDS, while at pH 10, the adsorption was suppressed, which suggested a synergic adsorption via the interaction between alkyl chains at low pH.³⁶

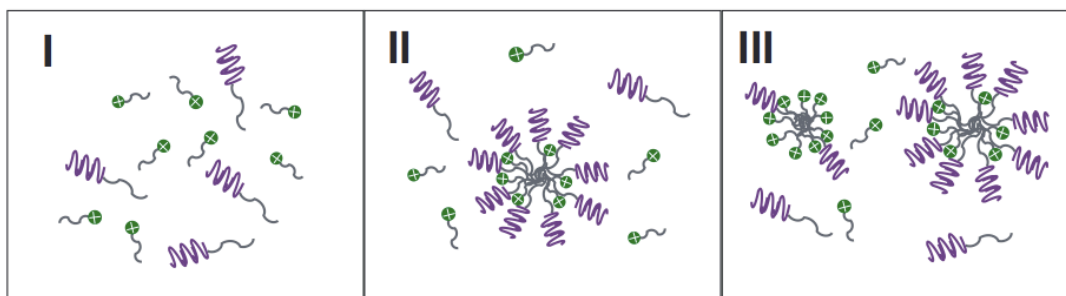


Figure 2.3 Schematic model of the binary surfactant system of TTAC and NP-15. Region I, no micelles in the mixed solution; region II, surfactants began to form aggregates; region III, TTAC-rich and NP-15-rich mixed micelles coexisted in the solution.³⁷

The micellization of nonionic surfactant pentadecyl ethocylated nonylphenol (NP-15) and cationic surfactant tetradecyltrimethylammomium chloride (TTAC) in a mixture solution was studied by ultrafiltration technique. The results suggested a coexistence of mixed micelles, which is of importance in guiding colloidal behavior of surfactant mixtures. On the basis of concentration measurements and phase behavior model, Huang et al. divided the micellization behavior into three regions (Figure 2.3). In region I, the concentration of surfactant is very low that only surfactant monomers exist. In region II, since the nonionic surfactant is more surface-active, NP-15-rich micelles are formed first and cationic surfactant

TTAC dissolves in the micelles as concentration increases, thereby changing the micelle composition. Region III is designated as the region where two types of micelles coexist leading to variations in the individual monomer concentrations.³⁷ The coexistence of two micelles in the same surfactant mixture system was later confirmed using analytical ultracentrifuge that suggested the practical implications in the stability and efficacy of the system (Figure 2.4).³⁸

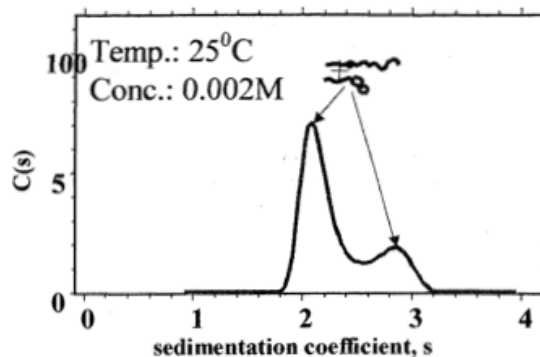


Figure 2.4 Analytical ultracentrifuge of mixed surfactants: coexistence of two micelles.³⁸

The micellization behavior of ionic and nonionic surfactant mixtures in homogeneous solutions has been intensively studied in the past few years.³⁹ Models describing the interactions between similar and dissimilar surfactants in bulk solutions were used to determine the interaction parameters. By modeling the interaction, prediction of synergic or competitive adsorptions of the mixture system may be achieved.

2.2.3 Polymer-surfactant interactions

Polymer and surfactant combinations are commonly observed in various types of personal care and cosmetic products, as well as paints, foods, drugs and pesticides formulations. In majority of the cases, polymer and surfactant have a synergistic effect in order to generate formulations with preferable colloidal stability, emulsification, flocculation, dispersability, viscosity, etc. Thus, polymer and surfactant systems have received a great deal of attention in the past decades. Systematic studies have been reported on their different behaviors compared to individual solutions of polymer or surfactant. Their properties are significantly altered with respect to phase behavior, interfacial, thermodynamic and rheological properties.

Surfactants self-assemble to form micelles at the cmc in polymer-free solutions, while in the presence of polymers, association of surfactant monomers on the polymer chains was observed at a concentration much lower than the cmc, and this concentration is commonly referred to as the critical

aggregation concentration (cac). For instance, in Figure 2.5, the first deviation of surface tension curves in the presence of polymer is the aggregation of SDS on PVP due to hydrophobic binding, which can be assigned as cac. Another critical concentration, called C_2 , shown as the second deviation denotes the saturation of polymer chains and the formation of free micelles in the bulk.⁴⁰

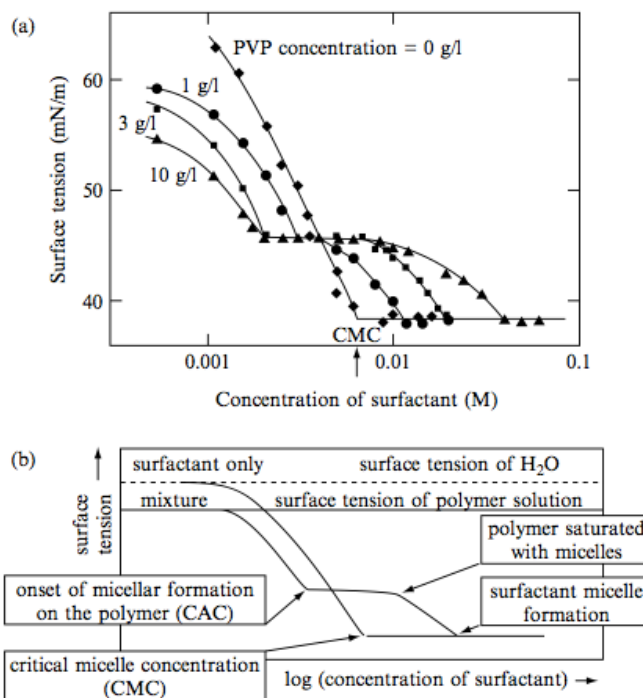


Figure 2.5 (a) Surface tension of SDS in the presence of varying concentrations of poly(vinyl pyrrolidone) (PVP). (b) A schematic plot of surface tension for individual surfactant and polymer-surfactant system.⁴⁰

Generally, polymer-surfactant interactions can be divided into two categories, one is between all types of surfactants with non-charged polymers, and the other is between charged surfactants with polyelectrolytes. Numerous studies have been conducted to study the interactions between uncharged polymers and ionic surfactants, such as poly(ethylene oxide) (PEO) and sodium dodecyl sulfate (SDS) such as those reported by Jones et al.⁴¹, who used surface tension method to study the system. Hydrophobic force is considered to contribute to their interactions, and at very low molecular weight of PEO, no interaction was observed. The same interaction was studied in detail by Dai et al.⁴² using isothermal titration calorimetry (ITC). They revealed the dependence of the interaction on PEO molecular weight at low, moderate and high ranges. When the molecular weight of PEO is below 400 Daltons, the hydrophobic interaction is too small that hydrophilic natured polymer chain had no interaction with SDS,

which was also confirmed by Gao et al. using NMR paramagnetic relaxation method.⁴³ (Figure 2.6, a) At the range of 900 to 1450 Daltons, an endothermic peak was observed on the thermograph and increased with molecular weight. (Figure 2.6, b) When SDS monomers are induced to aggregate at the hydrophobic domain on PEO chains, the dehydration and solubilization of PEO segments from the water phase to hydrophobic core of SDS aggregations result in an endothermic peak.⁴⁴ The onset of the peak is designated as the cac of the system, which decreases for PEO of higher molecular weights due to the increase of hydrophobicity. The cooperative binding of SDS results in an increase in the aggregation number until the saturation point of PEO chain is reached. The electrostatic repulsion between anionic head groups of SDS retard further aggregation. As the molecular weight of PEO increases to 3350 Daltons, an distinctive exothermic peak can be observed on the thermogram. The exothermic peak is attributed to the rehydration of PEO hydrophobic domains from the core of SDS aggregates to water phase, upon which the PEO chain would further surround the SDS micelles. The driving force of the rehydration is ion-dipole association between EO segments and hydrophilic head groups of SDS. These newly formed structures are stabilized due to reduced electrostatic repulsion of SDS head groups as well as the reduced contact between SDS hydrophobic cores and water by wrapped PEO chains. (Figure 2.6, c)

For cationic surfactants, they display less activity towards non-ionic polymers than anionic surfactants. The explanation for this difference is a combination of large ionic head groups and the different structure of water cage surrounding the surfactant. Studies have pointed out that changing the counter ions binding at cationic surfactant would significantly alter their activity toward non-ionic polymers.⁴⁵

Regarding charged polymer and oppositely charged surfactant systems, electrostatic attraction dominates the binding of monomers to the adsorption sites on polymers at low surfactant concentration, since electrostatic force is the most dominant physical forces. Upon adsorption, surfactant ion acts as a nucleating site for aggregate formation of other monomers. The adsorption process is very energetic and favorable that it turns the polymer interface to become more hydrophobic. However, in most cases, with further adsorption and aggregation of surfactants, the interface would become more hydrophilic with ionic head groups of surfactants facing outward, resulting in the solubilization of the polymer.

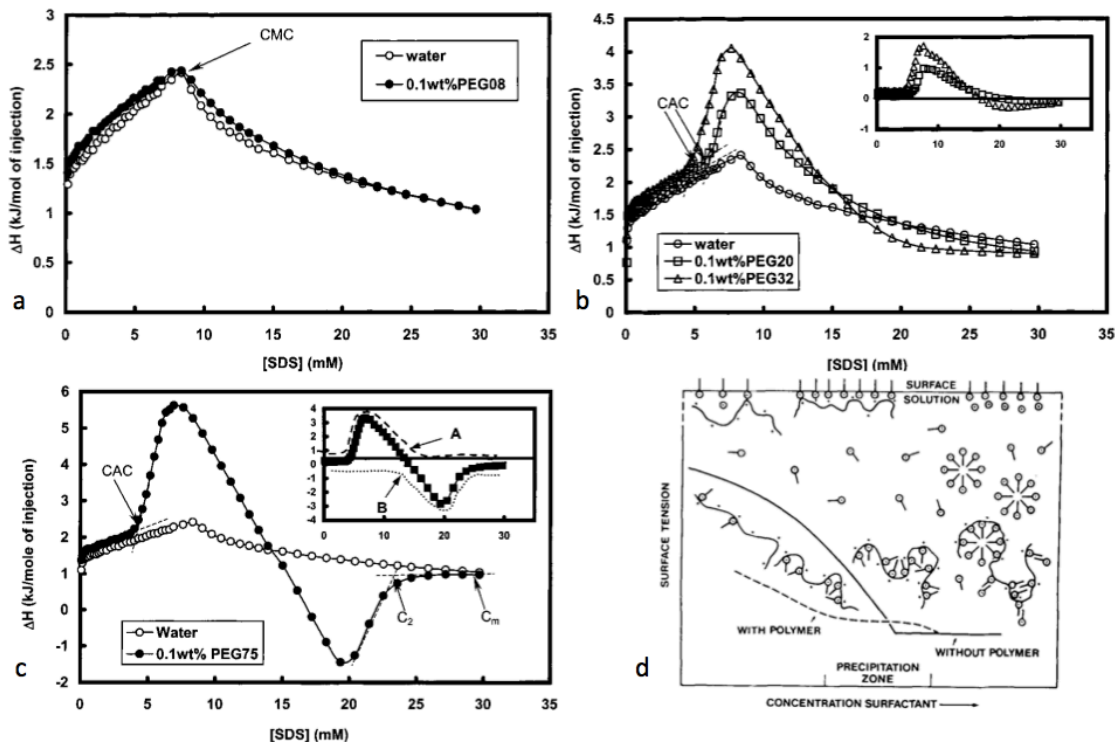


Figure 2.6 (a) ITC curve of 0.2M SDS titrating into water and 0.1wt% PEO (400 Da); (b) ITC curve of 0.2M SDS titrating into 0.1 wt% PEO (900 Da) and PEG (1450 Da); (c) ITC curve of 0.2M SDS titrating into 0.1 wt% PEO (3350 Da); (d) schematic of the dehydration and rehydration of non-ionic polymer interacting with surfactant. ⁴⁴

Surfactant selective electrode (SSE) is commonly used to determine the cac and bound number of surfactant monomers per charged group of polymer. This method is based on the equilibrium of surfactant activity, thus it is difficult to be used in the presence of oppositely charged polymers. Compared with SSE, a novel method has been reported to determine the binding isotherm of surfactant.⁴⁶ The method does not rely on equilibrium measurements of surfactant activity, but on the measurement of electrophoretic mobility with respect to increasing surfactant concentration. The amount of bound surfactant per polymer charged group and equilibrium surfactant concentration can be calculated from mass balance of the system under certain assumptions and be used to determine the binding isotherm of surfactant on oppositely charged polymers. Recently, transient electrical birefringence (TEB) was used to monitor the binding process at the microscope level. ⁴⁷ The technique is based on the counterion polarization mechanism, which describes the different contribution of two types of counterions. Free counterions are polarized perpendicular to the polymer axis giving a negative contribution to the

birefringence, while condensed counterions polarized parallel to the polymer axis giving a positive contribution. When surfactants bind to the charged group on polymer chain, the binding replaces free counterions thus reduces the negative contributions, which can be detected by measuring the change of birefringence of the system.

In addition to the driving force of polymer-surfactant interactions, other aspects will also influence the system's behavior. The flexibility of polymer chains determines the extent of polymer wrapping on surfactant micelles. Hydrophobic nature and surface activity of polymer also impacts its activity towards ionic surfactants, for example, PVA, PEO, PPO have increasing interactive activity towards surfactants.

2.3 Cellulose Nanocrystals (CNC)

2.3.1 Cellulose

Cellulose is the most abundant biopolymer resource in the world. It is widely recognized as a renewable and biodegradable raw material with applicable advantages and properties. Cellulose is consisted of β -1,4-linked anhydro-D-glucose units, in which the glucoses are 6-carbon rings linked by single oxygen between C¹ and C⁴. Each glucose is corkscrewed 180° to its neighbors thus two glucoses are usually taken as one unit (Figure 2.7a). The polymerization degree on each chain is up to 20,000, which is dependent on the source.⁴⁸⁻⁵⁰ Cellulose chains have a linear configuration that stabilizes the linkage between glucose units by forming intra-chain hydrogen bonding between hydroxyl groups and oxygen of neighboring glucose units. Meanwhile, van der Waals and intermolecular hydrogen bonding promote parallel stacking of multiple chains to form elementary cellulose segments. Further aggregation of the segments forms larger microfibrils in the size of 5-50 nm in diameter and several microns in length.⁵¹ These elementary segments are the main reinforcement phase for the source, such as trees, plants, algae, bacteria and tunicates. Within cellulose fibers there are regions that cellulose chains are arranged in a highly ordered structure as well as regions that are disordered (Figure 2.7b). The cellulose chain network formed by forming inter and intra-chain hydrogen bonding with crystalline structure ensures the stability of cellulose fiber and makes it highly stiff in axial direction, while the amorphous regions make the materials flexible and resistant to bending or fracture. The crystalline regions contained in the cellulose fibers can be extracted to obtain cellulose nanocrystals (Figure 2.7c).⁵⁰

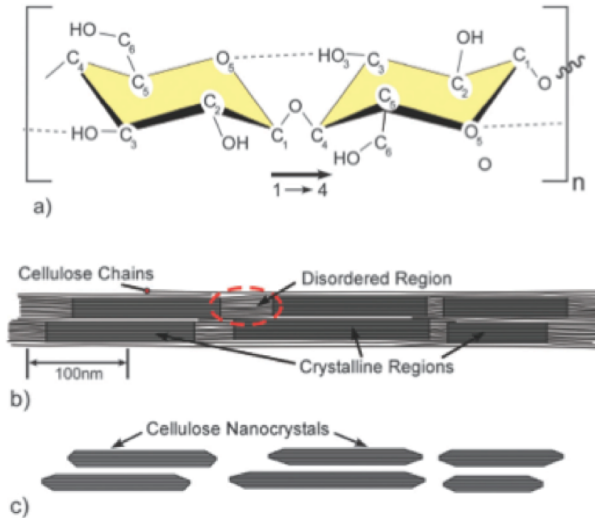


Figure 2.7 (a) Structure of single cellulose chain repeat unit, the direction of 1-4 linkage and intra-chain hydrogen bonding are shown; (b) Schematic of cellulose microfibrils with crystalline and amorphous regions; (c) Schematic of cellulose nanocrystals after amorphous regions are dissolved by acid hydrolysis.⁵⁰

Cellulose has different polymorphs ascribed as cellulose I, II, III and IV.⁴⁸ Cellulose I is mostly found in plants or bacteria cellulose crystalline segments, which is consisted of metastable cellulose I with all the cellulose chains in a highly parallel arrangement.⁵² It is thermodynamically stable and can be converted to cellulose II or III. Up to date, the most stable structure regarding technical applications is cellulose II. It can be produced by two methods: one is solubilization and recrystallization, the other is sodium hydroxide treatment in aqueous suspension.⁵³ Cellulose II has been widely used in producing transparent films (Figure 2.8)⁵⁴ and synthetic textile fibers. From liquid ammonia treatment of cellulose I and II, cellulose III can be obtained. Further thermal treatment of cellulose III generates cellulose IV.

Structure of cellulose I is most intensively studied due to its availability and cost-efficiency. There are two polymorphs in cellulose I, called I α (a triclinic structure) and I β (a monoclinic structure). They coexist in cellulose fibres with varied proportions depending on the source.⁴⁸⁻⁵⁰ For example, I α polymorph is found to be the largest proportion in algae and bacteria, while I β is highly dominating in tunicate and higher plants.⁵⁵ I α polymorph can be converted to I β by high temperature treatments in organic solvent or helium gas^{56,57}, and by hydrothermal treatment at about 260°C in alkaline solution⁵⁸⁻⁶⁰. I α polymorph conversion is mostly done using I α -rich algae and bacteria. Though the conversion efficiency can be controlled by varying the treatment conditions, complete conversion has not been achieved.^{57,58,60}

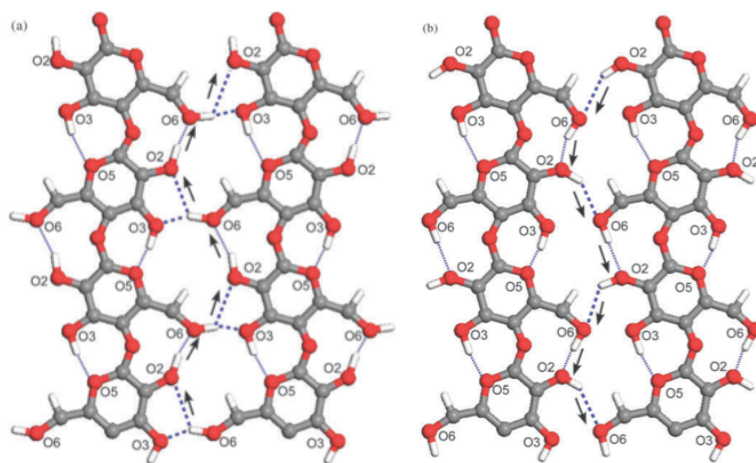


Figure 2.8 Schematics of two hydrogen bonding networks within cellulose fibre. Thin dotted lines are intra-chain bondings, thick dotted lines are inter-chain bondings.⁵⁴

Hydrogen bonding within I α and I β polymorphs is very important for the differences in their stability and properties. Two coexisting hydrogen bonding networks are mostly agreed upon as shown in Figure 2.8.⁶¹ The intra-chain hydrogen bonding are mainly formed by the strong O3-H \cdots O5 bonds, while there are other intra-chain hydrogen bonding configurations that are harder to be characterized because they are possibly linkages with chains outside of the plane.⁵⁶ These intra-chain hydrogen bonding contribute to the high axial stiffness of I α and I β polymorphs.^{62,63} Proportion of intra-chain hydrogen bonding in I β polymorph is higher than that in I α polymorph and distributed in a region of better bonding geometry.⁶⁴ Inter-chain hydrogen bonding coexists with intra-chain bonding in both of the polymorphs, but it is believed that inter-chain hydrogen bonding in I β polymorph is stronger than that in I α , results in a higher stability of I β polymorph. It also explains the reason of I α polymorph thermally degrades at a lower temperature than I β polymorph does.⁵⁹

2.3.2 CNC synthesis

Cellulose nanocrystals are derived from acid hydrolysis of wood fiber, plant fiber, microfibrillated cellulose, microcrystalline cellulose or nanofibrillated cellulose.⁶⁵⁻⁶⁷ They are rod-like or whisker shaped particles with dimension 5-20 nm in width and 50-500 nm in length and a high aspect ratio. The main proportion of its crystalline structure is I β polymorph. Its crystalline structure can be highly affected by hydrolysis procedure and conditions, the resulting product can be either insufficiently or too severely hydrolyzed. If removal of amorphous region is incomplete, the crystallinity will decrease in the product and particle morphology may be changed. Also, too much hydrolysis will result in a reduction of the

aspect ratio or even producing spherical particles.^{68,69} Cellulose nanocrystal has very good thermal stability, where the onset of its thermal degradation is between 200-300°C, depending on the type of particle and surface modification.^{70,71}

Acid hydrolysis is the main process for preparing CNC. Upon acid treatment, amorphous region of cellulose is preferentially hydrolyzed, while crystalline regions are more resistant to acid treatment due to hydrogen bonding network and thus, they remain intact.⁷² The resulting crystalline region, the main constituent of cellulose fibres, are rod-like particles with sizes in the range of 10 to 20 nm in diameters and several hundreds of nanometers in length⁷³. The size of CNC varies with the hydrolysis procedures, such as reaction time, temperature and types of acid, as well as the source of cellulose. The main sources of CNC are wood, cotton, tunicate, bacterial, ramie and sisal cellulose. The morphology and crystallinity of crystalline blocks remain the same as the original fibers as confirmed by TEM, AFM and XPS.

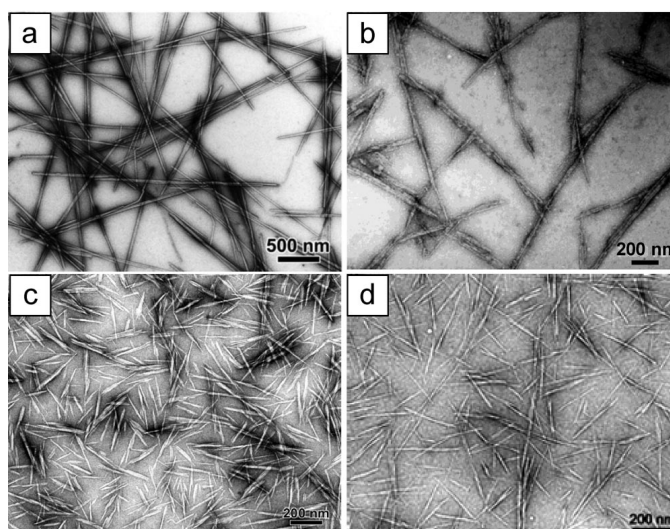


Figure 2.9 TEM images of dried dispersion of CNC derived from (a) tunicate (b) bacteria (c) ramie (d) sisal

65,74–76

Table 2.1 shows examples of length (l) and diameter (d) of CNCs from different sources⁷³. CNC from bacterial cellulose have a larger dimension compared with those derived from wood and cotton fibers since they have longer crystalline regions and lower fractions of amorphous region.⁷⁷ Polydispersity index (PDI) of CNC depend on the distribution of amorphous region along cellulose fibers. Since bacterial cellulose have more randomly distributed amorphous regions, the PDI of CNC products is relatively higher under the same hydrolysis conditions.⁷⁸ Thus far, CNC from wood and cotton are mostly produced due to their abundant supply, high cellulose content and uniformity.⁷⁹

Source	L (nm)	D(nm)	Aspect ratio (L/D)	Technique
Bacterial	100-1000	150	2-100	TEM
Cotton	100-150	5-10	20-30	TEM
	150-210	5-11	15-42	E-SEM
MCC	~500	10	50	AFM
Ramie	50-150	5-10	5-30	TEM
Sisal	100-500	3-5	20-167	TEM
Tunicate	1160	16	73	DDLS
	100-several 1000	15-30	3-67	TEM
Valonia	>1000	10-20	50-100	TEM
Wood	100-300	3-5	20-100	AFM

Table 2.1 Sizes of CNC form various resources.

During acid hydrolysis, the reaction conditions are also the determinants of CNC morphologies. Although hydrolysis occur randomly along the CNC surface, a higher ratio of acid to cellulose, longer reaction time or higher reaction temperature result in shorter and narrower CNC particles, while the polydispersity index (PDI) is decreased.^{74,80} Sulfuric acid and hydrochloric acid are extensively used for CNC production. CNCs prepared by hydrolysis in sulfuric acid undergo protonation of glucosidic oxygen or cyclic oxygen by protons in the acid⁸¹. Then the addition of water will further split of glucosidic bonds yielding shorter chains, however the basic structure of cellulose backbone is preserved (Figure 2.10a). After chain scission, esterification of hydroxyl groups occurred on CNC surface resulting in an excellent dispersity of the CNC in aqueous as well as some organic solutions, such as alcohol, dimethylformamide, dimethyl sulfoxide due to electrostatic repulsion between anionic sulfate groups on surface, which compromises the thermostability of nanoparticles (Figure 2.10b).⁷⁵ While CNCs prepared in hydrochloric acid have poorer stability and tend to flocculate.⁸² Post-treatment of hydrochloric acid-generated CNCs by sulfuric acid has been studied to introduce a controlled amounts of sulfate groups onto the CNC surface.^{83,84} A combination of sulfuric acid and hydrochloric acid during hydrolysis steps generate CNC nanoparticles with spherical instead of rod-like appearances, which have better thermal stability due to

increased amount of sulfate groups on the surface.^{69,85} Hydrolysis using phosphoric and hydrobromic acids have also been reported.⁸⁶

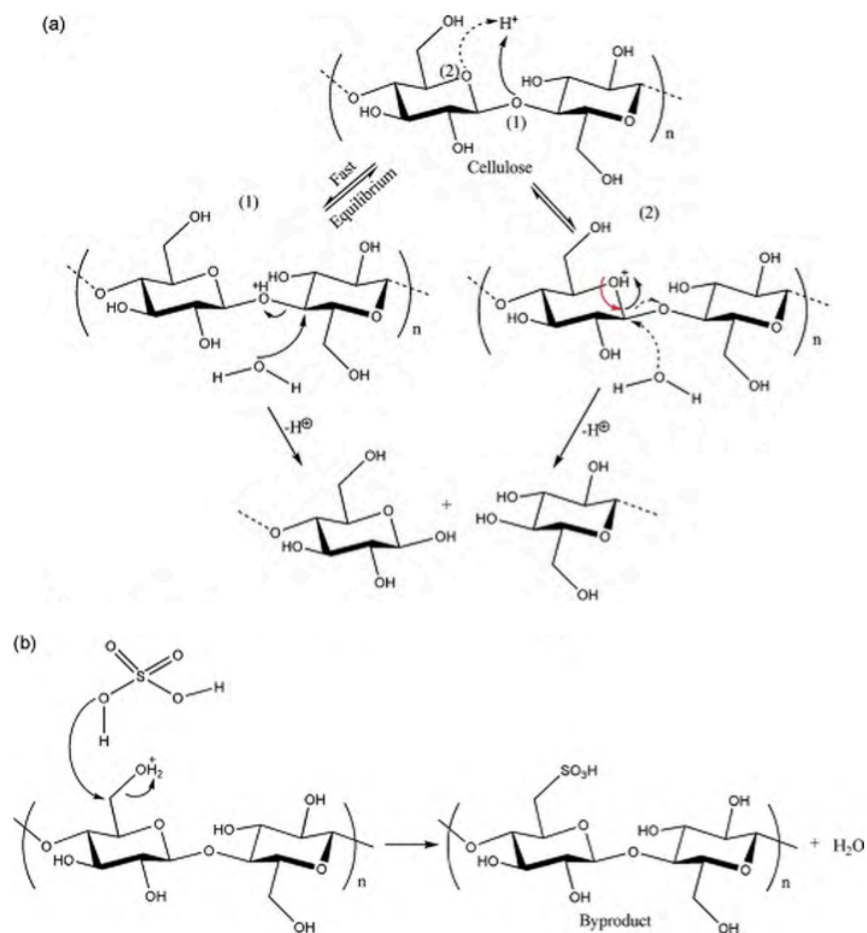


Figure 2.10 (a) Acid hydrolysis mechanism, (b) esterification of cellulose nanocrystal surface.⁷⁵

Cellulose nanocrystals in the dimension of several to hundreds nanometers have much larger amount of reactive hydroxyl groups on the surfaces than microcrystalline cellulose or cellulose fibres. Since the negatively charged sulfate groups are vulnerable under mild alkaline conditions, modifications are needed to introduce more stable negative or positive electrostatic charges onto surface of CNC to increase the stability. Furthermore, hydroxyl groups make CNC highly hydrophilic on the outside so that the compatibility is usually poor for applications in nanocomposite. Thus, surface energy of CNC needs to be tuned by introducing nonpolar or hydrophilic segments in order to increase its compatibility while preserving the inner crystalline structure so that the excellent mechanical property can be maintained and transferred to the matrix.

2.3.3 CNC properties

CNC has very good dispersability in aqueous solution due to the negative charges from acid hydrolysis. CNC suspension is isotropic at very low concentration when the particles are randomly oriented, and when the concentration increases to a critical value the suspension becomes anisotropic with a chiral nematic ordering and forms a liquid crystalline phase.⁸⁷ With further increase in the CNC concentration, a shear birefringence phenomenon can be observed. The explanation to this behavior was derived by analyzing the critical concentration of CNC as a function of its aspect ratio, charge density and osmolarity. It was reported that the application of AC electric or magnetic field on CNC suspension can also introduce ordering of the nanoparticles.^{88,89} Habibi et al.⁹⁰ observed that application of AC field resulted in the alignment and orientation of CNC suspensions, and the film formed from aligned suspensions is more homogeneous with increasing electronic field strength. Pan et al.⁷ conducted a similar study and reported factors that control the chiral nematic property of CNC films. They found that the magnetic field did not influence the formation of chiral nematic phase, however, it increased the chiral nematic pitch of the suspension. Due to the polyelectrolyte nature of CNC nanoparticles, they are highly sensitive towards electrolytes and counterions, as well as polymers. Studies on the addition of electrolyte to CNC suspensions and monitoring the phase behavior of CNC suspensions have been conducted. For example, HCl, NaCl and KCl were found to significantly reduce the volume fraction of anisotropic phase.⁹¹ Beside ionic strength, the types of counterions and polymers in solution all have an influence on phase separation behavior of CNC suspension.^{92,93} Addition of surfactants was used to improve the dispersability of CNC in non-polar solvents for applications in nanocomposites. It was reported that with the addition of surfactants, a layer of surfactant coating was formed around CNC particles, but the chiral nematic phase was still observed.⁹⁴

2.3.4 CNC modification

Non-covalent modification with surfactants was mostly studied for the purpose of improving the dispersability of CNC in nonpolar solvents. Thin layer of surfactants consisting of mono-/di-esters of phosphoric acid and alkylphenol tails was detected using SANS in the form of 15 Å coating layer on the surface of CNC. This layer of non-ionic surfactants transformed the CNC and produced a well dispersed suspension in nonpolar solvents.^{77,95-98} Anionic and non-ionic surfactants were also used to enhance the compatibility of CNC in poly(lactic acid) (PLA) and polystyrene-based composite fibers.⁹⁹⁻¹⁰¹

CNCs generated from sulfuric acid hydrolysis form homogeneous nanoparticle suspension in aqueous and some organic solvents due to the negative sulfate groups on the surfaces. However, since the

sulfate groups may take up as much as 40% of the most reactive hydroxyl groups and make them unreactive. Studies to investigate the influence of residual sulfate groups on gelling and thixotropic behavior of cationized CNCs¹⁰², different ways of CNC desulfation were conducted.

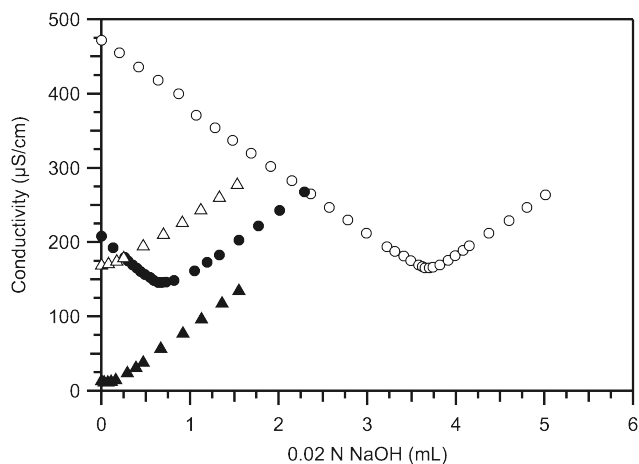


Figure 2.11 Conductometric titration curves for H_2SO_3 -hydrolyzed CNC (open circle), HCl-hydrolyzed CNC (open triangle), HCl-desulfated CNC-seventh step (solid circle), solvolytically desulfated CNC (solid triangle).¹⁰³

Hasani et al.¹⁰² reported a CNC desulfation procedure under the condition of 2M NaOH treatment at 65 °C for 5 hours. However, it was also indicated that alkaline-catalyzed desulfation of CNC resulted in 3:6- and 2:3-anhydride structures.^{104,105} Other methods include acid hydrolysis and solvolytic desulfation. Desulfation by acid has a drawback in that the glycosidic linkages in polysaccharides are susceptible to acid hydrolysis. Depolymerization may take place when treated with strong acids. Another limitation is that the desulfation process can be stereo-selective.¹⁰⁶ Desulfation of CNC using hydrochloric acid shows only partial sulfate groups are hydrolyzed yielding a decreasing sulfate content with repeated hydrolysis.¹⁰³ Solvolytic desulfation involves heating of pyridinium salt of polysaccharide in the mixture of dimethyl sulfoxide and methanol.^{107,108} This method resulted in a nearly complete desulfation within a single step (Figure 2.11).¹⁰³

(2,2,6,6-Tetramethylpiperidine-1-oxyl)-mediated (TEMPO) oxidation is a process to introduce carboxylic groups to the position of hydroxymethyl groups on CNC surface. This reaction has a very distinguish substitution towards primary hydroxyl groups, while the secondary hydroxyl groups remained mostly unreacted. This makes TEMPO oxidation green and simple to conduct.⁷⁸ TEMPO, a stable nitroxyl radical, and oxidizing agents sodium bromide (NaBr) and primarily sodium hypochlorite (NaOCl)

are applied for oxidation reaction. By varying the amount of primary oxidizing agent, the degree of oxidation on surface of HCl-hydrolyzed CNC can be predicted and achieved. Meanwhile, the birefringence patterns of TEMPO-CNC aqueous suspension are preserved and no flocculation observed (Figure 2.12).¹⁰⁹

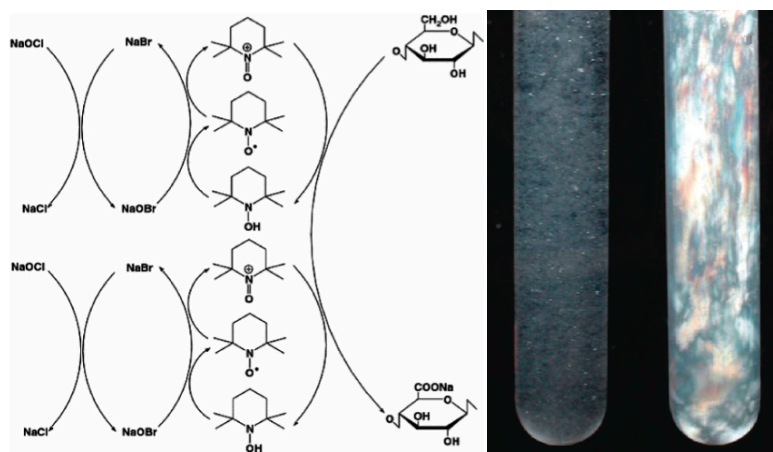
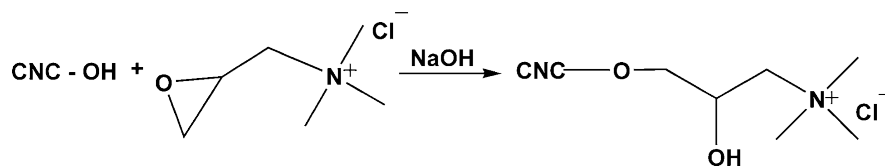


Figure 2.12 Scheme of TEMPO-mediated oxidation of primary hydroxyl groups on the surface of CNC (left); suspension of HCl-hydrolyzed CNC suspension in the left tube and TEMPO-oxidized CNC in the right tube observed between crossed polarizers (right).¹⁰⁹



Scheme 2.2 Reaction scheme of cationization of CNC with GTMAC.

Cationization of CNC by grafting epoxypropyltrimethylammonium chloride (GTMAC) via the addition of alkali-activated hydroxyl groups to epoxy moiety of GTMAC was studied by Hasani et al. (Scheme 2.2)¹⁰² A zeta-potential of $+30 \pm 5$ mV was observed for GTMAC-CNC compared to -39 ± 3 mV for the original CNC, indicating a reversed surface charge after modification. Due to the fact that side reaction of GTMAC in alkaline solution is determinative to its grafting efficiency, Zaman et al.¹¹⁰ investigated the influence of various reaction parameters, such as water content, reaction molar ratio and reaction media. They found that the optimized reaction media to be 36wt% of water in aqueous media and 0.5 water to DMSO in mixture solvent media.

Grafting of polymers onto the surface of CNC was conducted in two different methods: grafting-

to and grafting-from. Grafting-to is an approach where polymers such as polycaprolactone (PCL) with various molecular weights¹¹¹, presynthesized waterborne polyurethane¹¹², amine-functionalized PEG^{83,113}, DNA oligomers¹¹⁴, etc. are directly grafted on the CNC surfaces. The peptide-coupling reaction between carboxylic groups on TEMPO-CNC and amine groups using EDC/NHS carbodiimide chemistry at room temperature is the most widely used approach.¹¹³⁻¹¹⁵ Grafting-from approach is to grow polymer chains from surface of CNC via atom transfer radical polymerization (ATRP), which ensures a precise control on the polydispersity of grafted polymers.¹¹⁶ Methods of ring-opening polymerization⁷⁶, microwave irradiation^{117,118}, in-situ solvent exchange¹¹⁹, etc. are also used to graft various polymers onto CNC surface.

2.3.5 Interactions between cellulose, CNC, CNC derivatives and surfactants

As a renewable, biodegradable and sustainable material from vast natural sources, cellulose and its derivatives have attracted increasing attentions. Cellulose and its derivatives have been applied as additives in food, drug, paint and personal care industries to enhance the performance of formulations. The study of interaction between cellulose derivatives and surfactants is one of the most important and intensively studied topics. Both cooperative and competitive interactions were observed in the high concentration range of surfactants.

The interactions between anionic surfactants and non-ionic cellulose derivatives, ethyl(hydroxyethyl) cellulose (EHEC) and hydroxypropyl methyl cellulose (HPMC) were studied by Ridell et al. using fluorescence probe techniques together with microcalorimetry and dye solubilization.¹²⁰ EHEC is water-soluble cellulose modified by hydrophilic group (-CH₂CH₂OH) and hydrophobic group (-CH₂CH₃) that are distributed randomly along the polymer backbone. The anionic surfactants studied were dodecyl sulfate with different counterions (KDS, NaDS and LiDS). It was found that counterions played a small but important role in the interactions. With more hydrated counter ion Li⁺, the micelles of surfactant and polymer-surfactant aggregates are both loosely packed and fragile, resulting in a higher cac and cmc. This effect in the order of Li⁺>Na⁺>K⁺ was confirmed by all three methods used. Due to the fact that EHEC is more hydrophobic than HPMC, it interacted more strongly with dodecyl sulfates than HPMC and gave a much lower cac value. Calorimetric measurements further confirmed the endothermic and entropy driven adsorption of surfactants onto polymers, as well as the exothermic interaction when more and more surfactant aggregates are formed on polymer chains.

Interactions between EHEC and cationic surfactants were also studied. Bloor et al.¹²¹ investigated the binding profile of cetyltrimethylammonium bromide (CTAB) with several non-ionic polymers

including EHEC using a surfactant selective electrode. They observed significant binding and saturation of the polymers by bound surfactants. The occurrence of free micelles in the bulk before the saturation of polymers was also reported. The same system was also studied by Zana et al.,¹²² who reported the increased ionization degree and reduced micelle aggregation number. They found that the effects were more significant at high temperature, indicating the increase of polarity of polymers and stronger interaction with surfactants. Wang and Olofsson¹²³ systematically studied the interactions between EHEC and a series of cationic surfactants including dodecylammonium chloride and alkyltrimethylammonium halides RTAX, where R represents the length of alkyl chain with 12, 14, 16 carbons and X represents Br or Cl. They compared the interactions of cationic surfactants and SDS and observed the difference in their binding sites on EHEC polymer. From viscosity and calorimetric measurements, it was observed that SDS interacts with ethyl and ethylene groups on EHEC, while cationic surfactants only interact with the alkyl substitutes.

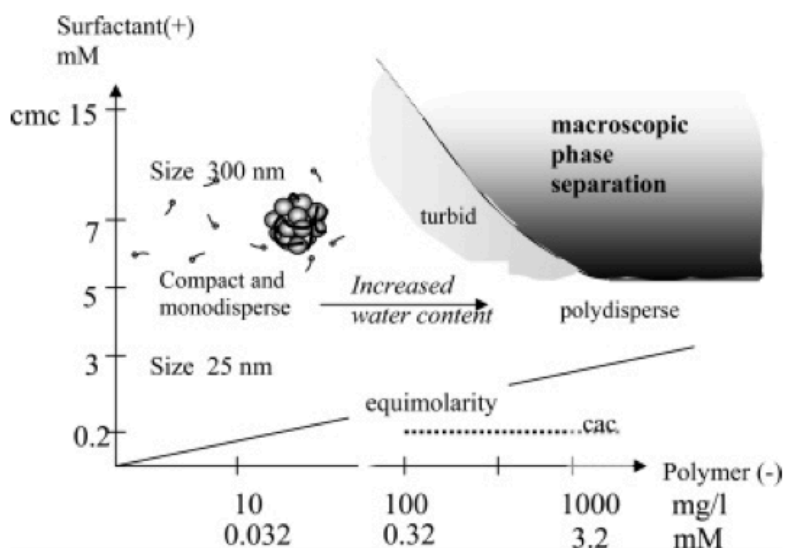


Figure 2.13 Scheme of the phase diagram indicating the different regions with dense aggregates, loose aggregates, and precipitates in the case of DTAB-NaCMC mixed solutions.¹²⁴

Cellulose derivatives bearing negative charges were synthesized and their interactions with various surfactants were studied. Carboxymethylcellulose (CMC) is negatively charged cellulose ether derived by alkali-catalyzed reaction of cellulose with chloroacetic acid. It is usually found in the form of sodium salt above pH 4, namely sodium caroxymethyl cellulose (NaCMC).¹²⁵ The interactions between NaCMC and oppositely charged surfactants have been extensively studied. It was found that NaCMC

behaved as synthetic anionic polymers in cationic surfactant solutions, where a cac can be observed at low surfactant concentration due to the strong electrostatic attraction. Wang and Tam reported the non-cooperative interaction even below cac, while it became more cooperative above the cac.¹²⁶ Trabelsi et al.¹²⁴ studied the interactions between NaCMC and two cationic surfactants, CTAB and DTAB, using light scattering, surfactant selective electrode, viscometer and zeta-potentiometer, and reported the influence of surfactant concentration, polymer concentration and length of surfactant hydrophobic tail on the morphology, size and charge of polymer-surfactant aggregates. In general, with the increase of surfactant concentration, charged binding groups on polymers are gradually saturated by surfactants. Then, hydrophobic effects become more significant than electrostatic interactions, resulting in the precipitation and phase separation in the solution. In NaCMC-CTAB system with low polymer concentration, polymer-surfactant aggregates are spherical, rigid and monodispersed at low surfactant concentrations, while at higher surfactant concentration the size increases exponentially. With the increase of polymer concentration, the aggregates become larger, polydisperse and softer. (Figure 2.13) They also found that the difference between hydrophobic tail length significantly influenced the behavior of polymer-surfactant aggregates. For the CTAB-NaCMC, the aggregates are much larger than DTAB-NaCMC possibly due to the fact that CTAB cannot completely neutralized the charges on polymer even above the concentration at which the total amount of surfactant monomers is similar to the charges on the polymers. Mata et al.¹²⁷ obtained similar results with DTAB, tetradecyltrimethyl-ammonium bromide (TTAB) and CTAB.

The interactions between cellulose nanocrystal and surfactants were also studied. Due to the crystalline nature and rod-like structure of this nanomaterial, CNC behaves differently comparing with cellulose polymers in surfactant solution. Dhar et al.¹²⁸ studied the interaction mechanism of tetradecyl trimethyl ammonium bromide (TTAB) and CNC system using surface tensiometer, isothermal titration calorimetry (ITC), conductivity titration and phase separation. They indicated that the interaction is controlled by electrostatic and hydrophobic forces, which resulted in the non-cooperative binding at higher TTAB concentrations (>CMC) and cooperative binding at very low TTAB concentrations (Figure 2.14). Interactions between surfactants and polymer-grafted CNC were also studied. Peng et al.¹²⁹ grafted polypropylene glycol (M600) onto CNC surface. The oxypropylene segments of the resulting polymer have strong hydrophobic interactions with hydrophobic tails of sodium dodecyl sulfate (SDS) as indicated by a large endothermic peak observed in the ITC thermogram. Cationic dodecyltrimethylammonium bromide (DTAB) had strong electrostatic interaction due to the neutralization of opposite charges (Figure 2.15).

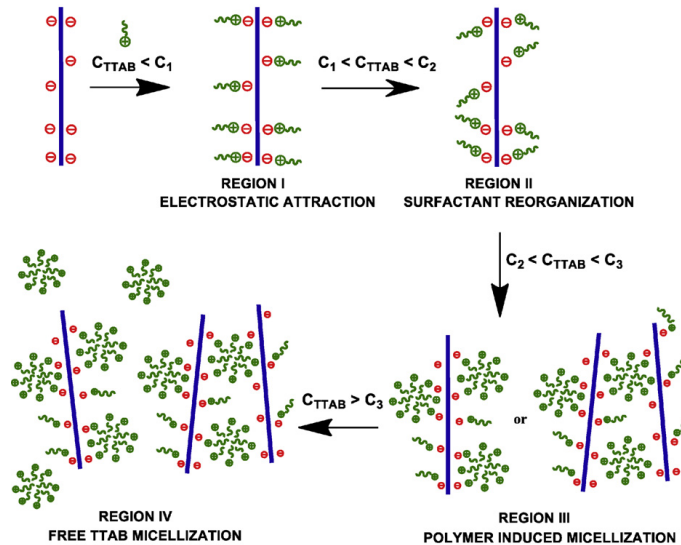


Figure 2.14 Mechanism of CNC-TTAB binding from ITC experiments. ¹²⁸

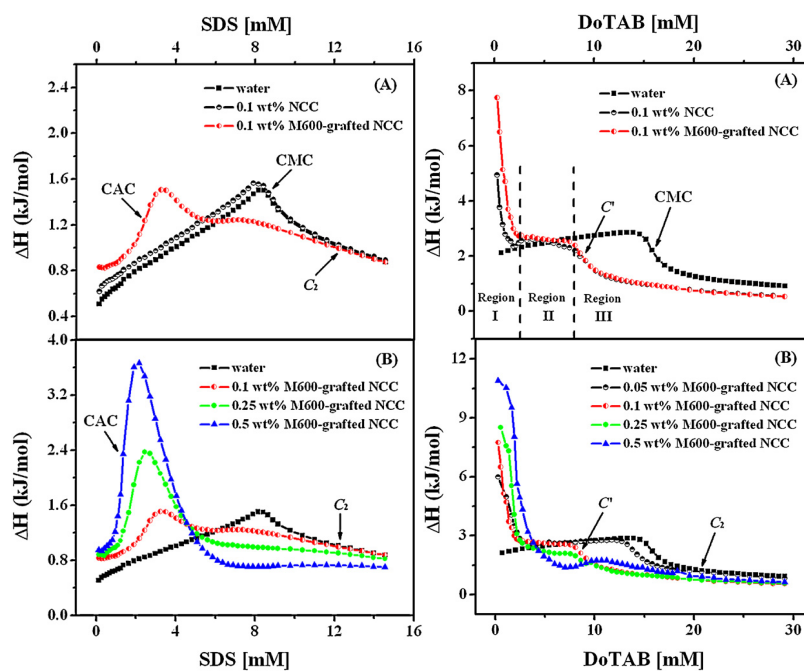
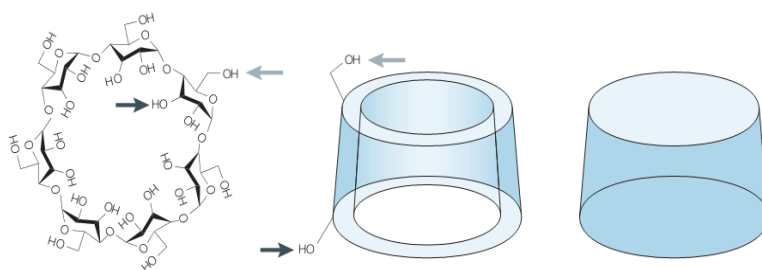


Figure 2.15 Calorimetric titration curves of SDS into CNC or M600-CNC suspensions (left); Calorimetric titration curves of DoTAB into CNC or M600-CNC suspensions (right). ¹²⁹

2.4 Cyclodextrin and Cyclodextrin Polymers

2.4.1 Structure and properties

Cyclodextrins are cyclic oligosaccharides composed of six, seven or eight α -D-glucose units linked by α -(1,4) bonds, which are called α , β and γ -cyclodextrin respectively. Cyclodextrins can be produced by intramolecular transglycosylation reaction from starch degradation by cyclodextrin glucanotransferase (CGTase) enzyme¹³⁰. The very first cyclodextrins were discovered and reported in 1891⁶, when nothing was known about the structure of these crystalline materials obtained from starch digest of *Bacillus amylobacter*. Several years later, Schardinger was able to isolate a new organism that can produce acetone and ethyl alcohol from starch-containing plants, as well as large amount of crystalline dextrans. He named the isolated two dextrans 'crystallised dextrin α ' and 'crystallised dextrin β '.¹³¹ But the structure of these dextrans were still unknown until 1942 by X-ray crystallography.¹³² In 1948, the ability of these cyclodextrins to form inclusion complex was recognized and it attracted a wide range of attentions.



Scheme 2.3 Chemical structure of β -cyclodextrin.

In cyclodextrins, the secondary hydroxyl groups (C_2 and C_3) are located on the wider edge of glucose ring and primary hydroxyl groups (C_6) are on the narrower edge, while inside of the ring are hydrogens of C_5 and ether-like oxygens on the bridge. This kind of structure results in molecules comprising of a hydrophilic exterior and hydrophobic interior, forming a micro heterogeneous environment to form inclusion complex with one or more hydrophobic molecules that can then dissolve in water (Figure 2.16).¹³³

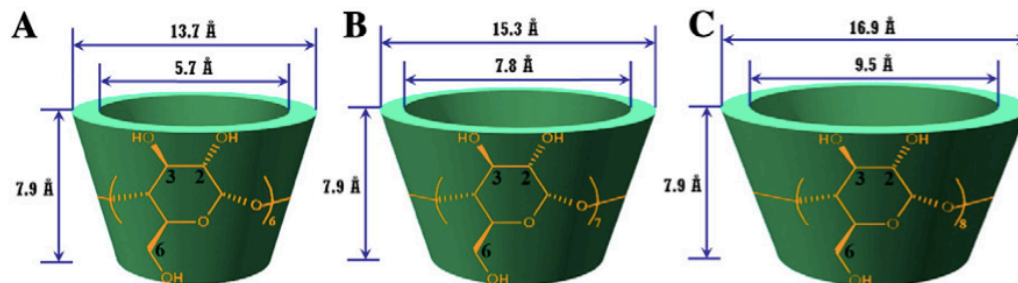


Figure 2.16 Chemical structure of α , β and γ cyclodextrins (left to right).

The properties of the three major kinds of cyclodextrins are α , β and γ cyclodextrins are summarized in Table 2.2¹³⁴. β -cyclodextrin is the most widely available, lowest-priced, mostly widely studied and also turned out to be the most useful. β -cyclodextrin is found to be less irritating than α -cyclodextrin after injection. It can bind with cholesterol and very small amount is absorbed by upper intestinal tract in the absence of metabolism. Metabolism by bacteria can only be found in caecum and colon. These facts also make β -cyclodextrin the most commonly used system in pharmaceutical and health care formulations.

Property	α -cyclodextrin	β -cyclodextrin	γ -cyclodextrin
Number of glucopyranose units	6	7	8
Molecular weight (g/mol)	972	1135	1297
Solubility in water at 25°C (% w/v)	14.5	1.85	23.2
Outer diameter (Å)	14.6	15.4	17.5
Cavity diameter (Å)	4.7-5.3	6.0-6.5	7.5-8.3
Height of torus (Å)	7.9	7.9	7.9
Hydrate water molecules	2	6	8.8

Table 2.2 Properties of cyclodextrins.

Aside from naturally generated or enzyme degraded cyclodextrins, modified cyclodextrins are also widely produced and studied. Usually, aminations, esterifications and etherifications of primary and secondary hydroxyl groups are used to produce CD with varying solubility.

2.4.2 Inclusion complex formation and characterization

The most notable property of cyclodextrins is its ability to form inclusion complex with a wide range of gas, liquid or solid compounds, such as straight or branched chain aliphatics, aldehydes, ketones, alcohols, organic acids, fatty acids, aromatics, gases and polar compounds such as halogens, oxyacids and amines, etc.¹³⁵ The ability of complexation can be explained by their special torus structures described above, relying on a dimensional fit between host and guest molecules. The hydrophobic cavity of cyclodextrin comprised of a microenvironment that only molecules with properly sized non-polar groups can enter to form a stable complex.¹³⁶ Thus, the ability of forming inclusion complex varies between cyclodextrin families. For α -cyclodextrins, only molecules with low molecular weight or with aliphatic side chains can insert into the cavity. For β -cyclodextrin, molecules with aromatic and heterocyclic moieties are preferred to form inclusion complexes, while γ -cyclodextrin has the same preference but with a ability of including larger molecules with macrocycles due to a larger cavity size.

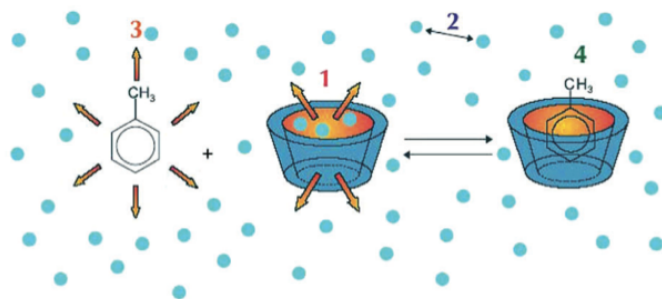


Figure 2.17 Formation of inclusion complex

Another important factor is thermodynamic interactions between host and guest molecules¹³⁷. Formation of inclusion complex does not break nor form covalent bonds, and it is a dynamic equilibrium process.⁶

A typical inclusion complex formation process involves several stages (Figure 2.17): 1. Polar water molecules are displaced from the non-polar CD cavity; 2. Displaced water returns to the bulk and form increasing numbers of hydrogen bonds; 3. Repulsion interaction between the hydrophobic guest molecule and the aqueous environment is reduced; 4. Guest molecules inserts itself into the non-polar CD cavity through increased hydrophobic interaction and forms hydrogen bonds.⁶ Inclusion complex can be formed in solution or in crystalline state. Water is commonly used as solvent, while co-solvent or non-aqueous solvent can also be used.

Methods for preparing inclusion complex include kneading, co-precipitation and freeze-drying. In

kneading method, only small amount of water is used to produce a cyclodextrin slurry. Then liquid or dissolved guest molecules are kneaded with this slurry in a mortar, followed by drying. This method is useful for poorly water-soluble guest molecules that dissolve slowly with the formation of inclusion complex. Though the yield is very good but kneading is not suitable for large-scale preparations. Coprecipitation means that guest molecules in organic solution is mixed with cyclodextrin aqueous solution, then upon heating and cooling, inclusion complex will precipitate as microcrystalline powder. This method is very useful for water-insoluble guest molecules. However, the yield is relatively poor due to the inhibition of competitive organic solvent inclusion. It is also not suitable for large-scale preparation since the cooling process is very time consuming. Freeze-dry is a very efficient method for preparing inclusion complex of water-soluble molecules. The powdered products usually have a very good yield and it is possible to scaled-up the procedure.¹³⁸

Cyclodextrin inclusion complex formation can be characterized by Infra-red (IR) spectroscopy. This technique is used to estimate the interaction between host and guest molecule in solid state.¹³⁹ Inclusion complex formation can be determined from band shift of guest molecules. However, bands assigned to the included part of guest molecules often overlap with specific bands of cyclodextrin when the fraction of guest molecules in inclusion complex is less than 25%.^{140,141} Thus the limitation of using IR is that guest molecules having some characteristic bands like carbonyl or sulfonyl groups.^{142,143} It has been observed that broken hydrogen bonding due to inclusion complex formation results in the shift of absorbance band to a higher frequency, while deformation vibration bands were less sensitive to hydrogen bonding, which result in small decrease in the frequency.¹⁴⁴ X-ray diffraction is used to detect changes in the diffraction pattern and crystalline nature of drug after it is included in cyclodextrin cavity. Sharpening of existing peaks, appearance of new peaks and shift of certain peaks all provide information on the inclusion complex formation.^{145,146} On the other hand, included molecules may result in an amorphous complex that result in the disappearance of certain peaks, less sharpen peaks compared with physical mixture of host and guest molecules.^{147,148} Differential scanning calorimetry (DSC) is a thermo-analytical method that is used to determine whether there are any structural changes of guest molecules taking place before the degradation of host cyclodextrin. Guest molecules may be evaporating, melting, decomposing, oxidating or changing polymorphic structure after included in cyclodextrin cavity. These changes all indicate the formation of inclusion complex. Usually, cyclodextrin have the influence on guest molecules suggested by the broadening, shifting, appearance or disappearance of peaks in DSC graph. However, if the interactions between host and guest molecules are very weak, shift of endothermic peaks is very hard to observe.

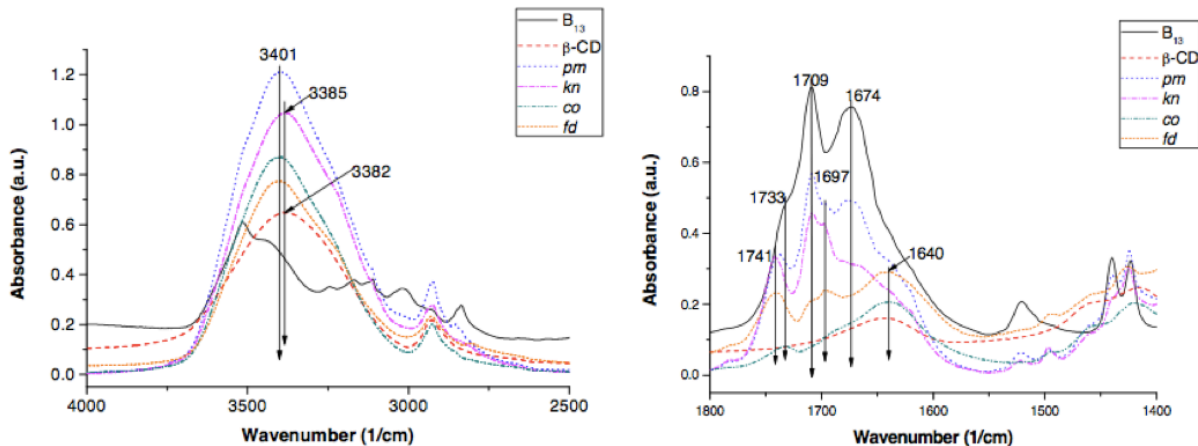


Figure 2.18 FTIR spectrum of cyclodextrin, orotic acid and their inclusion complex by kneading, co-precipitation and freeze-dried methods. ¹³⁸

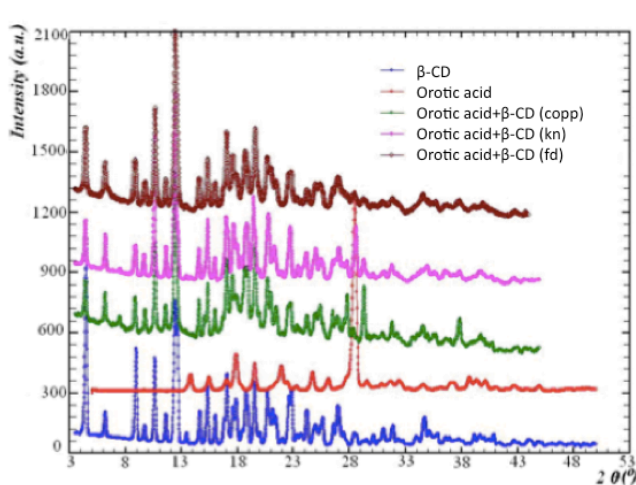


Figure 2.19 X-ray diffraction spectrum of cyclodextrin, orotic acid and their inclusion complex by kneading, co-precipitation and freeze-dried methods. ¹³⁸

As an example, inclusion complex of β -cyclodextrin and orotic acid was characterized by using FTIR (Figure 2.18), X-ray diffraction (Figure 2.19) and DSC (Figure 2.20). In FTIR spectrum, diminished C=O, C=C stretching peaks at 1709, 1674 cm^{-1} and shifted N-H deformation peaks indicate formation of hydrogen bonding between orotic acid and cyclodextrin. X-ray diffraction pattern shows different crystalline/amorphous ratios between samples due to different crystallization processes. Thermogram from DSC shows specific degradation curve of β -cyclodextrin compared with those of inclusion complex. A decrease in the dehydration endothermic peak of cyclodextrin as well as gradually disappearing melting

peak of orotic acid were observed, which also indicates that the preparing method determines the structural information of the inclusion complex.¹³⁸

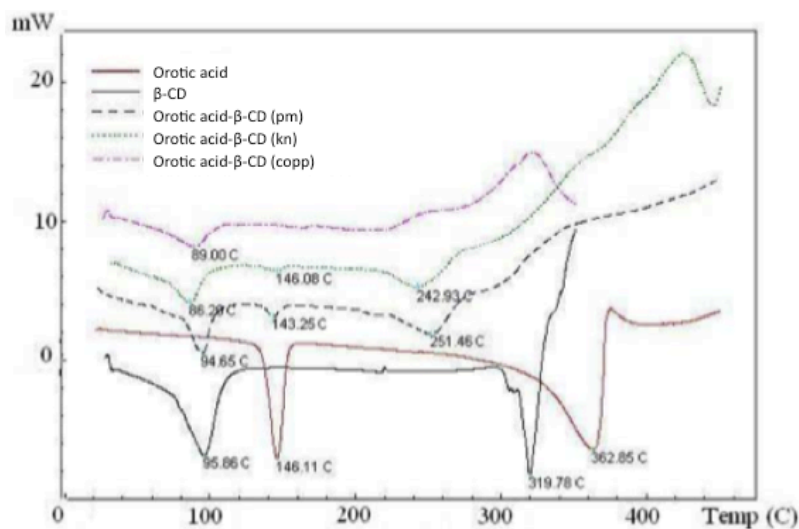


Figure 2.20 DSC spectrum of cyclodextrin, orotic acid and their inclusion complex by kneading, co-precipitation and freeze-dried methods.¹³⁸

2.4.3 Interaction between cyclodextrin and surfactants

Most of surfactant molecules are expected to form inclusion complexes with cyclodextrins by the inclusion of hydrophobic tail into the non-polar cavity. This behavior will possibly have an influence on both the process of micellization and the structure of micelles. Studies on the inclusion complex between cyclodextrin and surfactant have been a subject of interest since the behaviors of these systems can be used to mimic the effect of cyclodextrins on cell membrane, which is mainly consisted of phospholipids.^{145,149} Efforts are required to understand the biophysical, physicochemical properties and behavior of surfactants and cyclodextrins in bulk and on the surface. A number of researches have focused on the effects of cyclodextrin on the CMC and micellization process in aqueous solution, the thermodynamics of inclusion process, and the micro/macrostructure of inclusion complex upon addition of cyclodextrin.

Inclusion complex of surfactants and cyclodextrins and the formation process can be measured using various techniques, such as surface tensiometer, ITC, electromotive force (EMF), conductivity, NMR, fluorescence, etc. Dharmawardana et al.¹⁵⁰ used surface tensiometer to determine the binding constants of β-cyclodextrin and three ionic surfactants, SDS, cetylpyridinium chloride (CPC), and

cetyltrimethylammonium bromide (CTAB) in water. They observed that upon the addition of β -cyclodextrin, the surface tension of surfactant solution increased monotonically. When the amount of β -cyclodextrin was in excess of the surfactant concentration, the surface tension was close to that of pure water, indicating that none of β -cyclodextrin and inclusion complex were surface-active (Figure 2.21).

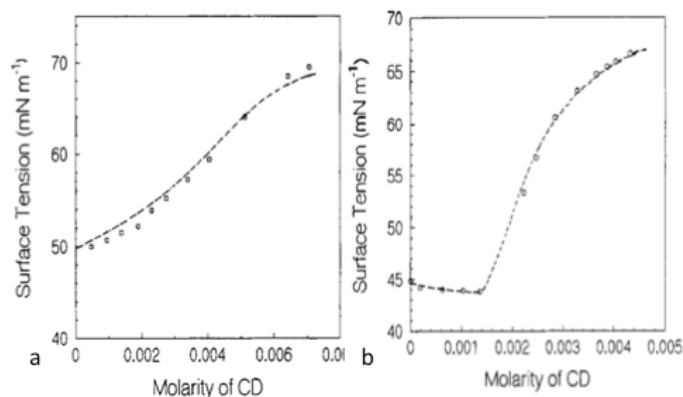


Figure 2.21 Surface tension result of SDS (a) and CPC (b) solutions containing 5.08 mM SDS and 2.00 mM CPC respectively upon addition of β -cyclodextrin.¹⁵⁰

Electromotive force measurement was used to determine the association constant and stoichiometry of inclusion complex of cyclodextrin and surfactant using a surfactant selective electrode. The electrode directly measures the concentration of surfactant monomers in solution in the presence or absence of additives. The information is then used to calculate inclusion complex equilibrium constants and determine the stoichiometry of the system. Rafati et al.¹⁵¹ constructed two kinds of ion selective electrode, membrane ion selective electrode and coating wire ion selective electrode, to investigate the behavior of tetradecyltrimethylammonium bromide (TTAB) and β -cyclodextrin inclusion complexes. They confirmed the formation of inclusion complexes corresponding with a 1:1 and 1:2 ratios of TTAB and β -cyclodextrin in the complex, and the thermodynamic parameters were then determined.

Isothermal titration calorimetry (ITC) is another powerful technique that measures the heat changes during titration to characterize the interaction between molecules. Dai et al.⁴² observed the behavior between poly(ethylene glycol) (PEG) and SDS using this technique, where the polymer saturation concentration, free SDS micelle formation concentration and most importantly, the critical aggregation concentration (CAC) were determined. And they were also able to investigate the influence of PEG molecular weights on these critical concentrations. ITC has also been widely used to characterize cyclodextrin-surfactant inclusion complex systems. Brocos et al. pointed out that even though β -

cyclodextrin-SDS system is by far the most studied system, the binding constant K determined using various techniques by different research groups varied over a large range of values (Table 2.3)¹⁵². One of the possible explanations for this inconsistency is the effect of non-inclusion complexes and cyclodextrin-induced aggregation. It was confirmed by conductivity and fluorescence methods: β -cyclodextrin-SDS inclusion complex serves as a hydrophobic source that further induces aggregation of SDS monomers upon titration. According to different reports, the critical aggregation concentration of SDS in the presence of β -cyclodextrin is between 0.8 to 6mM.^{153 154} Another explanation is the solvent influence and the technique sensitivity. Mwakibete et al. divided the available experimental techniques into two categories according to direct or indirect measurements of system compositions. They also pointed out that ITC is an exception to this rule, due to the fact that it is a technique specially designed to measure thermodynamic parameters and subsequently provide binding constants.¹⁵⁵

Inclusion complex of cyclodextrins and SDS were studied in detail by Brocos et al. using ITC¹⁵² From the ITC analysis combined with molecular dynamic simulations, they were able to plot the concentration of free β -cyclodextrin, free SDS, β -cyclodextrin : SDS = 1:1 complexes, β -cyclodextrin : SDS = 2:1 complexes as a function of molar ratio between SDS and β -cyclodextrin (Figure 2.22). These results are strong evidences indicating the dependence of 1:1 and 1:2 complexes concentration on the SDS and β -cyclodextrin molar ratio. Also, they suggested that interaction between SDS and cyclodextrin with a smaller cavity is mostly exothermic due to the preference of forming 1:2 inclusion complex, meanwhile cyclodextrin with larger cavity sizes mainly have positive heat changes when interacting with SDS because of the formation of 2:1 inclusion complexes and the electrostatic repulsion between two anionic SDS heads.

Cyclodextrin cross-linked polymers were synthesized originally for the column in separation chromatography. However, in the 1980s, studies were conducted on applying these materials in pharmaceuticals as drug-delivering polymer networks¹⁵⁶. The solubility of CD cross-linked polymer is largely dependant on the degree of cross-linking. As for the structure shown in Figure 2.23(A), only a small portion of CDs is bridged to each other. This polymer has even higher solubility than pristine CDs due to the modification, especially in the case of beta-CD. Solution of CD polymer with low cross-linking degree has very good stability and is suitable for use as solubilizers for guest molecules. Another type is highly cross-linked CD polymer. This polymer is not soluble in any solvent, but is very hydrophilic and has a good swelling property in water. Both of these two polymers can be used as drug delivery vehicles.¹⁵⁷

Table 2.3 Thermodynamic data for the formation of β -cyclodextrin-SDS inclusion complexes.¹⁵²

$10^{-3}K_{11}$ (M^{-1})	$10^{-3}K_{21}$ (M^{-1})	$10^{-3}K_{12}$ (M^{-1})	technique
0.453 ± 0.006^g			surface tension
23.0 ± 0.5^c			reaction kinetics ^o
49 ± 26^8			¹ H NMR spectroscopy ^m
0.294 ± 0.013^c			static conductivity
24.5^c			¹ H NMR spectroscopy ^m
3.021 ± 0.098^c			capillary electrophoresis ^r
			group II techniques ^b
25.6	0.22 ± 0.09		spectral displacement ^{s,t}
19 ± 1^c			spectral displacement ^{s,u}
18.5 ± 0.3^c			spectral displacement ^{s,v}
21	0.21		emf ^w
			ITC ^{x,y}
9.6 ± 0.5^c			spectral displacement ^{s,z}
$15 \pm 2^{c,\alpha}$			spectral displacement ^{s,\beta}
26.8 ± 2.5^z	0.44 ± 0.09^z		spectral displacement ^{s,\delta}
1.55^e		0.795^e	ITC ^e
8.15 ± 0.40^p			ITC ^y
48^q	0.21^q		capillary electrophoresis ^{op}
$18.0 \pm 5.0^{z,\lambda}$			spectral displacement ^{s,\mu}
18.2 ± 0.4^z	0.64^z		spectral displacement ^{s,\theta}
6.3^p			ITC ^{\alpha,\tau}
23.0 ± 0.8^c			ITC ^{\omega}
6.95^c			ITC ^{\psi}
20.8 ± 0.1	0.77 ± 0.03		ITC ^{\psi}

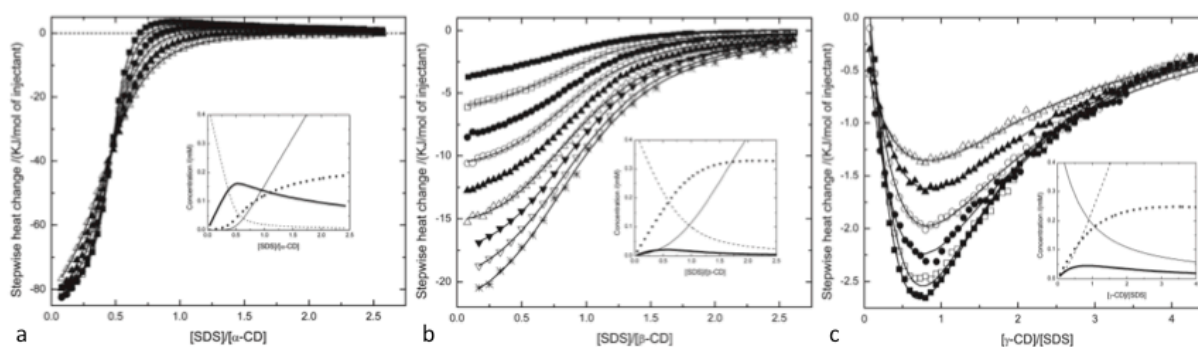


Figure 2.22 Integrated heat change per mole of injectant versus [cyclodextrin]/[SDS] molar ratio. Insert: concentration of free cyclodextrin (dashed thin line), free SDS (solid thin line), CD:SDS=1:1 complexes (dotted thin line), CD:SDS=2:1 complexes (solid thick line) as a function of [SDS]/[CD] ratio. ¹⁵²

2.4.4 Cyclodextrin grafted polymers

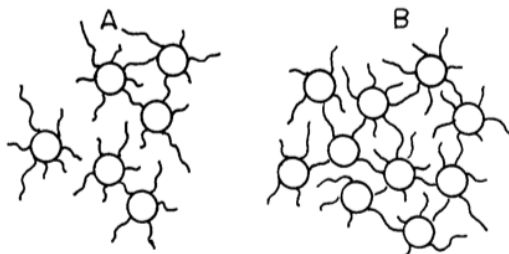


Figure 2.23 A) Cyclodextrin polymer with low cross-linking degree; B) Cyclodextrin polymer with high cross-linking degree

One of the most commonly used approaches to prepare CD cross-linked polymers is using bifunctional epichlorohydrin (EPI) as cross-linker to polycondense CDs in alkaline solution. Several studies reported the use of such kind of polymer networks to incorporate water-insoluble or poorly soluble drug molecules.^{158–160} In the study by Pinzauti *et al.*¹⁶⁰, both soluble and insoluble CD-EPI polymers were grounded with naproxen to enhance the solubility of the drug. It was found that both polymers were more effective than pristine CD or its hydroxyalkyl-derivatives in improving drug solubility to as high as 30 times. The solubility of CD polymers mainly determined the drug crystallinity in the final drug-carrier formulations. Rodriguez-Perez *et al.*¹⁵⁸ synthesized hydrogels from various CD derivatives and discussed their complexation capability towards estradiol. They found that pristine CD and anionic CD-derivatives are not suitable for hydrogel preparation via cross-linking, while hydrogels produced from hydroxypropyl- β -CD and methyl- β -CD exhibited very high swelling ratio in water and were able to load up 500 times more estradiol than the amount of free drugs dissolved in aqueous phase. These hydrogels also displayed sustained release of estradiol up to one week, depending on the affinity of drug towards different CD-derivatives. CD polymers were also used in composition materials as bone substitutes to deliver antibiotics locally. Martel *et al.*¹⁵⁹ incorporate pristine CD and CD polymers with hydroxyapatite (HA) by thermal fixation processing. Two model drugs ciprofloxacin and vancomycin were loaded. Although a burst release was observed in CD polymer-impregnated HA but not in pristine CD-HA, the former showed a prolonged antibacterial activity towards *S. aureus* and higher cytocompatibility to osteoblasts.

Cyclodextrins can also be conjugated onto other polymers in order to tailor the solubility, mechanical properties or morphologies using EPI, diepoxide or diisocyanate as cross-linking agents. CDs were covalently bonded to water-soluble polymers, such as poly(vinyl alcohol), poly(acrylic acid), poly(N-isopropylacrylamide), hydroxypropyl methylcellulose, etc.¹⁶¹ CD-containing polymers are able to deliver

drugs by forming inclusion complex with CD, directly conjugate drugs onto the polymer or loading drugs by hydrophobic interactions. Beta-CD functionalized hyperbranched polyglycerol (HPG) was synthesized by the reaction of amine and mono-tosylated beta-CD.¹⁶² Then insulin-loaded HPG-CD was prepared under mild conditions. Studies showed that these drug-loading NPs possessed a high loading capability and good biocompatibility. Due to the ability of CDs to enhance nasal adsorption of drugs by hampering enzymatic degradation, and the positive charge presenting on the surface^{163,164}, HPG-CD was able to enhance the nasal absorption of insulin by transporting it across the nasal barrier. Conjugation of drug molecules on CD-containing polymers is another effective way to protect drugs from degradation while delivering agents for various applications. Tang *et al.*¹⁶⁵ synthesized polyethylenimine-cyclodextrin-tegafur as pro-drug which can be co-delivered with enhanced green fluorescent protein reporter plasmid DNA. With a size of approximately 150 nm after condensing plasmid DNA and positive surface charge, this PEI-CD-tegafur NP is favourable for endocytosis delivery of therapeutic genes.

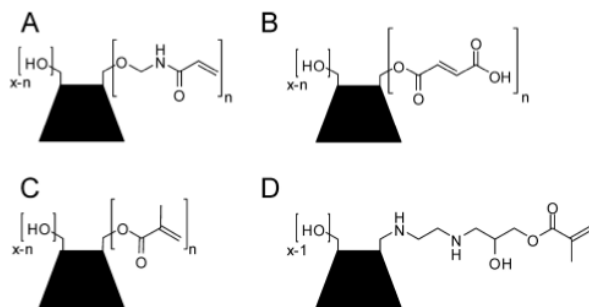


Figure 2.24 Polymerizable CD monomers. A) acrylamidomethyl-CD; B) maleic anhydride modified CD; C) methacryloyl-CD; D) mono-substituted vinyl CD.¹⁶⁶

Another approach to synthesize CD-contained polymers is copolymerization of above-mentioned polymers with polymerizable CD monomers, such as vinyl- or acryloyl-modified CDs (Figure 2.24). CD-containing-PAA hydrogel was synthesized by free radical polymerization of acrylamidomethyl-CD and N,N'-methylene-bis(acrylamide) as both delivery system for both hydrophilic and hydrophobic drugs.¹⁶⁶ Nanoparticles can also be functionalized with targeting ligands, such as galactose for hepatocyte, transferrin for cancer cell or antibodies, by forming ligand-coupled adamantane and CD complexations.^{167,168}

2.4.5 Application of cyclodextrin in personal care products

2.4.5.1 Enhanced stability

Forming inclusion complex within the cavity of cyclodextrin can protect certain guest molecules from light degradation or oxidation. Tea tree oil is a natural antimicrobial agent. Even though the pure oil can remain stable in the absence of light and oxygen for months, one of the essences, terpene, is very sensitive to these factors. Light or oxygen degradation can convert terpene into a highly irritating compound, p-cymene. Test results by CycloChemBio showed that all of the three kinds of cyclodextrins can form inclusion complex with α -terpinene by freeze-dry method and protect it under heating treatment. After heating for 24 hours under 50°C and 6 hours under 100°C, Gas-Chromatography analysis showed that the amount of free α -terpinene quickly decreased while amount of p-cymene significantly increased (Figure 2.25a). But with the inclusion complex formation, degradation of α -terpinene slowed down. Considerable amount of α -terpinene still remained even after 144 hours under 50°C and 20 hours under 100°C. Among which, α -cyclodextrin turned out to be the most effective to protect α -terpinene from heat-degradation (Figure 2.25b).

Retinol is always used in topical anti-aging formulations to reduce wrinkles and help restoration of damaged tissues due to excess exposure to UV light. However, retinol undergoes chemical reactions in the presence of light and oxygen, which act as initiators in retinol degradation. Being included in cavity of cyclodextrin, both stability and solubility of retinol are highly enhanced, while toxicity of retinol to human cell is reduced (Figure 2.26).¹⁶⁹ Weisse et al.¹⁷⁰ further mixed cyclodextrin-vitamin A inclusion complex with PVA to form an aqueous gel, which significantly improved the amount of vitamin A that penetrates different layers of human skin while not going into the circulation system.

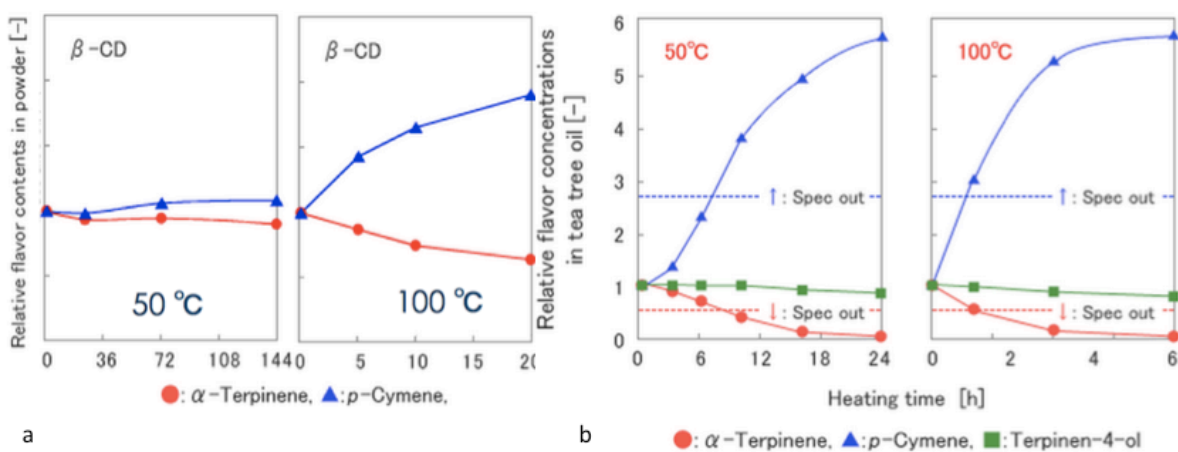


Figure 2.25 a) Effect of heat treatment at 50°C and 100°C on flavour content of tea tree oil; b) Effect of heat treatment at 50°C and 100°C on flavour content inclusion complex with β -cyclodextrin

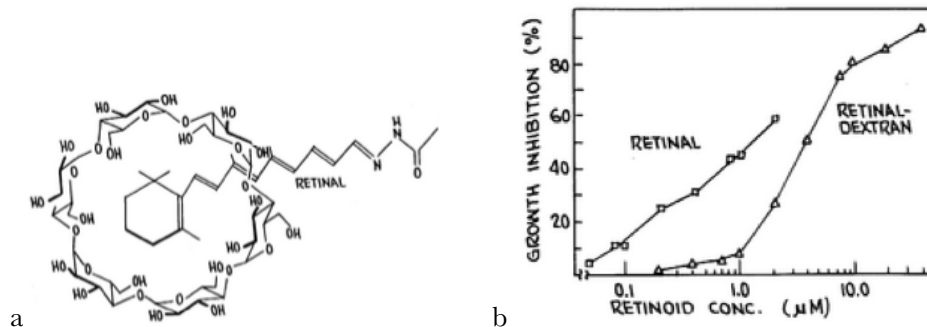


Figure 2.26 a) Structure of β -cyclodextrin-retinol inclusion complex. b) Toxicity of pure retinol and β -cyclodextrin-retinol inclusion complex. ¹⁶⁹

2.4.5.2 Increased solubility

Cyclodextrin's torus structure with a hydrophilic exterior and a hydrophobic interior enables enhancement of water solubility of guest molecules and further widen the range of applications. Fullerene is a non-polar molecule that has many promising properties. Inclusion complex of fullerene and cyclodextrin has been widely studied and mainly focused on γ -cyclodextrin due to its larger cavity. Even though cavity size of β -cyclodextrin is not large enough to fit fullerene and form inclusion complex, researches have been reported that β -cyclodextrins are able to form 2:1 complex with single fullerene molecule by using a mixed organic solvent system followed by stirring over a period of two weeks (Figure 2.25).¹⁷¹ Results showed that fullerene didn't intrude into the cavity completely but visible and accessible surface was increased by a factor of 8 compared with γ -cyclodextrin inclusion complex. These compounds have potential biomedical applications and toxicity problems were highly reduced compared with polymer-functionalized fullerene reported.

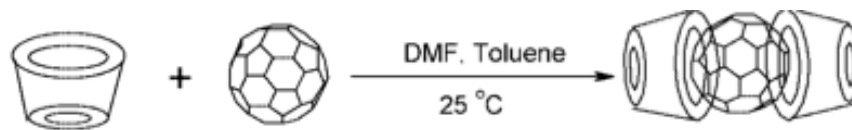


Figure 2.27 Synthesis of the β -cyclodextrin-fullerene inclusion complex. ¹⁷¹

A large portion of ingredients in personal care formulations is insoluble in water, such as vegetable oils, fatty acids and their esters, hydrocarbons, vitamins, hormones, antiseptics and preservatives, etc. All of these compounds can form inclusion complex with cyclodextrins. Not only the solubility of guest molecules is enhanced, but also irritating reactions are prevented due to a better homogeneity. Properties of antibacterial, keratolytic and disinfectant are improved in commercially available products

Bioclin Sebo Care Impure Skin Cream (Ganassini), menthol functioning products (Lipo Chemicals Inc.), Dexol A (Collaborative Laboratories), etc.¹³²

Cyclodextrins are also used to solubilize substances secreted by human skin. The skin fat forms complex with cyclodextrin and becomes soluble. Then they can be easily removed by water. Such kind of formulation can be found in the product named Gesichtstonic (Annemarie Börlind).

2.4.5.3 Elimination of malodours

The interaction of guest molecules with cyclodextrins produces a higher energy barrier for volatile guest molecules to evaporate, thus producing long-lasting fragrances. Cyclodextrin based compositions are also used to different formulations to reduce body odours such as perspiration control, dippers, as well as in dish washing and laundry detergent, fabric softener compositions. Meanwhile, cyclodextrins can also be added into formulations containing essential volatile compounds to reduce its unpleasant smell from the formulation while slowly releasing functional ingredients. This is the case in most of essential oil containing products.

2.5 Summary

In this chapter, a background on the applications of polymers for personal care application and the behaviors of polymer/surfactant system are comprehensively reviewed. Also, the chemical and physical properties of CNC and β -CD, their surface modification techniques and their interactions with surfactants are presented. Finally, the potential applications of CNC and β -CD in personal care products as viscosity modifier, delivery system, conditioning reagents, etc. are also described respectively. Based on this literature review, it can be concluded that the drawbacks of currently commercialized polymers can be resolved by the development of novel materials. And the applications of CNC and β -CD in personal care products are of great interest due to their advantageous properties. Thus, our objective is to design and characterize β -CD-functionalized CNC and investigate the behavior changes of this novel nanomaterial in surfactant solutions.

3 β -Cyclodextrin-Functionalized Cellulose Nanocrystals and Their Interactions with Amphiphilic Molecules

3.1 Introduction

Cellulose nanocrystals (CNC) are highly crystalline nanoparticles derived from the hydrolysis of native cellulose by acid treatment. From most cellulose sources, the particles are in rod-like crystalline morphology and are negatively charged when sulfuric acid is used in the hydrolysis process⁷⁴, yielding stable CNC dispersions². CNC as a biocompatible and sustainable nanomaterial has gained increasing interest from the scientific community. Their potential applications as nanocomposite additives, and in pharmaceuticals and personal care products stem from their attractive properties, such as high mechanical strength, large surface area, and unique optical properties.^{172,173}

Surfactants are widely used as emulsifiers and stabilizers in many formulations. Understanding the nature and characteristics of surfactant-polymer and surfactant-nanoparticle interactions is necessary to enhance the performance of many products.^{174,175} In the presence of polymers, surfactants tend to aggregate on the polymer chains due to electrostatic or hydrophobic attractions at the critical aggregation concentration (CAC). Polymer saturation by surfactant molecules and the formation of free surfactant micelles are described as C_s and C_m^* respectively. In a system comprising ionic surfactants and non-ionic polymers, such as sodium dodecyl sulfate (SDS) and poly(ethylene-oxide) (PEO), the temperature and the molecular weight of the polymer are two important parameters controlling the interaction characteristics^{42,176}. For oppositely charged surfactants and polymers, hydrophobic chain length, hydrophilic head groups and the ionic strength of the solvent have a significant influence on their interactions.^{177,178} Oppositely charged surfactants and polymers tend to be unstable and will phase separate due to the formation of large surfactant-polymer complexes. These structures either in bulk or at interfaces were thoroughly studied by Bain *et al.*¹⁷⁹

In order to incorporate CNC into surfactant solutions, it is vital to understand the behavior of CNC in the presence of surfactants due to its polyelectrolyte character. Interactions between CNC and anionic surfactants have been studied to improve the dispersability and stability of CNC in nonpolar solvents⁷⁷ and poly (lactic acid) solutions⁹⁹. Kim *et al.*¹⁰⁰ and Rojas *et al.*¹⁰¹ have used non-ionic surfactants to disperse CNC particles in polystyrene-based composites. The interaction between pristine CNC and the cationic surfactant tetradecyl trimethyl ammonium bromide (TTAB) has been reported by Dhar *et al.*¹²⁸ under various ionic strengths. They found that dispersion and phase separation were mainly

dominated by electrostatic interaction, polymer-induced micellization and hydrophobic interaction, while the addition of electrolyte weakened the electrostatic interaction by charge shielding. Interactions between thermo-responsive CNC and surfactants with identical alkyl chain but different charged head groups have also been investigated.¹²⁹ Non-ionic poly (ethylene glycol) dodecyl ether (Brij 30) and cationic dodecyl trimethyl ammonium bromide (DoTAB) have been found to have no significant interactions with pristine CNC, while polypropylene glycol grafted CNC induced aggregations of both anionic and cationic surfactants by hydrophobic and electrostatic interactions respectively.¹²⁹

β -cyclodextrin is a cyclic oligosaccharide composed of seven α -D-glucose units linked by α -(1,4) bonds. Because the primary and secondary hydroxyl groups are located on the exterior of the cyclic structure, the surface of β -cyclodextrin is hydrophilic while the interior is hydrophobic¹³⁰. Thus, non-polar molecules or compounds, are able to replace bound water molecules in the cavity of β -cyclodextrin to form inclusion complexes.⁶ Due to its unique property of forming host-guest inclusion complexes with varieties of non-polar molecules, β -cyclodextrin and its derivatives have been extensively studied and applied in medical, pharmaceutical, health and personal care products to enhance the water solubility, stability, bioavailability and biocompatibility of active reagents, or to eliminate undesirable component from solutions.^{131,180,181} Grafting of β -cyclodextrin enables the fixation of active reagent carriers on the surface of CNC, which imparts new properties and enriches its potential applications. However, since surfactants are amphiphilic molecules, most of them can form complexes with β -cyclodextrin by the inclusion of the hydrophobic segment in the non-polar cavity. Scamehorn *et al.*¹⁸² has reported that the surface tension of the ionic surfactants SDS and hexadecyl-trimethyl-ammonium bromide (CTAB) increased upon the addition of β -cyclodextrin, indicating the loss of the surface-activity of surfactant after the formation of the inclusion complex. Rafati *et al.*¹⁵¹ have studied the interaction between β -cyclodextrin and TTAB. The formation of the 1:1 and 1:2 TTAB/ β -cyclodextrin inclusion complex was reported and the thermodynamic parameters were calculated. , β -cyclodextrin induced surfactant aggregation has also been observed by Jiang *et al.* using fluorescent probes.¹⁵³

Since surface activity and micellization behavior of surfactants have been reported to be significantly influenced by β -cyclodextrin, a comprehensive understanding on the behavior of β -cyclodextrin grafted CNC in the presence of ionic and non-ionic surfactants will facilitate the use of such nanomaterials in pharmaceuticals and personal care products. In this paper, we report on the synthesis of β -cyclodextrin grafted CNC (CNC-CD) using cyanuric chloride as the cross-linker. The reaction conditions required to enhance the grafting of β -cyclodextrin are elucidated, and FTIR and UV are used to confirm the grafting. Interactions between CNC-CD and three surfactants were investigated by micro-

calorimetry, surface tensiometry, conductivity, and zeta potential measurement, and the physical mechanisms describing these interactions are proposed.

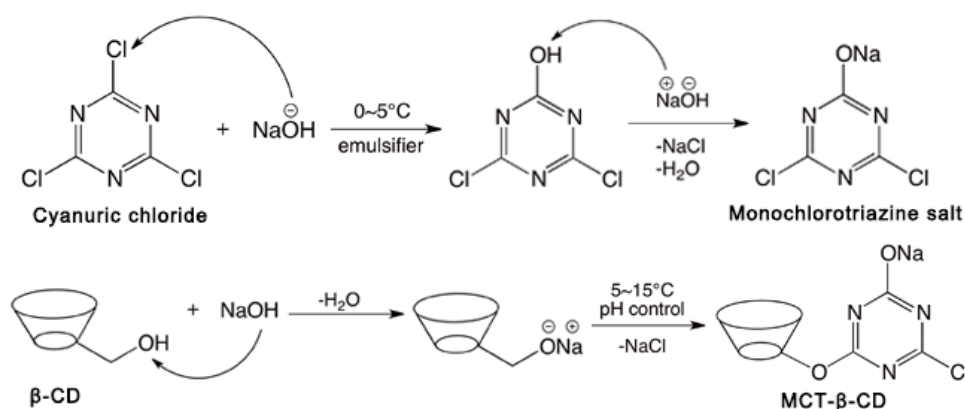
3.2 Experimental

3.2.1 Materials

Spray-dried cellulose nanocrystals (CNC) were supplied by CelluForce Inc. CNC suspensions were prepared by vigorous mixing using a 500W IKA T-25 homogenizer followed by sonication in a 700W 42kHz Branson sonication bath. Cyanuric chloride, β -cyclodextrin hydrate (99%), phenolphthalein, 4-octylphenol polyethoxylate under the trade name of Triton X-100 (TX-100), sodium dodecyl sulfate (SDS) (>99%), hexadecyl-trimethyl-ammonium bromide (CTAB) (>99%) were purchased from Sigma-Aldrich and used as received. Deionized Milipore water was used for all sample preparations.

3.2.2 Synthesis

The synthesis of monochlorotriazine- β -cyclodextrin (MCT- β -CD) was conducted according to the procedure reported by Yu *et al.*¹⁸³ A clear solution of dichlorotriazine sodium salt was obtained by dispersing cyanuric chloride in a NaOH solution in an ice bath for 1h. β -CD solution at pH 12 was then added to allow reaction with the dichlorotriazine at a temperature of about 10°C until the pH approached neutral. (Scheme 3.1) The MCT- β -CD was purified using acetone and DMF to desalt and precipitate repetitively. Finally the product was filtered and dried in a vacuum oven until a constant weight was achieved.



Scheme 3.1 Procedure for MCT- β -CD synthesis.

The optimum reaction conditions for the synthesis of β -cyclodextrin grafted cellulose nanocrystals (CNC-CD) to obtain a high β -cyclodextrin grafting ratio were determined. CNC concentration, sodium

bicarbonate content, heating temperature and time were all found to have an influence on the β -CD grafting ratio. In the optimized procedure, a 2 wt% suspension of CNC was first activated in 0.02 w/w NaCO_3 solution for 3h, followed by the addition of a varied amounts of MCT- β -CD at room temperature. The water content in the mixture was then reduced to around 10 wt% on a Heidolph Laborota 4011 rotating evaporator at 45°C. The grafting reaction was conducted by heating the concentrated mixture at 130°C for 5min. Un-reacted MCT- β -CD molecules were removed by dialysis against water over 2 weeks. CNC-CD in dimethyl sulfoxide (DMSO) was synthesized in 2 wt% CNC DMSO suspension under 80 °C for 24h with the similar molar ratios between reactants.

3.2.3 Spectroscopy

Ultraviolet absorbance of cyanuric chloride, CNC and CNC-CD was measured on a Varian (Carey 100 Bio) UV-visible spectrometer at room temperature. Transmittance was also measured on the same instrument at 600 nm. Fourier Transform IR (FTIR) spectra of samples in compressed KBr powder were obtained on a Bio-Rad (Excalibur series) FTIR spectrometer over scanning wavelengths of 400-4000 cm^{-1} .

3.2.4 Transmission electron microscopy (TEM)

TEM images were taken on a Philip CM10 electron microscopy to visualize the inclusion complex induced SDS aggregates on the surface of CNC-CD. The TEM samples were prepared by depositing one drop of 0.02 wt% suspension onto a carbon coated copper grid. Samples with surfactants were prepared by placing copper grids on a filter paper and excess liquid was removed by the filter paper, and the dried nanoparticles were retained for analysis.

3.2.5 Grafting ratio

The grafting ratio of β -CD was measured by the phenolphthalein (PHTH) inclusion method. Freshly prepared solution of 0.1mM PHTH in 0.02M NaCO_3 buffer was used for all the measurements. CNC-CD suspensions were mixed with PHTH, stirred and equilibrated overnight before measuring the absorbance of the solutions. Samples without PHTH were also prepared as blank controls. The amount of β -CD was determined by a calibration of $\log(\text{absorbance of PHTH}/\beta\text{-CD mixture})$ against $\log(\text{concentration of } \beta\text{-CD})$. Grafting ratio was then determined from the equation:

$$\text{Grafting ratio} = \frac{C(\beta\text{-CD})}{C(\text{CNC-CD})} \times 100\% \quad \text{Equation 3.1}$$

where $C(\beta\text{-CD})$ and $C(\text{CNC-CD})$ are weight concentrations of β -CD and CNC-CD in mg/ml,

respectively.

3.2.6 Surface tensiometry

Surface tension measurements were conducted on a DCAT 11 (Dataphysics) tensiometer. Continuous dosing was performed by a liquid dispensing unit (LDU) that is capable of dosing microliters of titrants. The Wilhelmy plate method was used to measure the dynamic surface tension at the air-water interface. 2 mM of TX-100, 30 mM of SDS were titrated into 40 mL of water, CNC and CNC-CD suspensions at 25°C respectively. 5 mM of CTAB was titrated into 40 mL of water, CNC and CNC-CD suspensions at 28°C. In this paper, the concentration of CNC, CNC-CD suspensions was 0.6 wt% for interactions with TX-100 and SDS, and 0.1 wt% for the interaction with CTAB.

3.2.7 Isothermal titration calorimetry (ITC)

The interactions between CNC, CNC-CD and surfactants were studied using a Microcal VP-ITC instrument. Stock solutions of 100 mM SDS, 5 mM TX-100 and 10 mM CTAB were prepared in advance and loaded into a 282 μ L syringe. CNC and CNC-CD suspensions with the concentrations described above were loaded in the 1.455 mL sample cell. The titrants were injected into the sample cell at pre-determined volumes of 1-10 μ L in each injection. The enthalpy change of the interactions were measured and reported in kJ/mol of injectant and plotted against surfactant concentration.

3.2.8 Zeta potential

Mixtures of surfactant and CNC or CNC-CD suspensions were prepared at selected surfactant concentrations described on the ITC thermograms. Zeta potential measurements were conducted in polystyrene cuvettes on a Malvern Zetasizer Nano ZS90. The samples were sonicated and measured without dilution. This method was used to determine the overall surface charge of CNC, CNC-CD samples in the presence of ionic surfactants.

3.2.9 Phase separation

Coacervation and phase separation behavior were observed and examined in CTAB/CNC and CTAB/CNC-CD samples. All samples were mixed and stabilized for 2 weeks prior to the measurements. The height of the flocculation column was normalised to the height of the total solution column with each sample for ease of comparison.

3.2.10 Conductivity

The conductivity measurements were performed on the Metrohm 809 Titrando System equipped with Tiamo software, which is able to dose microliters of titrant in each injection. All the measurements were conducted in a jacketed vessel with a stirring speed of 4. The same temperature and concentrations of surfactants and CNC, CNC-CD suspensions were used as in surface tension measurements. The conductivity was measured using a conductivity electrode.

3.3 Results and Discussion

3.3.1 UV-vis and FTIR

CNC-CDs synthesized in water and DMSO were characterized by UV-vis (Figure 3.1) and FTIR (Figure 3.2) spectroscopy. MCT- β -CD possessed a specific absorbance at 245 nm, and upon the substitution of the third chlorine atom, the change in the electron distribution on the triazine ring induced a blue-shift from 245 to 230 nm. Pristine CNC did not display any specific UV absorbance, and the observed absorbance without any peaks was attributed to scattering from the CNC nanorods.

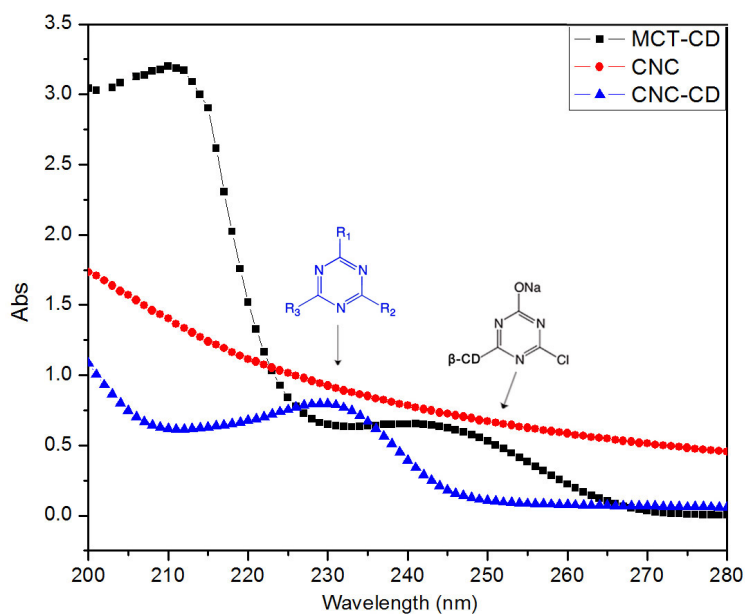
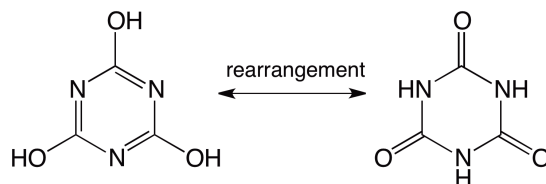


Figure 3.1 UV-vis spectra of MCT- β -CD, CNC and CNC-CD.

The FTIR spectra of cyanuric chloride and MCT- β -CD are compared in Figure 3.2, where the peaks centered at 1579 cm^{-1} and 1467 cm^{-1} were attributed to the triazine ring on the cyanuric chloride. The peaks between 1487 cm^{-1} and 868 cm^{-1} are the characteristic bands for β -CD molecules. And the new peak at 819 cm^{-1} is attributed to C-Cl bond that has red-shifted from 920 cm^{-1} due to the substitution of

chlorine atoms.¹⁸⁴

The spectra of CNC- β -CD (water) and CNC- β -CD (DMSO) both possessed new peaks at 1722 and 1770 cm^{-1} , which are attributed to C=O stretching from the rearrangement of triazine rings as shown in Scheme 3.2.¹⁸⁵



Scheme 3.2 Rearrangement of cyanuric acid in aqueous solution.¹⁸⁵

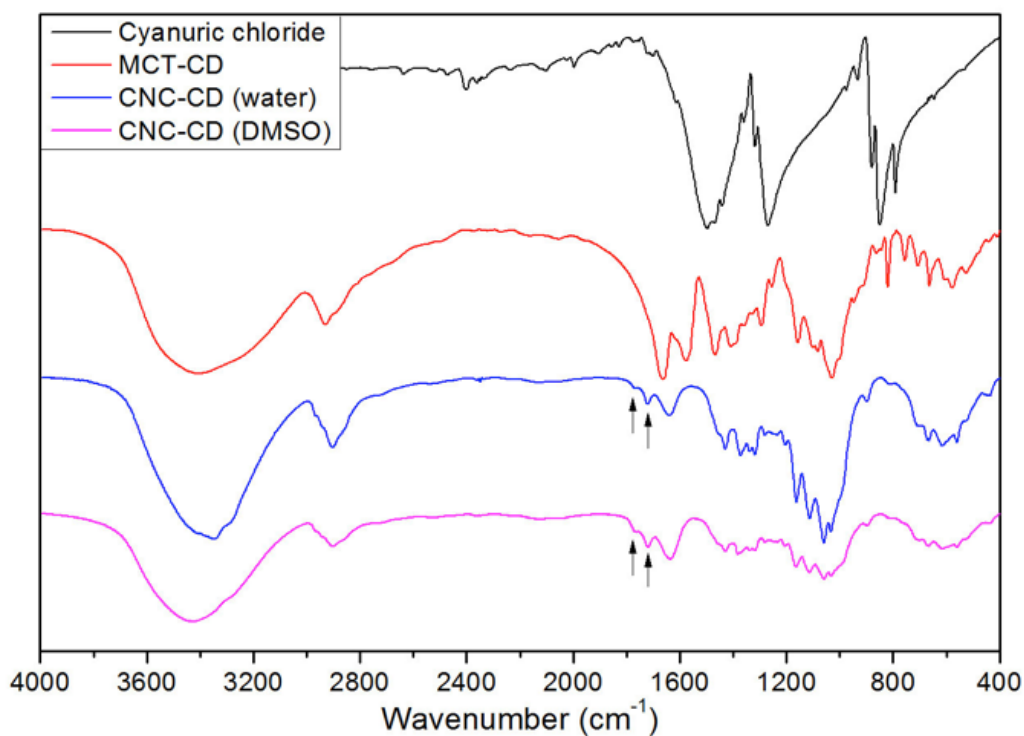


Figure 3.2 FTIR spectra of cyanuric chloride, MCT- β -CD, CNC-CDs synthesized in water and DMSO (top to bottom).

3.3.2 Grafting ratio of MCT- β -CD.

Phenolphthalein molecules deprotonate and form a 1:1 host-guest inclusion complex with β -CD above a pH of 8.2. Free PHTHs in the bulk phase possess a UV absorption peak at 552 nm, while those

forming an inclusion complex with β -CD no longer absorb at this wavelength. With the increasing β -CD concentration, the pink color of PHTH solutions gradually fades and the absorbance of PHTH solutions decreases proportionally, which yields a linear relationship between $\ln(\text{Abs of PHTH})$ and $\ln(\beta\text{-CD Concentration})$ (Figure 3.3, 3.4). Since pristine CNC is negatively charged due to sulfate groups on its surface, PHTH does not interact electrostatically with pristine CNC. The amounts of PHTH molecules included in the cavity of β -CD can thus be used to determine the weight percentage of β -CD in CNC-CD. The grafting ratio obtained from PHTH inclusion agreed with results obtained from elemental analysis. This method is also more efficient and convenient for determining the grafting ratio of β -CD since no filtration is required.

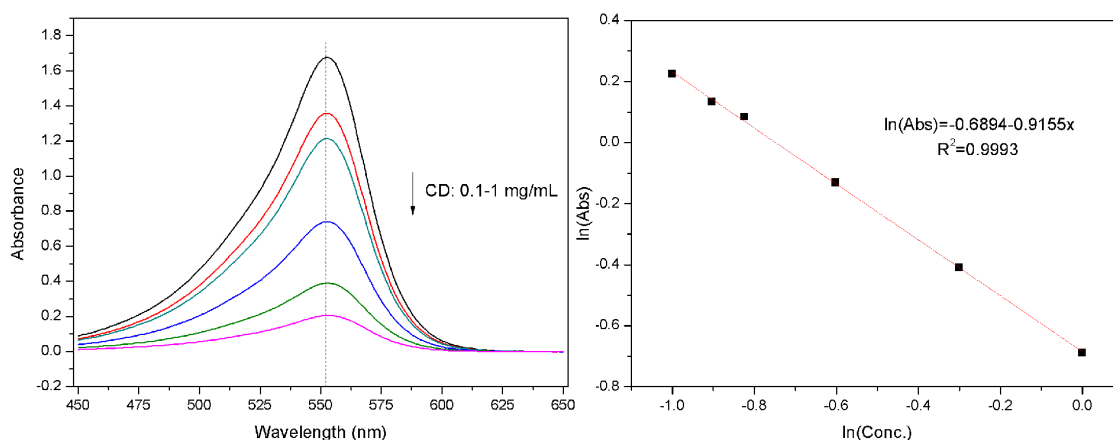


Figure 3.3 UV absorbance of PHTH/ β -CD solutions with increasing β -CD concentrations (left). Calibration curve of absorbance and β -CD concentration (right).



Figure 3.4 Phenolphthalein solutions with increasing β -CD concentration, where color faded from pink to colorless.

The grafting ratio of β -CD on CNC depends on the reaction conditions and the solvent

environment (Figure 3.5). For the reaction in water and DMSO, the average grafting ratios of β -CD were 3.32 and 4.92 wt%, respectively. The observed difference is related to the hydrolysis of chlorine atoms on MCT- β -CD, which reduced the reactivity with the hydroxyl groups on CNC. By reducing the water content in the reaction, β -CD grafting ratio was enhanced, but it was still lower than when using DMSO as the solvent, indicating that water content is critical in the reactions with cyanuric chloride.

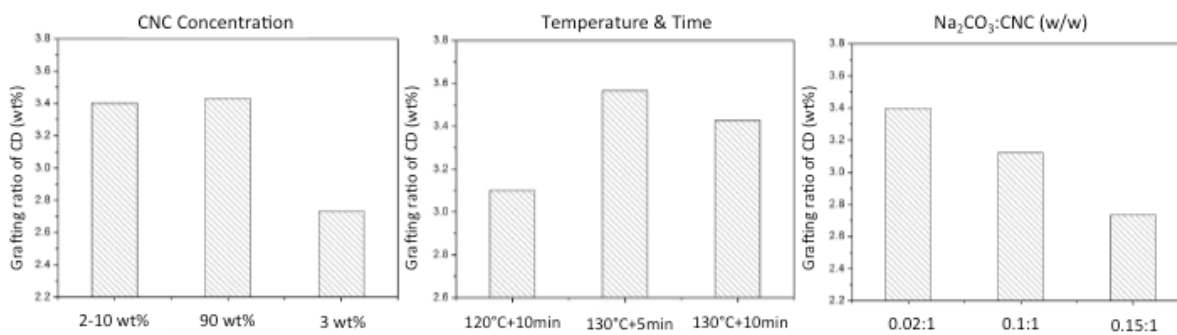


Figure 3.5 Impact of reaction conditions on the grafting ratio of β -CD: CNC concentration (left), temperature and time (middle), NaCO_3 : CNC ratio (right).

In addition to the impact of water, the hydrolysis of chlorine atoms on MCT- β -CD was affected by the concentration of sodium bicarbonate, reaction temperature and time. Sodium bicarbonate was used to scavenge hydrogen chloride (HCl) molecules generated from $-\text{Cl}$ substitution and the hydrolysis of $-\text{Cl}$ from the added base. The grafting ratio was enhanced by increasing the reaction temperature and reducing the heating time with an upper limit of 140°C , beyond which β -CD started to degrade and CNC began to discolour and become yellowish.

The reaction conditions for using cyanuric chloride as a linker to graft β -CD on CNC were optimized. In comparison to a previous study¹⁸⁶, where CNC was labeled with 5-(4,6-dichlorotriazinyl) aminofluorescein (5-DTAF), our grafting ratio was approximately 10^3 times ($29.7\mu\text{mol/g}$) better than 5-DTAF ($24\pm 1\text{ nmol/g}$) despite the molecular weight of β -CD being much larger than that of 5-DTAF.

3.3.3 Interactions with a non-ionic surfactant

Surface tension and enthalpy changes of a non-ionic surfactant, 4-octylphenol polyethoxylate (TX-100) in water, CD, CNC suspension and CNC-CD suspension were measured as a function of TX-100 concentration (6A). TX-100 possessed a critical micelle concentration (cmc) of 0.28 mM in water as determined from the inflexion point of surface tension and the first-order differential curve of the ITC

thermogram (Figure 3.7). The surface tension of TX-100 in a CNC suspension did not change much up to the inflexion point at 0.09 mM, where it started to decrease. This is attributed to the hydrophilic tail of TX-100 hydrogen bonding with the hydroxyl groups on the surface of CNC, while the hydrophobic domains remained surface active and partitioned to the air-water interface (Scheme 3.3-top left panel). Since CNC is much larger than TX-100 molecules, the interface became saturated much faster at a lower TX-100 concentration. The calculated surface area coverage was larger compared with TX-100 alone, signifying that the TX-100/CNC aggregates occupied a larger surface area at the air-water interface. However, the behavior of TX-100 in the CNC-CD suspension was different; the surface tension in CNC-CD decreased slower than in water, indicating a reduced surface activity of TX-100 at the same concentration. This can be explained by the hydrophobic segment of TX-100 forming a host-guest inclusion complex with β -CD, resulting in a loss in its surface activity by detachment from the interface and partitioning to the bulk solution (Scheme 3.3-top right panel). The identical cmc observed for TX-100 in water and CNC-CD is possibly due to a higher affinity of TX-100 monomers for the air-water interface than to β -CD.

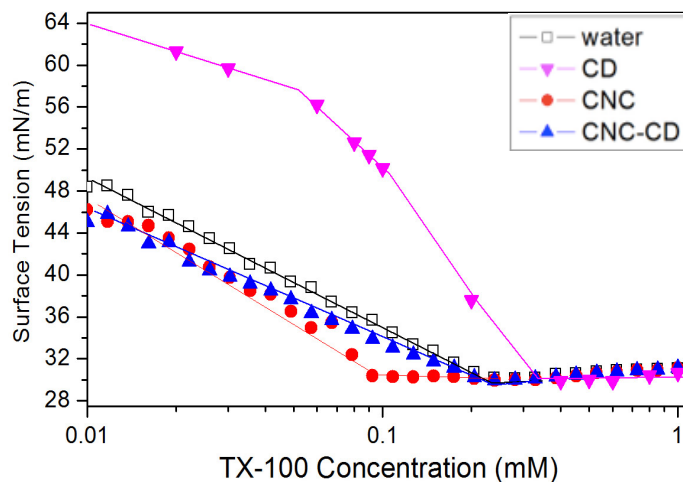


Figure 3.6 (A) Surface tension curves of water, 0.6 wt% CNC and 0.6 wt% CNC-CD suspensions with increasing TX-100 concentrations at 25°C.

From the calorimetric curves of TX-100 (Figure 3.7), the difference between titrations into water and into CNC suspension is negligible. However, the ITC thermograms of the TX-100/CNC-CD system revealed a large exothermic enthalpy change at very low TX-100 concentration, which was also observed in the TX-100/CD system. This confirmed the host-guest interaction between TX-100 and β -CD as postulated earlier from the surface tension data. The shift of the cmc to a higher value for both the CNC-

CD and β -CD were attributed to the inclusion complexation of TX-100 monomers and β -CD, thus more monomers were required to produce the micelles.

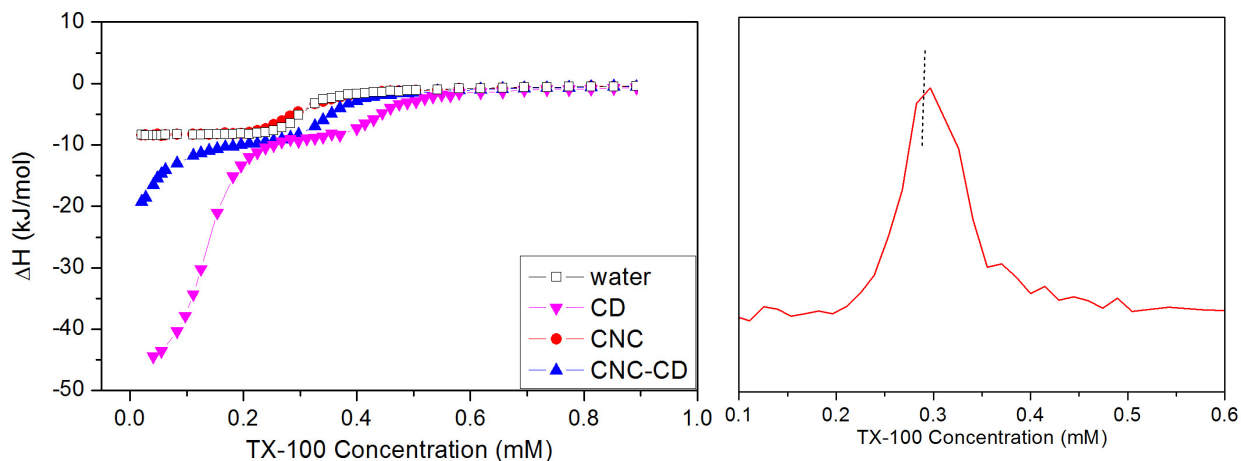


Figure 3.7 Thermograms from titrating TX-100 into water, 0.18 mM β -CD, 0.6 wt% CNC and 0.6 wt% CNC-CD suspensions at 25°C (left). First-order differential curve of TX-100 to water ITC thermogram (right).

3.3.4 Interactions with anionic surfactant

In the surface tension measurements (Figure 3.8A), the slopes ($dg/d\ln(c)$) (designated as Slope 1) prior to the cmc, the addition of SDS into water, CNC suspension and CNC-CD suspension were identical, and only Slope 2 for CNC-CD (after the cmc) was different. The valley in the surface tension curve is due to a trace contaminant arising from SDS synthesis or from hydrolytic reaction, which were frequently observed in studies on the surface activity of SDS. In the presence of the hydrophobic cavity of β -CD in the bulk phase, the removal of contaminants from the air-water interface was facilitated by the inclusion complexation phenomenon, resulting in a more rapid recovery of the surface tension for the CNC-CD system.

In the ITC thermogram from the SDS titration into CNC-CD, an exothermic interaction at low concentration was observed which was similar in trend to that of the titration into β -CD, which confirmed the inclusion activity of β -CD towards SDS monomers after it had been grafted on the CNC surface. In the concentration range of 7.4-10.8 mM, an obvious deviation in enthalpy change for the SDS/CNC-CD system was observed (Figure 3.8B). This exothermic interaction can likely be attributed to the inclusion complex induced aggregation of SDS.

To gain a clearer understanding of this interaction, transmittance and zeta potential were measured and compared with ITC results (Figure 3.9). The zeta potential of CNC-CD was less negative than pristine CNC due to the partial hydrolysis of sulfate groups during the grafting reaction. With increasing SDS concentration, CNC displayed a gradual increase in the zeta-potential, while CNC-CD showed an initial reduction up to Region II, then a slight increase at 10.8 mM. The formation of a host-guest complex between SDS and CNC-CD could be responsible for the drop in the zeta-potential due to the increased negative charge on CNC-CD. From transmittance measurements, SDS/CNC showed no obvious changes after the cmc, while CNC-CD became slightly cloudy in Region II, indicating the appearance of larger sized particles due to the agglomeration of SDS bound CNC-CD induced by hydrophobic interactions between free and partially bound C₁₂ alkyl chains (Scheme 3.3-middle right panel). In the photos taken under natural light, light scattering particles were evident in the SDS/CNC-CD samples of Region II and these disappeared at higher SDS concentration. The SDS/CNC samples remained translucent over the entire region (Figure 3.10). Conductivity measurements for the addition of SDS to CNC-CD also showed three regions (Figure 3.11). In Region II, a lower conductivity observed in the SDS/CNC-CD suspension suggested a reduced mobility of SDS monomers in the bulk due to the encapsulation of SDS monomers on β -CD grafted on CNC.

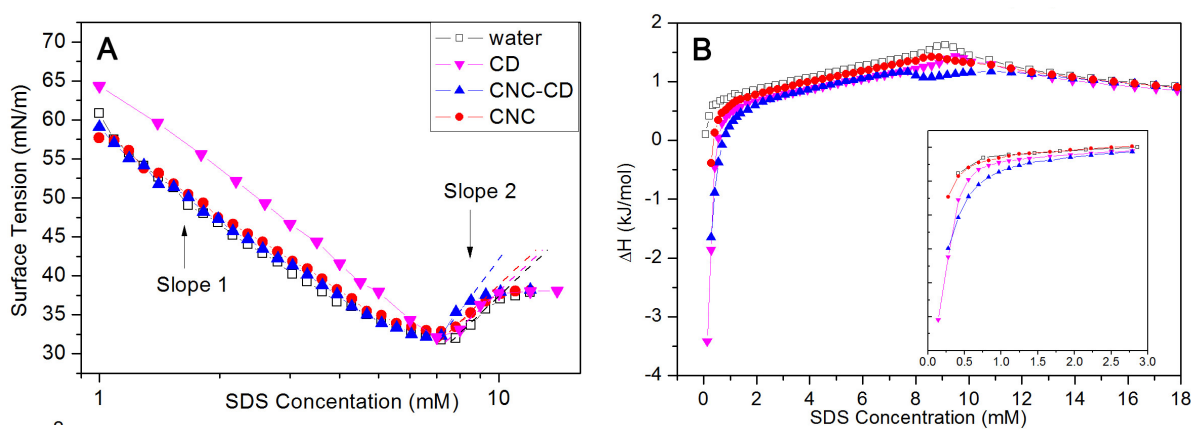
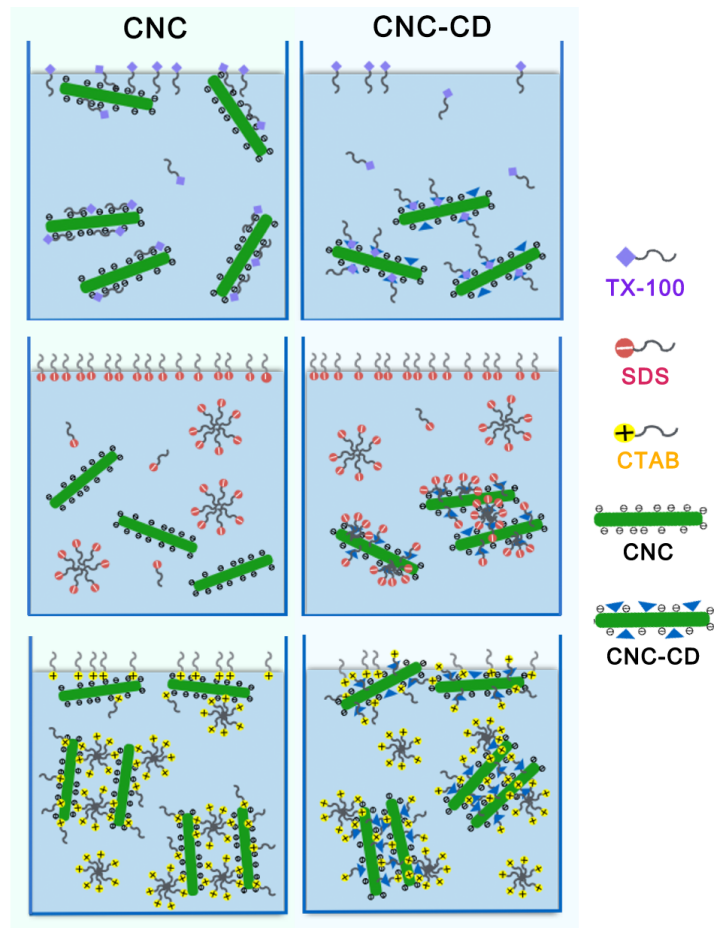


Figure 3.8 (A) Surface tension curves of water, 0.6 wt% CNC and 0.6 wt% CNC-CD suspensions with increasing SDS concentrations at 25°C. (B) Thermograms from titrating SDS into water, 0.18 mM β -CD, 0.6 wt% CNC and 0.6 wt% CNC-CD suspensions at 25°C. The insert is an enlargement of the region at low SDS concentration.



Scheme 3.3 Schematic diagrams describing the change in behavior of CNC-CD compared to CNC in differently charged surfactants. The concentration shown in the scheme is below the cmc for TX-100, and above the cmc for SDS and CTAB.

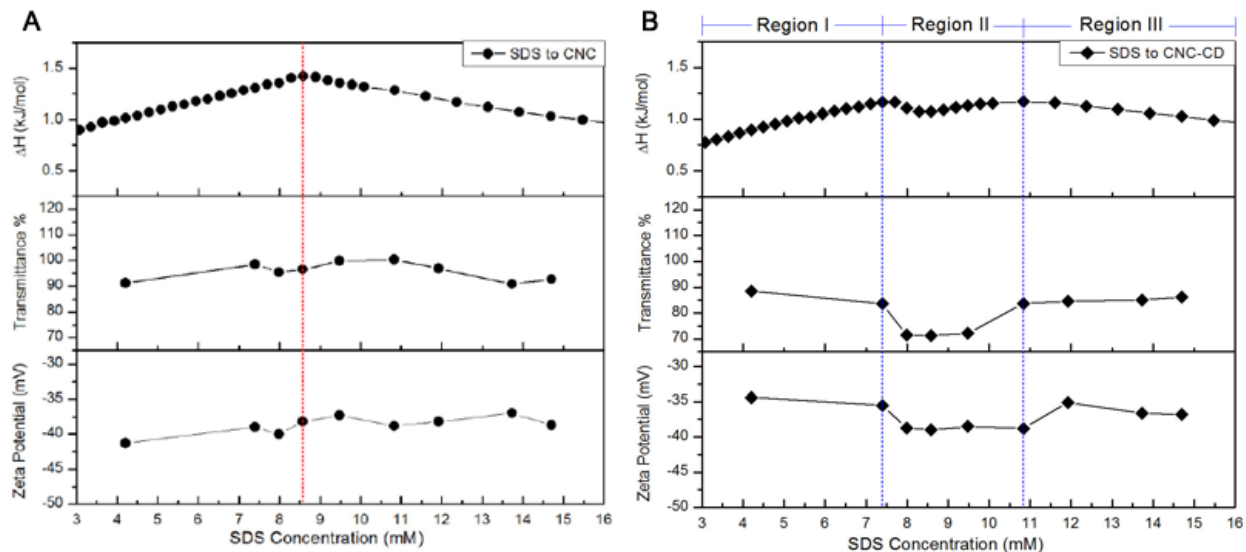


Figure 3.9 Comparison of ITC, transmittance and zeta potential results for CNC/SDS (A) and CNC-CD/SDS (B) samples.

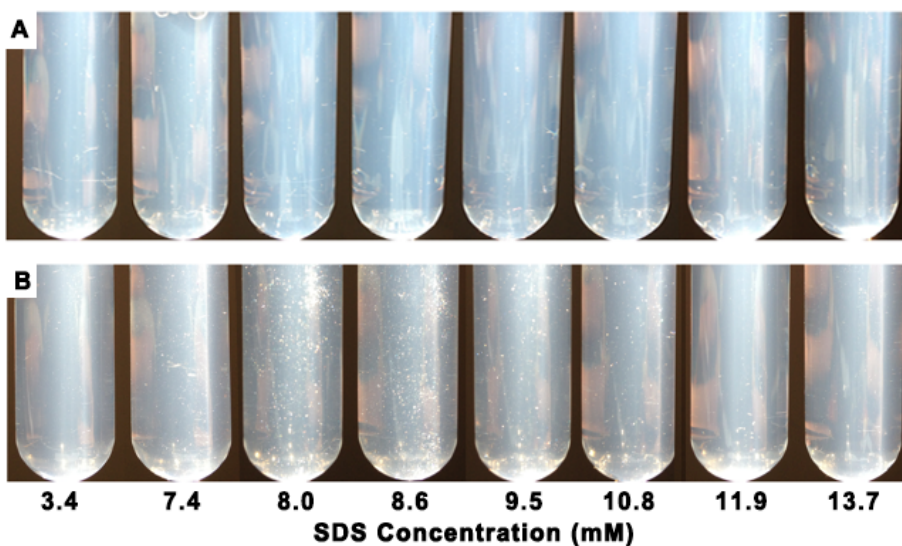


Figure 3.10 Photos of 0.6 wt% SDS/CNC (A) and SDS/CNC-CD (B) samples with increasing SDS concentration.

Images of SDS/CNC and SDS/CNC-CD revealed the aggregation of SDS induced by the inclusion complex on the surface of CNC-CD (Figures 3.12). The CNC and CNC-CD concentration were kept low to avoid the agglomeration of CNC-CD observed in Region II. From the images, both

CNC and CNC-CD were well dispersed, while the aggregation of SDS was only observed on nanorods of CNC-CD. In summary, at the SDS concentration in Region II, CNC did not interact with SDS monomers or micelles. With CNC-CD, aggregates, induced by the formation of SDS/ β -CD host-guest complexes on the surface of CNC, were formed at an SDS concentration of ~ 7.6 mM and dissociated at ~ 10.8 mM. In the SDS/ β -CD host-guest complexes, due to the length of the C12 alkyl chains and the length of the CD cavity, part of the hydrophobic chains were exposed. When SDS concentration was increased, the monomers nucleated around the inclusion complex driven by hydrophobic forces; this is a different mechanism than the polymer-induced aggregation of surfactant. Considering the size of the aggregates, it is highly likely that the aggregation of free or included SDS monomers could bridge with other SDS/CNC-CD complexes to form larger aggregates, which were then visible to the naked eyes. Beyond the cmc (~ 11 mM), the SDS aggregates on the CNC-CD complexes continued to grow leading to the dissociation of large SDS/CNC-CD aggregates to form smaller stable SDS/CNC-CD nanorods in water.

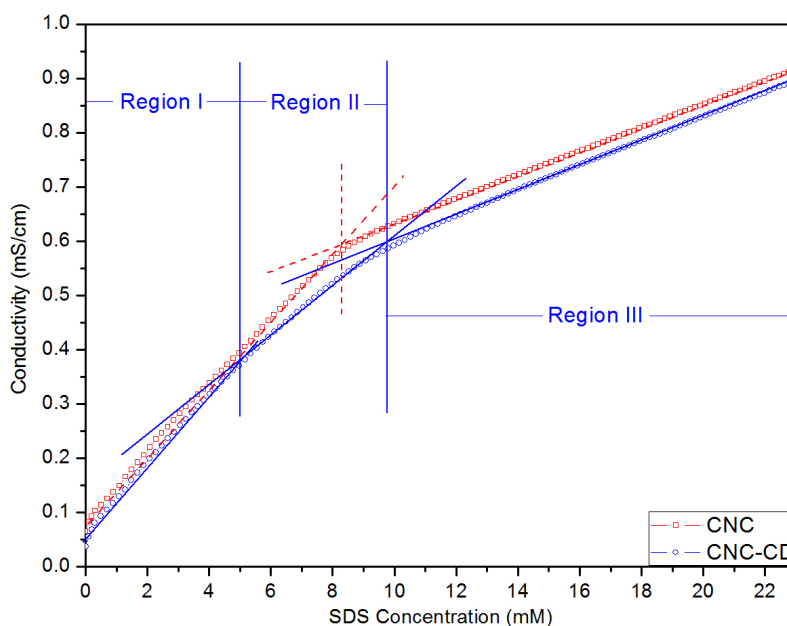


Figure 3.11 Conductivity of 0.6 wt% CNC and CNC-CD suspensions with increasing SDS concentration at 25°C.

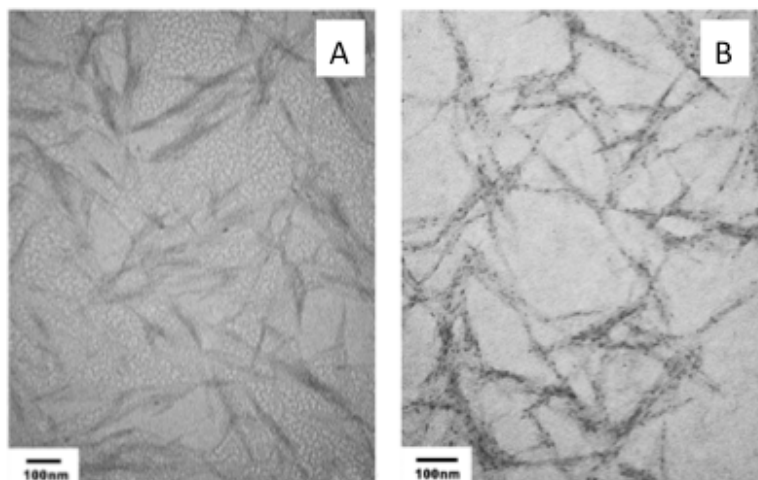


Figure 3.12 TEM images of 0.02 wt% of CNC (A) and CNC-CD (B) with 8.5 mM SDS.

3.3.5 Interactions with a cationic surfactant

The cmc of CTAB in water is ~ 1 mM as evident from the inflection point in the surface tension (Figure 3.13A) and the first-order differential curve of the ITC data. With CNC and CNC-CD suspensions, changes in the surface tension followed a similar trend, but they were different from the CTAB/water curve. The surface tension profile could be divided into three regions with different slopes. In the region with Slope 1, positively charged groups on the CTAB monomers were bound to the negatively charged CNC surface. Since the hydrophobic tails of CTAB monomers bound to the CNC were exposed to the bulk water, with increasing amount of bound monomers the hydrophobicity of CNC particles was enhanced. Thus, CNCs were driven to the interface due to the diminished hydrophilicity, resulting in the smaller Slope 1 comparing with the slope of CTAB dilution. CTAB aggregation induced by the bound monomers was also observed in this region (Scheme 3.3-bottom left panel). At the first inflection point on the curve, CNC became positively charged due to CTAB aggregation and were stripped from the interface resulting in a rapid drop of surface tension shown in Slope 2. Surface tension of CNC-CD was lower than CNC because of the higher hydrophobicity of CNC-CD aggregates adsorbed at the interface: The host-guest interactions between CTAB tails and CNC-CD enhanced the hydrophobicity and promoted the bridging between particles to form large hydrophobic aggregates adsorbed at the air-water interface in Slope 1. (Scheme 3.3-bottom right panel). The desorption of aggregates was more rapid was assigned to the facilitated CTAB aggregation induced by inclusion complexes of CTAB and β -CD.

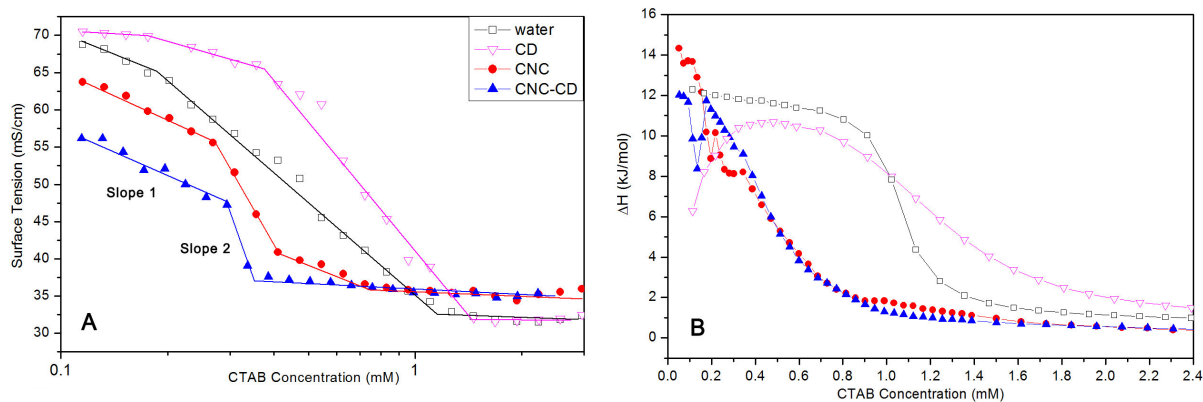


Figure 3.13 (A) Surface tension curves of water, 0.1 wt% CNC and 0.1 wt% CNC-CD suspensions with increasing CTAB concentrations at 28°C; (B) Thermograms of titrating SDS to water, 0.03 mM β -CD, 0.1 wt% CNC and 0.1 wt% CNC-CD suspensions at 28°C.

The host-guest interaction between CTAB and β -CD was described by a smaller ΔH at low concentration as seen in the ITC thermogram (Figure 3.13B). A similar reduction was also observed when CNC-CD was compared to CNC in the region where the electrostatic and host-guest interactions both contributed to the ΔH . At ~ 0.2 mM in CNC-CD and ~ 0.3 mM in CNC, the slight increase in the ΔH is attributed to the aggregation of CNC or CNC-CD particles in the bulk. Due to the bridging effect of CTAB/ β -CD complex, aggregation of CNC-CDs occurred at a lower concentration.

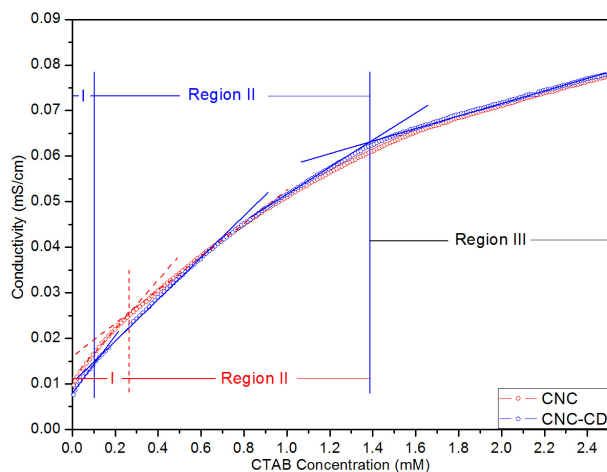


Figure 3.14 Conductivity of 0.1 wt% CNC and CNC-CD suspensions with increasing CTAB concentration at 28°C.

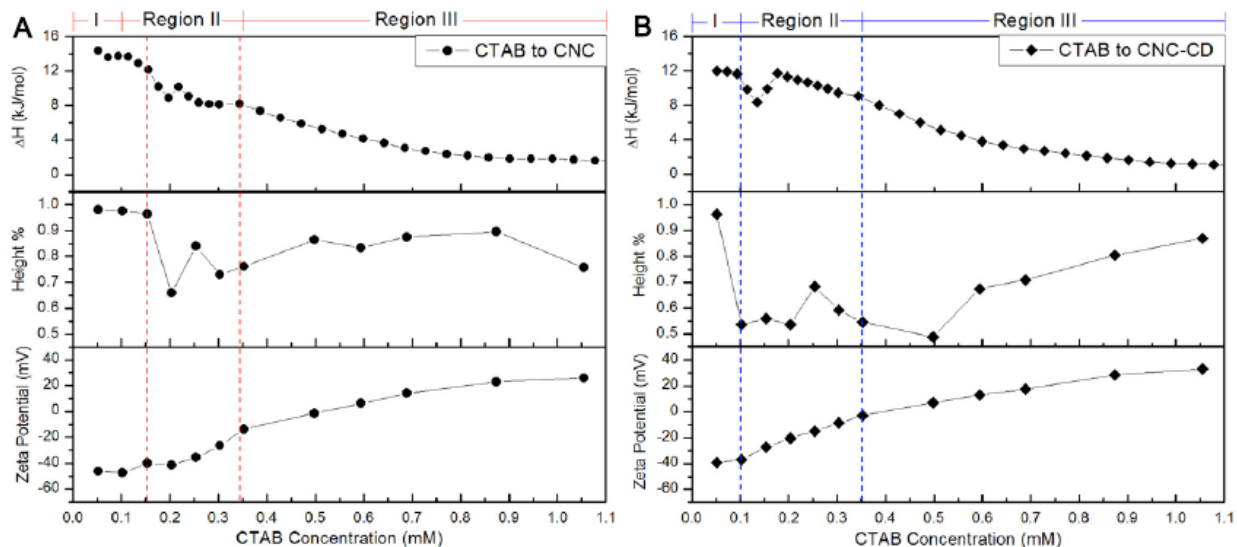


Figure 3.15 Comparison of ITC, transmittance and zeta potential results for CNC/CTAB (A) and CNC-CD/CTAB (B) samples.

Comparing the calorimetric, phase separation and zeta-potential results provided a comprehensive understanding on the aggregation behavior of CNC and CNC-CD in the presence of CTAB (Figure 3.15). In Region I, the zeta-potential increased slowly when bound CTAB monomers adsorbed the CNC and CNC-CD nanoparticles that produced small amounts of precipitates. At the onset of Region II, CNC-CDs were bridged by CTAB inducing a rapid aggregation and a faster precipitation, resulting in a less negative zeta potential. The second reduction in the column height of the precipitates at 0.25 mM CTAB corresponded to denser aggregates that settled into a more compressed structure with the zeta potential further increased to ~ 0 mV. At the end of Region II, the microstructure of the aggregates became less compact due to the continuous binding of CTAB molecules that dissociated the aggregates into smaller, relatively better-dispersed aggregates yielding an increase in the height of the aggregates in Region III. However, it was not possible for CTAB to entirely disperse CNC or CNC-CD nanoparticles to form transparent suspensions even at concentration above the cmc. The difference in CTAB induced precipitation of CNC and CNC-CD can be observed in Figure 3.16.

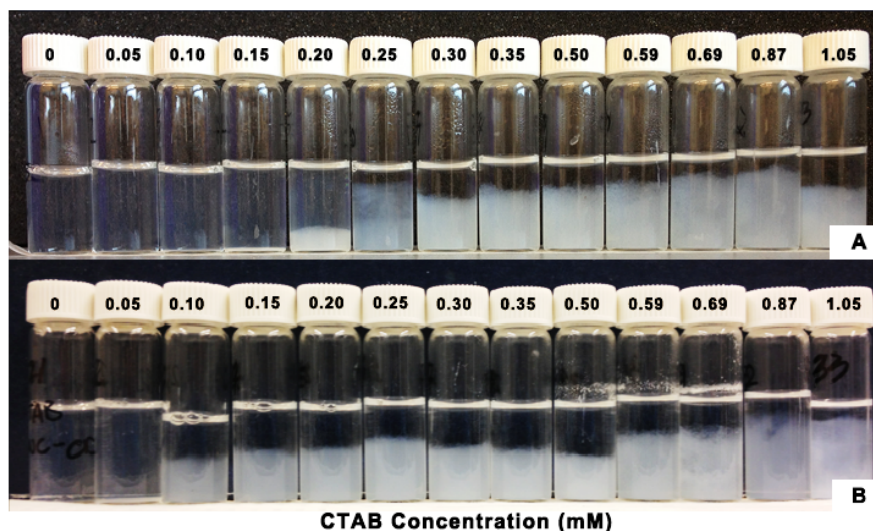


Figure 3.16 Phase separation of 0.1 wt% CTAB/CNC (A) and CTAB/CNC-CD (B) samples with increasing CTAB concentration.

3.4 Conclusions

β -CDs were successfully grafted on CNC where the grafting ratio of β -CD was determined by the phenolphthalein inclusion method. The interactions between CNC-CD nanoparticles and TX-100, SDS and CTAB were investigated via surface tensiometry, isothermal titration calorimetry, conductometry, transmittance, phase separation and zeta potential measurements. The primary interactions in the CNC-CD/TX-100 and CNC-CD/SDS systems are host-guest interactions between the hydrophobic domain of surfactants and β -CD. While hydrogen binding was also possible between TX-100 and pristine CNC. Adsorption and desorption of CNC and CNC-CD in CTAB solutions were observed from surface tension measurements, resulting from the electrostatic interactions between negatively charged groups on CNC and cationic CTAB molecules. Inclusion complex induced aggregation was observed in CNC-CD/SDS at low SDS concentration due to the incomplete inclusion of the SDS alkyl chain. Re-dispersion of CNC-CD aggregates at high SDS concentration was attributed to the inclusion complex-induced SDS aggregation. Both host-guest and electrostatic interactions between positively charged CTAB and negatively charged CNC-CD contributed to the formation of precipitates and the transition from loose to compact aggregates with increasing CTAB concentration. However, there was no re-dispersion of the aggregates observed due to the strong electrostatic interaction and high hydrophobicity of CTAB tails.

4 β -Cyclodextrin-functionalized Cellulose Nanocrystal Derivatives and Their Interactions with Amphiphilic Molecules

4.1 Introduction

There are many varieties of personal care products in the market that use cationic polymers in their formulations for the purpose of conditioning, grooming or moisturizing. Especially in shampoos, multi-functioning is required and additional benefits, such as ease of wet/dry combing, smooth feeling and pleasing appearance, are expected except for simple cleansing the hair. Cationic polymers play an significant role in providing most of these features. They can adsorb onto hair and skin by electrostatic interaction between the negatively charged substrate surface and positively charged segments of the polymer. Synthetic polymers and naturally derived polymers have all been incorporated into hair care products to deliver and promote the conditioning effects on hair. For example, polyquaternium-10 (PQ-10), being the first cationic polymer used in conditioning shampoos, is a quaternary ammonium salt of hydroxyethyl cellulose (HEC) which has been reacted with 2,3-epoxypropyltrimethylammonium chloride.²⁶ It was found that this polysaccharide has good film forming properties. The uniform, clear and glossy film can be translated into a better hair appearance. Also, due to the cellulosic nature PQ-10 has moderate substantivity without weighing down the hair, and a uniform deposition provides a smooth hair surface upon application.

In order to ensure that addition of polymers in formulations that usually contain various surfactants has no effects on the product's processing, appearance and functionality, insights on the behavior of mixed surfactant/polymer systems are necessary for practical applications. Interactions between ionic surfactants and non-ionic water-soluble polymer, polyelectrolytes are attracting widespread attentions because of the many practical uses of such systems and their inherently beneficial properties. Mixed system of surfactant and polymers are widely used in applications such as detergency, cosmetic products, rheology control, paints and pharmaceutical formulations. Variation of the property of these mixtures can be used to control and optimize the phase separation, rheological and interfacial property of the formulation in order to obtain ease of processing, better appearance or to impart other functionalities. It was well-defined that non-ionic polymer can induce surfactant aggregation by hydrophobic interactions. Conformational change of flexible polymers such as poly(ethylene glycol) (PEG)⁴² and polyvinyl pyrrolidone (PVP)¹⁸⁷, enable the polymer backbone to be dehydrated and solubilized in surfactant micellar cores in the form of string and beads, where string is the polymer and beads are surfactant micelles.¹²¹ At high surfactant concentration, polymer backbone rehydrates and wrap around on the

outside of surfactant micelles before the micellization took place in the bulk.

It was found that in the presence of non-ionic polymer, surfactants aggregate at much lower concentrations their cmc, meaning that the total concentration of surfactant monomer was reduced. The ability of hydrophobically modified polymer (HMP) to minimize irritation caused by surfactant-based cleansers was investigated and good tolerability and efficacy were observed.¹⁸⁸ Nevertheless, for polyelectrolyte and ionic surfactant systems, this effect is more significant due to the strong binding forces involved, and the reduction in monomer concentration would tend to be much more significant. Furthermore, non-ionic polymer can also reduce the surface/interface activity of ionic surfactants by forming weakly surface-active complexes, while complex of oppositely charged surfactant and polymer may provide a synergistic enhancement of the surface/interface activity of the mixture system. Emulsifying and foaming ability can be consequently improved by such enhancement.

On the basis of extensive testing on the influence of cationic cellulosic polymers on keratin, which are negatively charged and water-swelling, it was hypothesized that these polymers form protective films on keratin substrates by adsorbing on the latter through a cross-linking mechanism, rendering an intact keratin polypeptide chain network. The influence of SDS on the adsorption of cationic polymer on negatively charged substrates, such as keratin or skin, has been extensively studied. Small addition of surfactants was reported to progressively reduce the adsorption of polymer owing to the reduced positive charge density of polymer upon binding. However, high concentration of SDS was able to fully restore the adsorption.¹⁸⁹

Cellulose nanocrystals (CNC) was demonstrated to have very good film forming properties as well as optical functionalities. Its rigid crystalline structure with a high aspect ratio ensures a fast viscosity build-up with increasing concentration. Potential modifications on the vast amount of hydroxyl groups on CNC surface provide opportunities for imparting other functional groups or compounds that can be delivered with application of CNC. Furthermore, cationization of CNC has been reported by Hasani et al.¹⁰² and Zaman et al.¹⁹⁰ separately using glycidyltrimethylammonium chloride (GTMAC) as cationization agents, which reversed the surface charge of CNC, but the total charged density was reduced in Hasani's work. Nevertheless, stable suspension of cationic CNC was obtained, and the gelling, shear birefringence and rheological properties were studied. In this study, we grafted β -cyclodextrin (β -CD) onto cationically modified CNC nanoparticles, aiming to develop a system that possesses conditioning functionality and at the same time can deliver active reagents to hair care products. Since the size and morphology of CNC are very different from traditionally used amorphous cationic polymers, the

addition of β -CD grafted cationic CNC (dcCNC-CD) into formulations containing ionic surfactants may change their phase separation, rheological and interfacial properties. In addition, the existence of β -CD also changes the surface/interfacial activity of surfactants. Thus, it will be beneficial to study the interactions between surfactants and cationically charged CNC with or without grafted β -CD.

4.2 Experimental section

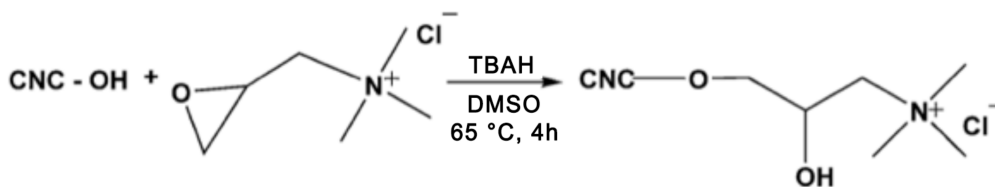
4.2.1 Materials

Spry-dried cellulose nanocrystals (CNC) were supplied by CelluForce Inc. MCT- β -CD was synthesized using the method previously described in Chapter 3. Phenolphthalein, sodium carbonate monohydrate (>99.5%), sodium bicarbonate (99.7-100.3%), tetrabutylammonium hydroxide (TBAH) (>98%), sodium dodecyl sulfate (SDS) (>99%), hexadecyl-trimethyl-ammonium bromide (CTAB) (>99%), silver nitrate (>99%), sodium chloride (NaCl) (>99.5%) were purchased from Sigma-Aldrich and used without any further purification. The CNC suspensions were prepared by vigorous mixing using a 500W IKA T-25 homogenizer followed by sonication in a 700W 42kHz Branson sonication bath. Surfactant solutions were prepared at least one day prior to the test. Deionized Millipore water was used in all the sample preparations and tests.

4.2.2 Desulfation and cationization of CNC

Concentrated NaOH(aq) solution was added to 3 wt% CNC aqueous suspension to obtain a NaOH concentration of 1 M. Then the suspension was heated at 60°C for 5 hours. The desulfated CNC was dialyzed against deionized water for three days and freeze dried overnight.

Cationization of desulfated CNC was synthesized in DMSO with small amount of water to catalyze the reaction while prevent hydrolysis of GTMAC. 1 g of TBAH was dissolved in 0.8 wt% of desulfated CNC suspension and sonicated in a Branson 1510 sonicator (Branson Ultrasonic Corporation, USA) for 10 min. Then the suspension was heated up to 65 °C followed by the addition of 3.31 mL GTMAC and 2 mL D.I. water. The reaction was allowed to proceed at 65 °C for 4 hours then terminated by the addition of approximately 3-fold of water. In order to purify the cationic desulfated CNC (dcCNC) and remove the DMSO, the suspension was dialyzed against D.I. water for a week.



Scheme 4.1 Reaction scheme of surface cationization of CNC with GTMAC in DMSO.

4.2.3 Grafting of MCT- β -CD

MCT- β -CD was synthesized as previously described in Chapter 3. Briefly, two chlorine atoms in the triazine ring of cyanuric chloride were hydrolyzed and substituted stepwise with β -CD by strictly controlling the temperature. MCT- β -CD was then grafted onto dcCNC in both aqueous solution and DMSO under optimized reaction conditions as discussed in Chapter 3, which are referred to dcCNC-CD and dcCNC-CD/DMSO respectively. Both of the β -CD grafted dcCNC and dcCNC-CD were dialyzed against D.I. water for at least 2 weeks in order to remove the free MCT- β -CD. All the dcCNC-CD in the following context were products synthesized in water without further specification.

4.2.4 Spectroscopy

Ultraviolet absorbance of MCT- β -CD, dcCNC, dcCNC-CD/water and dcCNC-CD/DMSO suspensions was measured on a Varian (Carey 100 Bio) UV-visible spectrometer at room temperature. Fourier Transform IR (FTIR) spectra of β -CD, dcCNC, dcCNC-CD/water and dcCNC-CD/DMSO samples in compressed KBr powder were obtained on a Bio-Rad (Excalibur series) FTIR spectrometer over scanning wavelengths of 400-4000 cm^{-1} .

4.2.5 Grafting ratio measurements

The grafting ratio of β -CD on dcCNC-CD synthesized in water and DMSO were determined using phenolphthalein (PHTH) method as described in Chapter 3. At pH higher than 8.2, PHTH was negatively charged and attracted to cationic CNC. However, the physical adsorption of PHTH on the surface of cationic CNC did not reduce the UV absorbance. Nonetheless, minor effects of dcCNC have been considered and deducted from all the measurements of dcCNC-CD used as controls. The amount of β -CD was determined by a calibration curve of $\log(\text{absorbance of PHTH}/\beta\text{-CD mixture})$ against $\log(\text{concentration of } \beta\text{-CD})$. The grafting ratio was then determined from Equation 3.1.

4.2.6 Surface tensiometry

Surface tension measurements were conducted on a DCAT 11 (Dataphysics) tensiometer. The Wilhelmy plate method was used to measure the dynamic surface tension at the air-water interface. 30 mM of SDS and 5 mM of CTAB stock solutions were prepared. Then, 40 mL of water, dcCNC 0.1 and dcCNC-CD 0.1 wt% suspensions were titrated manually using Eppendorf pipettes with SDS and CTAB stock solutions at 25 and 28 °C respectively to obtain increasing concentrations. After each titration, solutions were stirred for 30s followed by a 30s of equilibrium time before measuring the surface tension. Finally, the surface tension values were plotted against the logarithm(concentration) to identify the critical concentrations.

4.2.7 Isothermal titration calorimetry

Heat effects in micellization and surfactant/polymer interactions are relatively small and need very sensitive techniques to quantify. Modern calorimeters using micro-calorimetric technique are sensitive enough to monitor small heat changes of as low as 0.1 calorie per injection. Isothermal titration calorimetry has been used to extract thermodynamic parameters such as enthalpy change, entropy change, Gibbs free energy change and heat capacity of the system. These parameters are crucial for understanding the interactions between surfactants and polymers, such as determining critical aggregation concentration and critical micelle concentration.

In this study, we used Microcal VP-ITC to study the thermodynamic properties of dcCNC and dcCNC-CD in SDS and CTAB solutions. Stock solutions of 100 mM SDS and 15 mM CTAB were prepared in advance and loaded into a 282 μ L syringe. dcCNC and dcCNC-CD suspensions with concentration 0.1 wt% were loaded in the 1.455 mL sample cell. The titrants were injected into the sample cell by pre-programmed procedures with volumes of 1-10 μ L in each injection. The enthalpy change of the interactions were measured and reported in kJ/mol of injectant and plotted against surfactant concentration.

4.2.8 Zeta potential

Samples of desulfated CNC, dcCNC, dcCNC-CD/water and dcCNC-CD/DMSO, as well as mixtures of surfactants and dcCNC or dcCNC-CD suspensions were prepared at concentrations of around 0.1 wt% of nanoparticles in polystyrene cuvettes. Zeta potential values were determined on a Malvern Zetasizer Nano ZS90. The samples were sonicated and measured without dilution. This method was used to determine the overall surface charge of dcCNC, dcCNC-CD samples with or without the

addition of ionic surfactants.

4.2.9 Potentiometric titration

The degree of cationization was measured by potentiometric titration. A Metrohm 809 Titando automatic titrator was used and the conductivity of solution were measured. The titrator was controlled by a Tiamo software that can dose titrants at 1 μ L/injection. All the measurements were performed in a closed jacketed vessel at 25 °C with a stirring speed of 4. Around 40 mg of dcCNC and dcCNC-CD were suspended in 20 mL of D.I. water. The suspensions were degassed by bubbling argon gas into the solution for 15 min, then titrated with 0.025 M silver nitrate solution. The conductivity was measured until titrated volume of silver nitrate reached at 4 mL for dcCNC and 2 mL for dcCNC-CD. Finally, the conductivity values were plotted against concentration of silver nitrate (in mM), which was used to determine the content of GTMAC groups.

The conductivity titrations were performed on the same instrument. All the measurements were conducted in a jacketed vessel with a stirring speed of 4 to prevent formation of bubbles. The same temperature and concentrations of surfactants and dcCNC, dcCNC-CD suspensions were used as in surface tension measurements. The conductivity was measured using a conductivity electrode.

4.3 Results and discussion

4.3.1 Characterization of dcCNC and dcCNC-CD

4.3.1.1 Zeta-potential

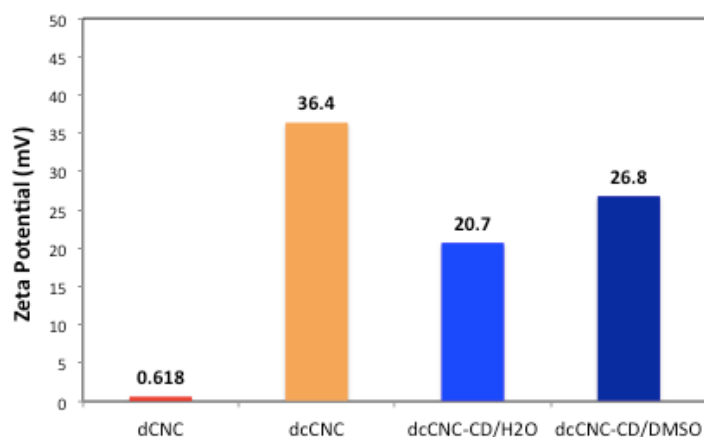


Figure 4.1 Zeta potential of desulfated CNC (dcCNC), desulfated-cationic CNC (dcCNC), CD grafted dcCNC synthesized in water (dcCNC-CD/H₂O) and in DMSO (dcCNC-CD/DMSO).

Zeta potential measurement showed that after desulfation, negatively charged sulfate groups on CNC were mostly removed resulting in a zeta potential close to zero. Cationic CNC synthesized using desulfated CNC (dcCNC) had a positive zeta potential of +36.4 mV, which contributed to a relatively good dispersability of dcCNC in aqueous solution. However, from the results of dcCNC-CD synthesized in water and DMSO, we observed a drop in zeta potential values below +30 mV. This can be explained by the hydrolysis of covalently bonded GTMAC on dcCNC. Since the reaction condition for grafting CD involved the addition of alkali and heat, both of these two factors can facilitate the hydrolysis of GTMAC in water. It can also explain the fact that dcCNC-CD synthesized in DMSO had a higher zeta potential compared to that synthesized in water, suggesting a lower degree of GTMAC hydrolysis. With zeta potential reduced to below +30 mV, the dispersability of dcCNC-CD decreased and light precipitation was observed after 3-4 days.

4.3.1.2 Conductometry titration

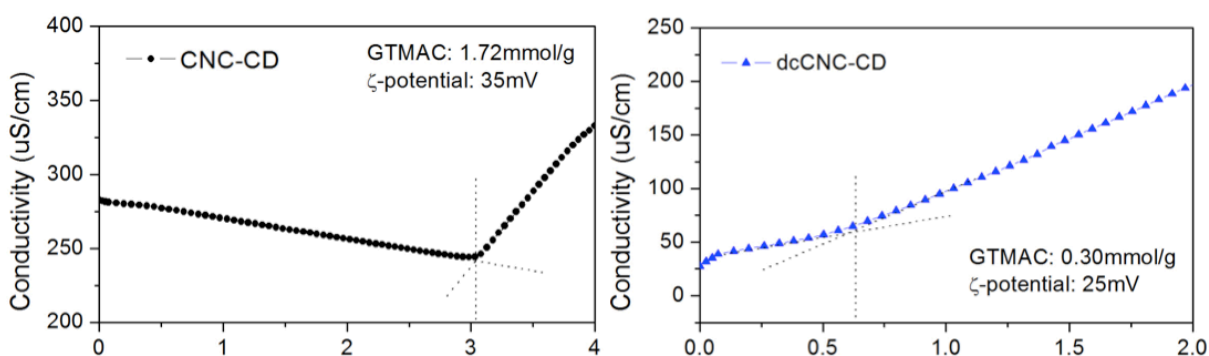
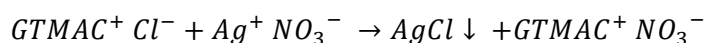


Figure 4.2 Conductometry titration of AgNO_3 2.5mM to dcCNC 40mg (A) and dcCNC-CD 42mg (B).



Scheme 4.2 Precipitation between GTMAC chloride and silver nitrate.

The degree of cationization was determined by measuring the conductivity of dcCNC and dcCNC-CD suspensions upon the titration of AgNO_3 . The counterion of GTMAC, Cl^- ion, forms white solid precipitates with Ag^+ ion upon titration (Scheme 4.2) and due to the decrease of ion concentration, conductivity drops while precipitating persists. In Figure 4.2A, the conductivity continued to decrease, and at the AgNO_3 concentration of 3.1 mM, Cl^- ions were completely consumed and ion concentration continues to increase resulting in the increase of conductivity. The degree of cationization of dcCNC was calculated to be 1.83 mmol/g using equation:

$$\text{Degree of cationization} = \frac{V_{AgNO_3} \times 0.0025M}{m_{dcCNC}} \quad \text{Equation 4.1}$$

In the titration profile of dcCNC-CD, we observed that the conductivity increased at low concentration of $AgNO_3$ with a slope smaller than that at higher $AgNO_3$ concentration. This can be explained by the interaction between Ag^+ and β -CD in addition to the $AgCl$ precipitation. It was reported that with an inner cavity diameter of 7-8 Å, it is possible for β -CD to include Ag^+ ions, whose hydrodynamic radius is 1.15 Å.¹⁹¹ Since host-guest interaction is an equilibrium process, part of Ag^+ ions titrated to dcCNC-CD suspension were included in β -CD cavity and hampered the precipitation with Cl^- . When the Ag^+ ions precipitated and the concentration decreased, included Ag^+ ions were released from β -CD cavity. Due to the incomplete precipitation of Ag^+ ions in each titration, the conductivity did not drop as in the case of dcCNC. After the Cl^- ions were completely precipitated, the conductivity slope became larger but still not as large as that of dcCNC due to the host-guest equilibrium.

4.3.2 UV-vis and FTIR of desulfated-cationic-CNC (dcCNC)

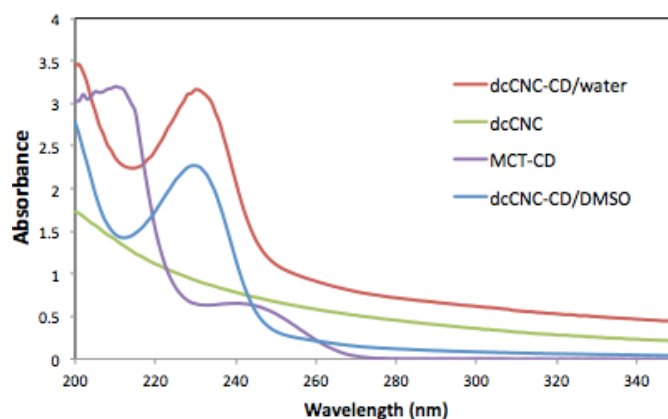


Figure 4.3 UV-vis spectra of MCT- β -CD, dcCNC, dcCNC-CD/water and dcCNC-CD/DMSO.

UV-vis spectra of dcCNC-CD synthesized in water and DMSO were compared with that of MCT- β -CD as shown in Figure 4.3. MCT- β -CD possessed a specific absorbance at 245 nm. Due to the substitution of the third chlorine atom in triazine ring of MCT- β -CD, the electron distribution was altered that resulted in a blue-shift of absorbance peak from 245 to 231 nm. The baseline shift of both dcCNC-CD/water and dcCNC-CD/DMSO were attributed to the light scattered by the rod-like nanoparticles of CNC, while no specific absorbance was observed.

Cationization of CNC and grafting of MCT- β -CD were confirmed by FTIR spectroscopy. (Figure 4.4) The characteristic bands of CNC were observed as previously reported¹⁹²⁻¹⁹⁵: the strong band

at 3418 cm^{-1} was assigned to hydroxyl (-OH) stretching, the 2904 cm^{-1} absorbance was due to symmetric C-H vibrations, an intense band at 1648 cm^{-1} originated from the moisture of the dcCNC, the band at 903 cm^{-1} was attributed to the C-H deformation of the glycosidic linkage between glucose units, and the absorbance between wavenumber $1134\text{-}1162\text{ cm}^{-1}$ designated the C-O stretching in major ether bands in CNC. Comparing the spectra of CNC and dcCNC, a new band can be observed at 1477 cm^{-1} , which was assigned to CH_2 bending mode and methyl groups of grafted GTMAC. For both dcCNC-CD/water and dcCNC-CD/DMSO, evident new bands appeared at 1538 cm^{-1} were noticed. This band was attributed to the amide II groups including C-N stretching, and N-H bending coupled vibrations, which were due to the grafted MCT- β -CD. The strong absorbance at 1488 cm^{-1} was assigned to be the specific peak of MCT- β -CD. The main difference between dcCNC-CD/water and dcCNC-CD/DMSO was seen at wavenumber 1724 cm^{-1} , which was attributed to the C=O bond due to the protonation then rearrangement of triazine ring in aqueous solution.

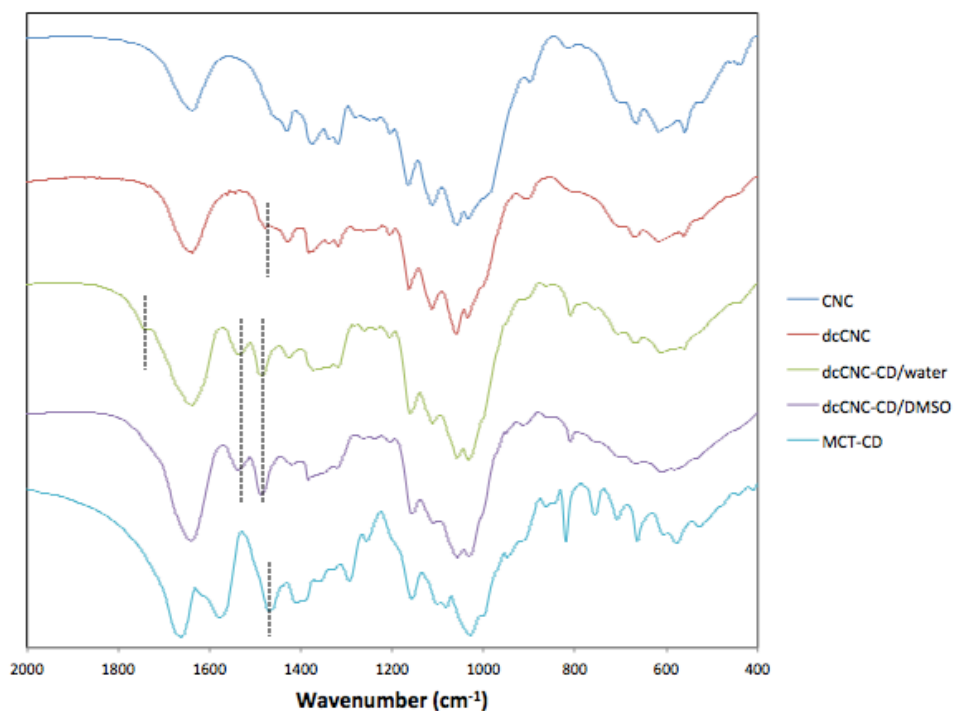


Figure 4.4 FTIR spectra of CNC, dcCNC, dcCNC-CD/water, dcCNC-CD/DMSO and MCT- β -CD.

4.3.3 Grafting ratio of MCT- β -CD

Table 4.1 Grafting ratio in wt% and $\mu\text{mol/g}$ of β -CD on dcCNC-CD comparing with that of CNC-CD.

Sample	wt %	$\mu\text{mol/g}$
CNC-CD	3.00 %	26.5
dcCNC-CD/water	7.05 %	62.15
dcCNC-CD/DMSO	6.66 %	58.65

The grafting ratio of β -CD on dcCNC-CD was measured using the phenolphthalein (PHTH) method described in Chapter 3. Briefly, due to the discoloring and loss of UV absorbance of PHTH upon complexation with β -CD, a calibration between PHTH absorbance and β -CD concentration can be used to determine the β -CD concentration in CNC-CD suspensions. Proper baseline correction was necessary due to the light scattering phenomenon from CNC-CD particles. From the calculations, the enhanced grafting ratio was observed for dcCNC-CD/water compared with that of CNC-CD synthesized under the same conditions. The increase in the grafting ratio was due to the increase of reactive sites, which are the $-\text{OH}$ groups on both CNC and GTMAC. Since the unreactive sulfate groups were removed before cationization and the resulting $-\text{OH}$ groups were substituted by GTMAC at 1:1 ratio, the total amount of $-\text{OH}$ groups on dcCNC increased. However, the grafting ratio of dcCNC-CD synthesized in DMSO was not higher than that of dcCNC-CD/water as expected, possibly due to the insufficient temperature during reaction.

4.3.4 Interactions between dcCNC, dcCNC-CD and cationic surfactants

The different behaviors of dcCNC and dcCNC-CD in the solution of a representative cationic surfactant, CTAB, were studied by tensiometry, calorimetry, conductivity, transmittance and zeta potential. In the following section, concentrations of dcCNC and dcCNC-CD were kept at 0.1 wt%. The concentration of surfactants was varied from low concentration to above cmc of CTAB, which is ~ 1 mM according to previously reported studies.

In tensiometry study, it was observed that surface tension of water barely decreased upon the titration of CTAB below the concentration of ~ 0.1 mM, after which the surface tension significantly decreased until the critical micelle concentration (cmc) was reached. (Figure 4.5) In the presence of β -CD, the reduction in the surface tension commenced at a higher concentration due to the formation of

inclusion complex between CTAB and β -CD that reduced the amounts of free monomers at the air-water interface. Thus, the cmc of CTAB in β -CD solution increased slightly. While in dcCNC and dcCNC-CD suspensions, the surface tension began to decrease at very low CTAB concentration and leveled off at concentrations below cmc. Unlike pristine CNC and CNC-CD, the lower surface tension of pure nanoparticle suspensions comparing with that of water indicated a low and slightly higher surface activity of dcCNC and dcCNC-CD respectively, which was possibly due to the modification with GTMAC. This also suggested that grafting of β -CD had a negative effect on the hydrophobicity of dcCNC.¹⁷⁴

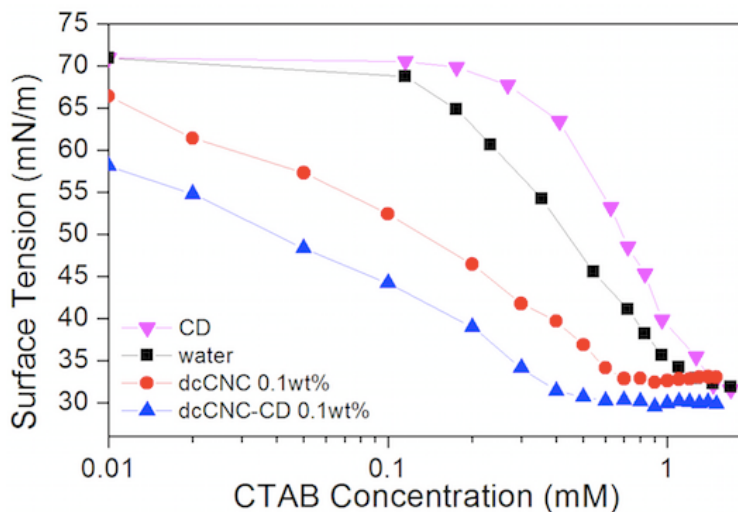


Figure 4.5 Surface tension of water, 0.35mM β -CD, 0.1 wt% dcCNC and 0.1 wt% dcCNC-CD with increasing CTAB concentration.

More significantly, the smaller slope of dcCNC and dcCNC-CD indicated their interactions with CTAB. Despite the electrostatic repulsion between cationically charged dcCNC and CTAB, CTAB may still interact with the backbone of dcCNC via hydrophobic interaction due to the inhomogeneous distribution of charged groups on dcCNC, which is similar as the interactions between nonionic polymer and ionic surfactants. In suspensions of dcCNC and dcCNC-CD, CTAB monomers attracted to the polymer backbone are partitioned to the air-water interface, as indicated by the reduced surface tension at low CTAB concentration. With increasing amounts of bound CTAB, dcCNC and dcCNC-CD particles became more hydrophilic and were progressively stripped from the interface. Thus, the surface tension eventually attains the value of polymer-free solutions. Although the formation of inclusion complex between CTAB and β -CD was believed to reduce the surface activity of CTAB leading to a higher cmc, the suspension surface was saturated at a lower CTAB concentration in dcCNC-CD compared to dcCNC

due to the compensative effects of dcCNC-CD surface activity.

The CTAB/dcCNC-CD interactions were more dominant in bulk solution than at the air-water interface. Thermodynamic study by isothermal calorimetry (ITC) provided detailed information on the difference between the interactions of CTAB/dcCNC and CTAB/dcCNC-CD in aqueous solution. In the thermogram of CTAB/dcCNC (Figure 4.6A), there was no obvious difference between CTAB/dcCNC and micelle dilution curve at low CTAB concentration (Region 1 in Figure 4.6C). Around C_{CTAB} slightly lower than cmc (C_1), the curve of CTAB/dcCNC started to deviate from CTAB dilution curve and decreased at a slower rate until it crossed the dilution curve at a concentration right around cmc (C_2). In Region 2, the enthalpy change was similar but slightly smaller than the dilution curve, possibly due to hydrophobic interactions between CTAB hydrophobic tails and dcCNC backbone. Beyond C_2 , the enthalpy change decreased slowly until it overlapped with the dilution curve (Region 3), which was much more obvious and this was attributed to the polymer-induced aggregation in the presence of dcCNC. This energetic interaction indicated that the aggregation of CTAB beyond cmc was more of a cooperative process than the binding of monomers onto CNC at low concentrations.

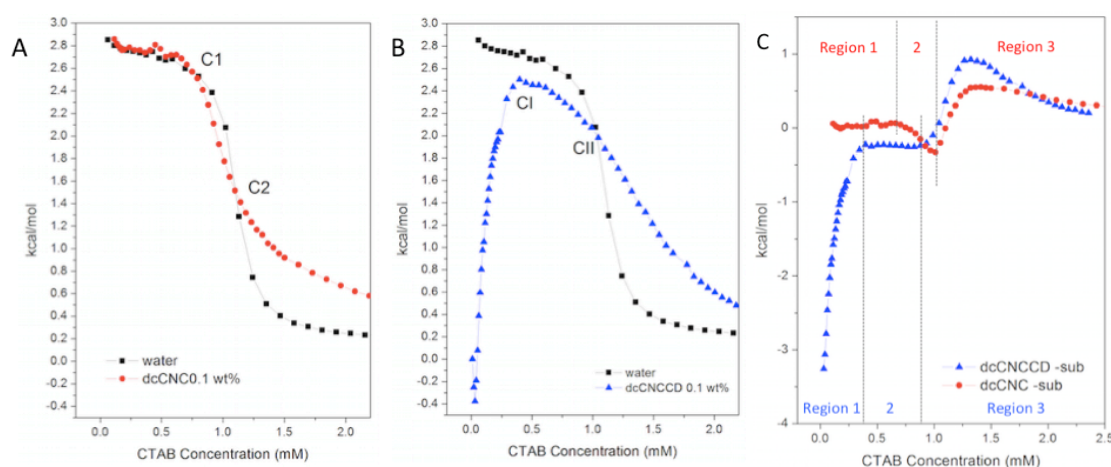


Figure 4.6 (A) Thermogram of CTAB titrations to water and dcCNC 0.1 wt%; (B) thermogram of CTAB titrations to water and dcCNC-CD 0.1 wt%; (C) enthalpy change of CTAB titrations to dcCNC 0.1 wt% and dcCNC-CD 0.1 wt% after subtracting CTAB dilution curve.

Similarly, in CTAB/dcCNC-CD thermogram, several critical concentrations could be assigned according to the binding isotherm. A pronounced endothermic peak was observed starting at 0 mM (Figure 4.6B), which corresponded to the binding isotherm of CTAB/ β -CD due to the host-guest interaction (Region 1 in Figure 4.6C). The thermogram approached a plateau at $C_{CTAB}=0.4$ mM

(designated as C_I), and at this concentration all the β -CDs on dcCNC-CD were saturated by CTAB. As more CTAB monomers were added, the enthalpy change started to decrease until it crossed the dilution curve at 0.8 mM (designated as C_{II}). The region between C_I and C_{II} was assigned as Region 2. As seen from the binding isotherm corrected for the dilution heat effect, Region 2 was a plateau indicating no specific interaction occurred in this region and at the temperature of 25 °C. Subsequently, the curve gradually decreased in Region 3 until it merged with the dilution curve at $C_{CTAB}=3.2$ mM (predicted value from the trend, designated as C_m). This region characterized the formation of surfactant aggregates on the surface of dcCNC-CD induced by inclusion complex and hydrophobic domains on dcCNC-CD's backbone. C_m corresponds to the dcCNC-CDs that are completely saturated by CTAB and free micelles started to form in bulk solution, thus only the heat of micelle dilution was evident.

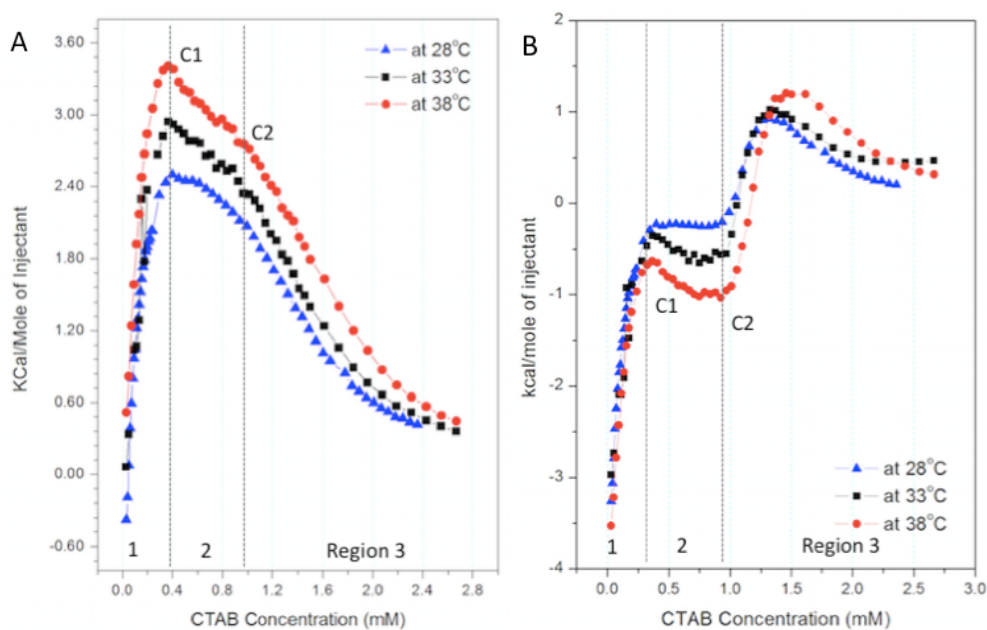


Figure 4.7 Thermogram of CTAB titrations to dcCNC-CD 0.1 wt% at 28, 33 and 38 °C (A) and corresponding curves corrected for the heat effect of dilution (B).

Hydrophobic interactions are likely to be affected by changes in the temperature, since at higher temperature, water molecules become more dynamic and the water cage surrounding the surfactant is weakened, which changes the hydrophobicity of the surfactant tails.¹⁷⁶ Thus, the binding isotherm of CTAB and dcCNC-CD interactions was investigated at 28, 33° and 38°C (Figure 4.7). The most discernable difference upon increasing the temperature was observed in Region 2, where the enthalpy change started to decrease at C_I instead of maintaining a plateau as observed at 25°C. A clear inflexion at

C₂ was observed in the original thermogram. This interaction was attributed to the rearrangement of CTAB hydrophobic tails on surface of dcCNC-CD. At 25 °C, the heat generated by the rearrangement was undetectable, while the hydrogen binding of the water cage became less efficient with increasing temperature, and the exothermic hydrophobic attraction between CTAB tails became more dominant. Furthermore, the polymer-induced and inclusion complex-induced aggregation process in Region 3 was prolonged resulting in a larger C_m upon the temperature increase, also denoting an enhanced attraction of hydrophobic domains to CTAB monomers on the surface of dcCNC-CD, thus more CTAB participated in the aggregation that delayed the formation of free micelles.

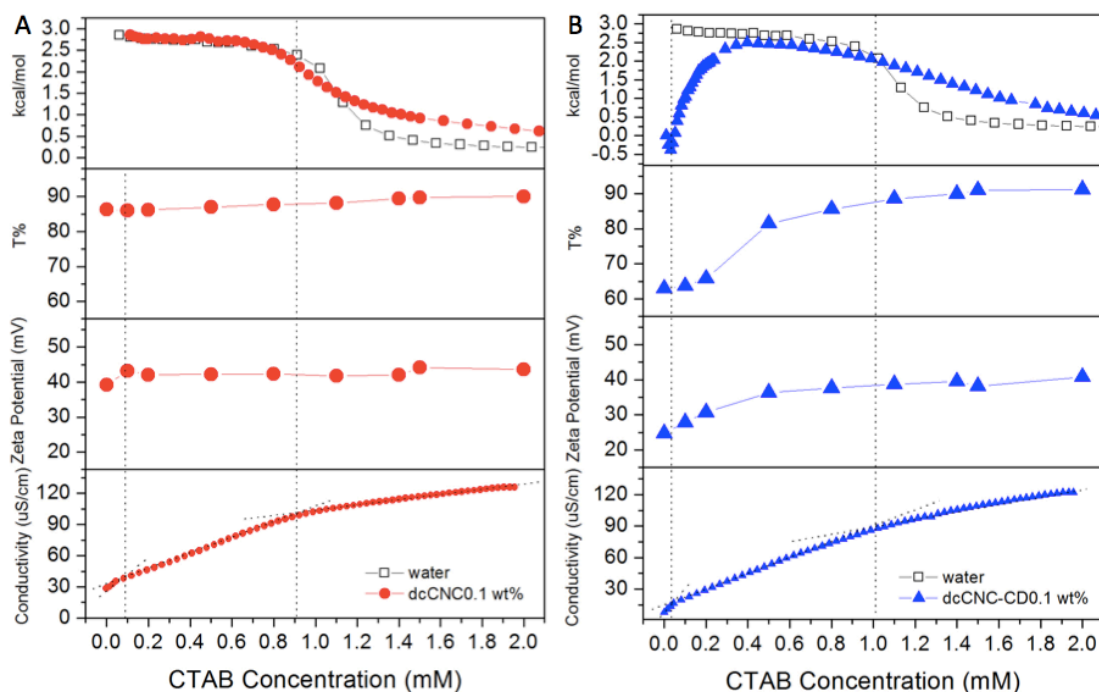


Figure 4.8 Comparison of T%, zeta potential and conductivity results of CTAB to dcCNC 0.1 wt% (A) and dcCNC-CD 0.1 wt% (B).

In order to obtain a clearer picture on the interactions, the two systems were also characterized using transmittance, zeta-potential and conductivity as a function of surfactant concentration and the results were plotted together for comparison. (Figure 4.8) The T% of dcCNC suspension remained unchanged with increasing CTAB concentration, while that of dcCNC-CD suspension became more translucent with increasing CTAB concentration (Figure 4.9B). This observation further suggested that aggregates of dcCNC-CD (resulting from association due to inadequate electrostatic stabilization) were dissociated by the enhanced electrostatic repulsion between the surfactant inclusion complex on dcCNC-

CD. This explanation was also supported by an increase in the zeta potential as shown in Figure 4.8B. However, the dcCNC induced CTAB aggregation in this region was difficult to detect due to the lack of sensitivity of these methods compared to micro-calorimetry. Furthermore, although the conductivity of dcCNC-CD suspension followed the same trend as dcCNC, it was smaller due to the lower conductivity of the CTAB bound monomers with β -CD. The slight increase observed in the zeta potential and conductivity curves at very low CTAB concentrations were possibly due to the electrostatic interaction with the sulfate groups resulting in the release of the bound counter ions.

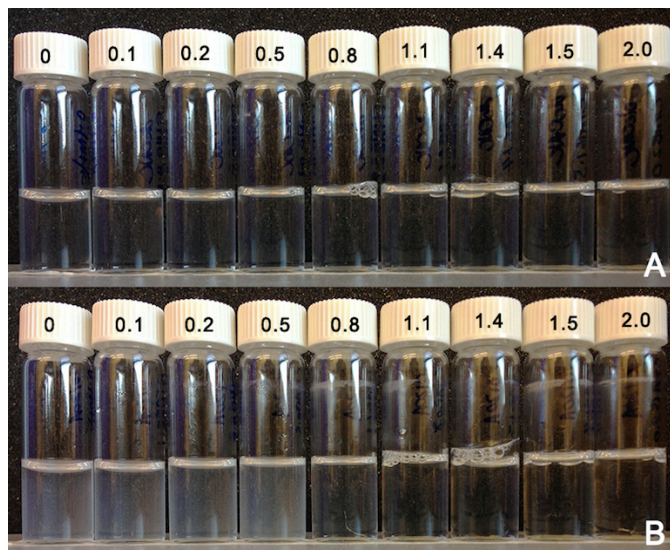


Figure 4.9 Image of dcCNC (A) and dcCNC-CD (B) suspensions with increasing CTAB concentration (mM).

In conclusion, host-guest interactions between dcCNC-CD and CTAB were observed in all the measurements resulting in significant change in the behavior of the nanoparticles. The inclusion complex induced aggregation facilitated the CTAB micellization on surface of dcCNC-CD and reduced the amount of free monomers over a wide range of CTAB concentrations. Furthermore, the aggregation was found to be more significant at higher temperature. This effect is considered beneficial in personal care applications for the efficient remover of dirt as well as reduced irritations due to a lower level of free surfactant monomers. In addition, although there was no considerable electrostatic interaction, dcCNC can also induce surfactant aggregation at high CTAB concentrations. However, this interaction is not as energetic and discernable since the hydrophobic attraction between CTAB tails and dcCNC backbone is somewhat weak.

4.3.5 Interactions between dcCNC, dcCNC-CD and anionic surfactants

The interactions between anionic surfactant, sodium dodecyl sulfate (SDS), and cationically modified CNC nanoparticles are very similar to that of other oppositely charged surfactant/polyelectrolyte systems with respect to the electrostatic attractions. It was reported that adsorbed surfactant ions on oppositely charged groups can act as nucleating sites for cluster formation of additional surfactant monomers. This process is similar to the polymer induced aggregation in ionic surfactant/non-ionic polymer systems, but is more energetic and favorable.¹⁷⁴ However, due to the crystalline nature of CNC, its limited flexibility hinders the conformational changes when interacting with surfactant micelles, as well as the hydration of polymer backbone by the hydrophobic core of micelles. These aspects result in different interfacial and solution behaviors of cationic CNC nanoparticles in the presence of anionic surfactants when compared to water-soluble and flexible cationic polyelectrolyte, such as poly(ethyleneimine), polyacrylamide, etc.

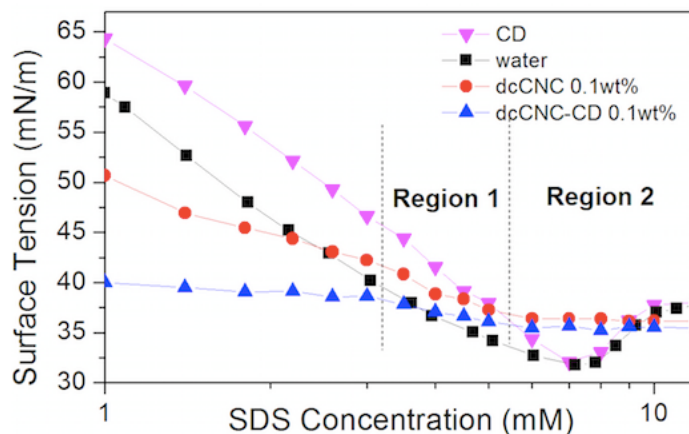


Figure 4.10 Surface tension of water, 0.35mM β -CD, 0.1 wt% dcCNC and 0.1 wt% dcCNC-CD with increasing SDS concentrations.

In surface tension measurements of water and β -CD solution with increasing SDS concentrations, an increased cmc was observed in the presence of β -CD due to the host-guest interactions between SDS hydrophobic tails and β -CD cavity, which reduced the amount of free monomers at the air-water interface, resulting in a higher surface tension comparing to water. For the 0.1 wt% suspension of dcCNC and dcCNC-CD, electrostatic interaction played a major role in the co-adsorption of polymer and surfactant to the air-water interface. The surface tension of dcCNC-CD below $C_{SDS}=4$ mM was lower than that of dcCNC due to the partially hydrolyzed GTMAC and the higher hydrophobicity. The curves of both dcCNC and dcCNC-CD displayed similar profiles, which can be divided into three regions. In

Region 1, part of the SDS monomers titrated to dcCNC/dcCNC-CD suspensions were adsorbed on the nanoparticles due to electrostatic interactions, thus the surface tension decreased at a slower pace than that in water. On the other hand, similar association of positively charged CNC particles and SDS monomers took place at the air-water interface, which also inhibited further adsorption of surfactants. At the end of Region 1, hydrophobic tails of adsorbed SDS nucleated more SDS monomers to form aggregates on cationic CNC particles surface. These complexes became more hydrophilic and they gradually desorbed from the interface in Region 2. In contrast to the ionic surfactant/non-ionic polymer systems, there was no plateau above the c_{ac} , which can be explained by the lack of conformational change of polymers due to the rigidity of CNC nanoparticles. After the cationic CNCs were completely transported from the air-water interface, the surface tension reached the value of polymer-free SDS solutions in Region 3. Furthermore, the "valley" near the cmc of SDS caused by impurities in SDS disappeared in the presence of cationic CNCs, indicating that the impurities were solubilized within the polymer induced SDS aggregates at concentrations below the cmc, which precluded them from partitioning to the air-water interface. This observation is in agreement with the preference of impurities to be solubilized in micelles than participating to air-water interface upon micellization.

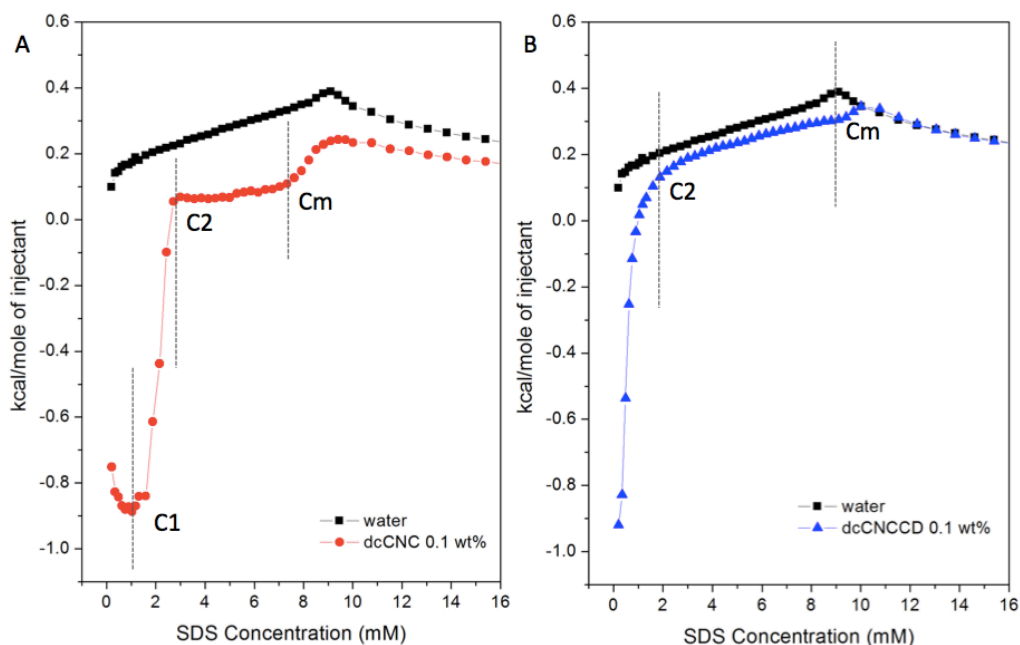


Figure 4.11 Thermograms of SDS titration to (A) water and dcCNC 0.1 wt%, (B) water and dcCNC-CD 0.1 wt%.

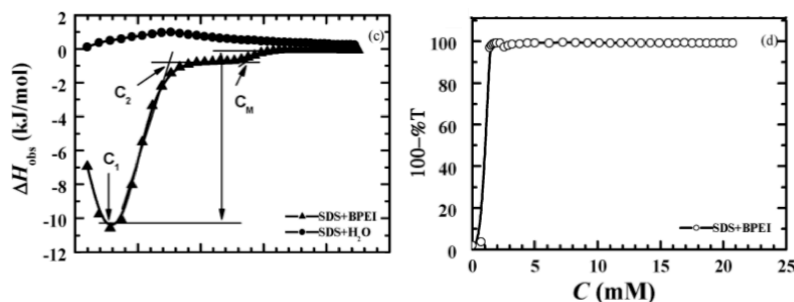


Figure 4.12 ITC curve for titrating 50 mM SDS into pure water and branched PEI solution (c) and (d) corresponding transmittance % curve.¹⁹⁶

Although cationically modified CNC nanoparticles are rigid rod-like polymers that behave differently from flexible polymers at air-water interface, their interactions with anionic surfactant SDS characterized by ITC were very similar to SDS/poly(ethyleneimine) (PEI) systems under various pH values respectively.¹⁹⁵ Thermograms of SDS/dcCNC and SDS/dcCNC-CD titration at 28 °C are shown in Figure 4.11. There were three distinct critical concentrations that could be assigned to SDS/dcCNC thermogram. C_1 designated as the first exothermic peak at $C_{\text{SDS}}=0.1$ mM, beyond which enthalpy change increased rapidly until C_2 . Upon the titration of SDS, the anionic headgroups bound to high-affinity sites of dcCNC cationic groups through electrostatic attraction. As evident from the phase separation images (Figure 4.13), light precipitations were observed at $C_{\text{SDS}}=0.5\sim 2$ mM, while at 2 mM large flocculates can be seen in the upper solution, indicating a structural change of the aggregates at C_2 (Figure 4.11A). A plateau was observed with increasing SDS concentrations till C_m was reached. At $C_2 < C_{\text{SDS}} < C_m$, SDS monomers tended to aggregate around the hydrophobic tails of bound SDS monomers on dcCNC, which increased the hydrophobicity of the particles. The aggregates were partitioned to the air-water interface due to the enhanced hydrophobicity. Formation of large and loose dcCNC clusters was observed from the transmittance results and was attributed to the interactions of the hydrophobic tails of adsorbed SDS. At $C_{\text{SDS}}=5$ mM, the precipitates disappeared and large clusters of aggregates floated to the upper half of the solution. Beyond C_m , the dcCNC clusters were fully saturated with SDS aggregates, hence free SDS micelles started to form in the bulk solution and ΔH gradually decreased and followed the trend of the dilution curve. The binding isotherm of SDS/dcCNC resembled the interaction between SDS and branched PEI at pH 10, where the polymer-induced aggregation was not able to dehydrate the polymer backbone into micelle cores and rehydrate at higher concentration as in the case of SDS and linear PEI interactions. (Figure 4.12) This can be explained by the strong steric hindrance of the hyperbranched structure of branched PEI that hindered the transfer of EI groups from water to the dehydrated micelle

core. Similarly for dcCNC, the crystallinity of dcCNC backbone prevented the rehydration thus only the ΔH of SDS aggregation was detected.

In SDS/dcCNC-CD thermogram (Figure 4.11B), C_1 was not discernable due to the hydrolysis of GTMAC on dcCNC-CD. Since less binding sites were available for SDS, the ΔH started to increase at a very low concentration and reached C_2 at $C_{SDS}=2.0$ mM. However, we noticed from the phase separation images (Figure 4.13) that the structure of the precipitates in this concentration range was not as compact as those in SDS/dcCNC, suggesting that different interactions might have occurred. Considering the host-guest interaction between SDS and β -CD, it was likely that the headgroup of included SDS also bound to the charge groups on dcCNC-CD nanoparticles in vicinity facilitating the bridging of the particles to form multi-chain aggregates. Since the electrostatic interaction was weaker than SDS/dcCNC, the identical ΔH of -0.92 kcal/mol at both C_1 also suggested the existence of exothermic host-guest interactions. Unlike SDS/dcCNC, the ΔH of dcCNC-CD did not display a plateau following C_2 . Instead, it gradually increased in parallel to SDS dilution curve until it reached C_m . Also, the clusters did not adsorb at the air-water interface due to the clusters becoming less hydrophobic. These were attributed to the reduced hydrophobicity of bound SDS monomers forming inclusion complex with β -CD. In addition, the surfactant aggregations on cluster surface also enhance the hydrophilicity of dcCNC-CD clusters. Since there are less conformational rearrangement involved, less heat was released during this process as reflected in the binding isotherm.

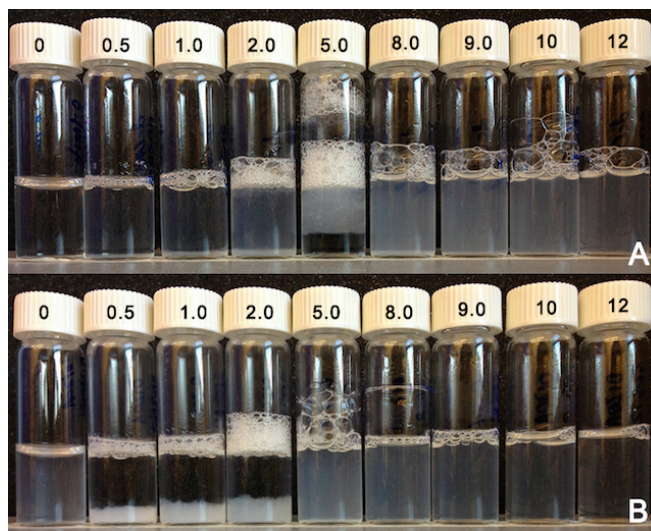


Figure 4.13 Phase separation of (A) dcCNC 0.1 wt% and (B) dcCNC-CD 0.1 wt% with increasing SDS concentrations in mM.

By comparing the transmittance, zeta potential and conductivity measurements of SDS/dcCNC and SDS/dcCNC-CD, it was found that at below $C_{\text{SDS}}=C_1$ in SDS/dcCNC, $T\%$ and zeta potential decreased less rapidly than at $C_1 < C_{\text{SDS}} < C_2$, which suggested that electrostatic binding was not a cooperative process. (Figure 4.14) Only after the charged groups were partially neutralized and hydrophobicity of dcCNC increased, did cooperative binding take place, which included both electrostatic and hydrophobic interactions, resembling those between SDS and linear PEI at low concentration range. However, due to the higher hydrophobicity of dcCNC-CD as well as the existence of host-guest interaction, which took place at the first SDS injection, cooperative binding was observed from the beginning in SDS/dcCNC-CD system. Furthermore, C_2 in both systems was at the concentration where zeta potential approached 0 mV, confirming that electrostatic interactions between SDS and dcCNC-CD dominate. After the complete neutralization of positively charged dcCNC or dcCNC-CD, SDS monomers started to aggregate due to hydrophobic attraction of the alkyl chains. The zeta potential of SDS/polymer clusters was further reduced to negative values upon the addition of SDS, which then levelled off when $C_{\text{SDS}}=C_m$, and aggregation and charge accumulation ceased. In addition, the inflexion points of both conductivity titration curves also corresponded to the free micelle concentration C_m in the thermograms, indicating a continuous growth of SDS aggregates on the CNC until free micelles started to form. Another very interesting observation in the transmittance measurements showed that dcCNC/SDS clusters cannot be completely redispersed, and only a $\sim 30\%$ recovery compared to 100% recovery for SDS/dcCNC-CD. This indicates that the mechanisms driving the dcCNC and dcCNC-CD interactions are different.

In the system of ionic surfactant and oppositely charged polyelectrolyte, especially inflexible polymers, charge density and hydrophobicity of the polymer have significant influence on their interactions. It is well-known that ionic strength can shield the surface charge of both polyelectrolyte and surfactant micelles to reduce the electrostatic repulsions. Thus, they are expected to have significant impacts on the surfactant/polyelectrolyte interaction of our system as well.¹⁷⁹ Thereafter, we performed ITC titrations of SDS to dcCNC and dcCNC-CD at varying NaCl concentrations in order to study the influence of charge density on the behavior of our inflexible nanoparticles. In the SDS dilution curves, the cmc decreased with increasing NaCl concentration due to the diminished electrostatic repulsion between negative head groups, thus in the binding isotherm of SDS/dcCNC and SDS/dcCNC-CD, the concentration was normalized by the corresponding cmc in order to eliminate the effects of micellization. (Figure 4.15) When electrostatic binding of SDS neutralized the surface charge, the hydrophobicity of polyelectrolyte was enhanced and the system resembled that of non-ionic polymer in SDS solutions,

where hydrophobic interactions dominated and became the driving force of polymer-induced surfactant aggregation. Similarly to SDS/dcCNC, increasing amounts of surface charge were shielded by the additional counterions, thus the cooperative binding was facilitated by hydrophobic interaction indicated by an increasing C_2 . At $C_{\text{NaCl}}=0.1$ M, C_2 was even higher than the cmc due to the prolonged binding process, and the formation of free micelles was delayed. For SDS/dcCNC-CD system, only in 0.1 M NaCl, an endothermic ΔH was observed at $C/\text{cmc}=1$. This peak was attributed to the fact that more heat was need to re-dispersing the dcCNC-CD clusters due to the enhanced hydrophobicity.

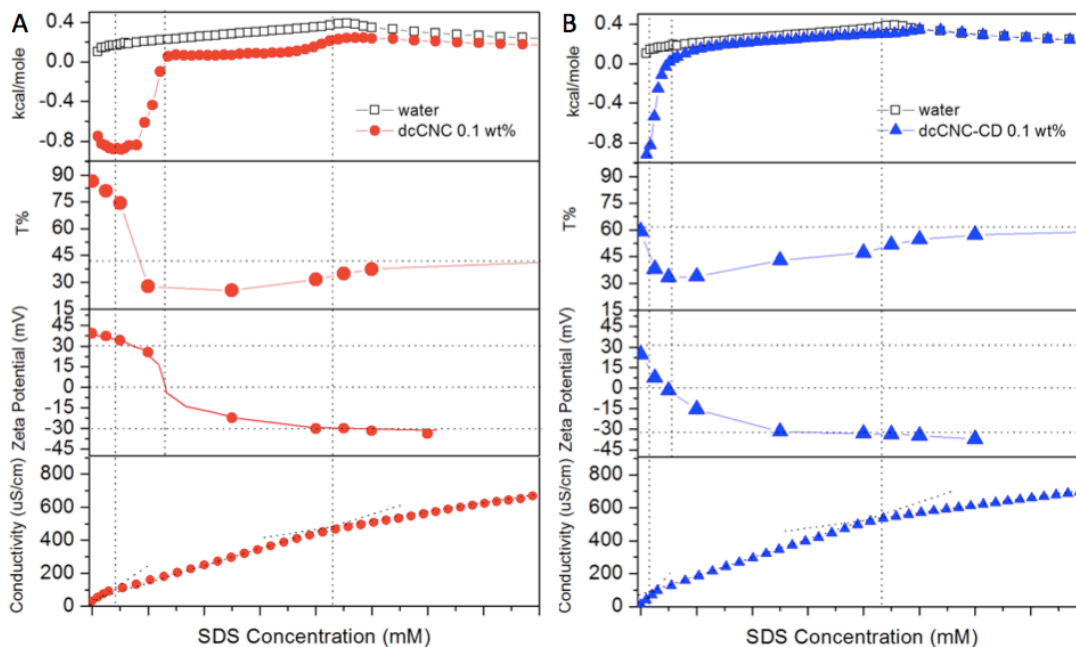


Figure 4.14 Comparison of ITC thermogram, transmittance%, zeta potential and conductivity measurements of (A) SDS/dcCNC and (B) SDS/dcCNC-CD with increasing SDS concentration.

Concentration of dcCNC and dcCNC-CD was kept at 0.1 wt% in all the measurements.

Oppositely charged SDS monomers are bound to dcCNC and dcCNC-CD via electrostatic and hydrophobic interactions. The surfactant bound complex induced aggregation and the dcCNC clusters cannot be completely dissociated compared to the dcCNC-CD system. It was reasoned that bridging of β -CD inclusion complex loosened the structure of nanoparticle clusters thus made it easier to be redispersed. These observations also confirmed that due to the rigidity and crystallinity of dcCNC and dcCNC-CD nanoparticles, intramolecular binding and polymer chain solubilization were not likely to occur. Therefore, multi-chain aggregates formation and disassembling were observed in both system, and the

structure depended on the change of charge density as well as hydrophobicity of cationic nanoparticles.

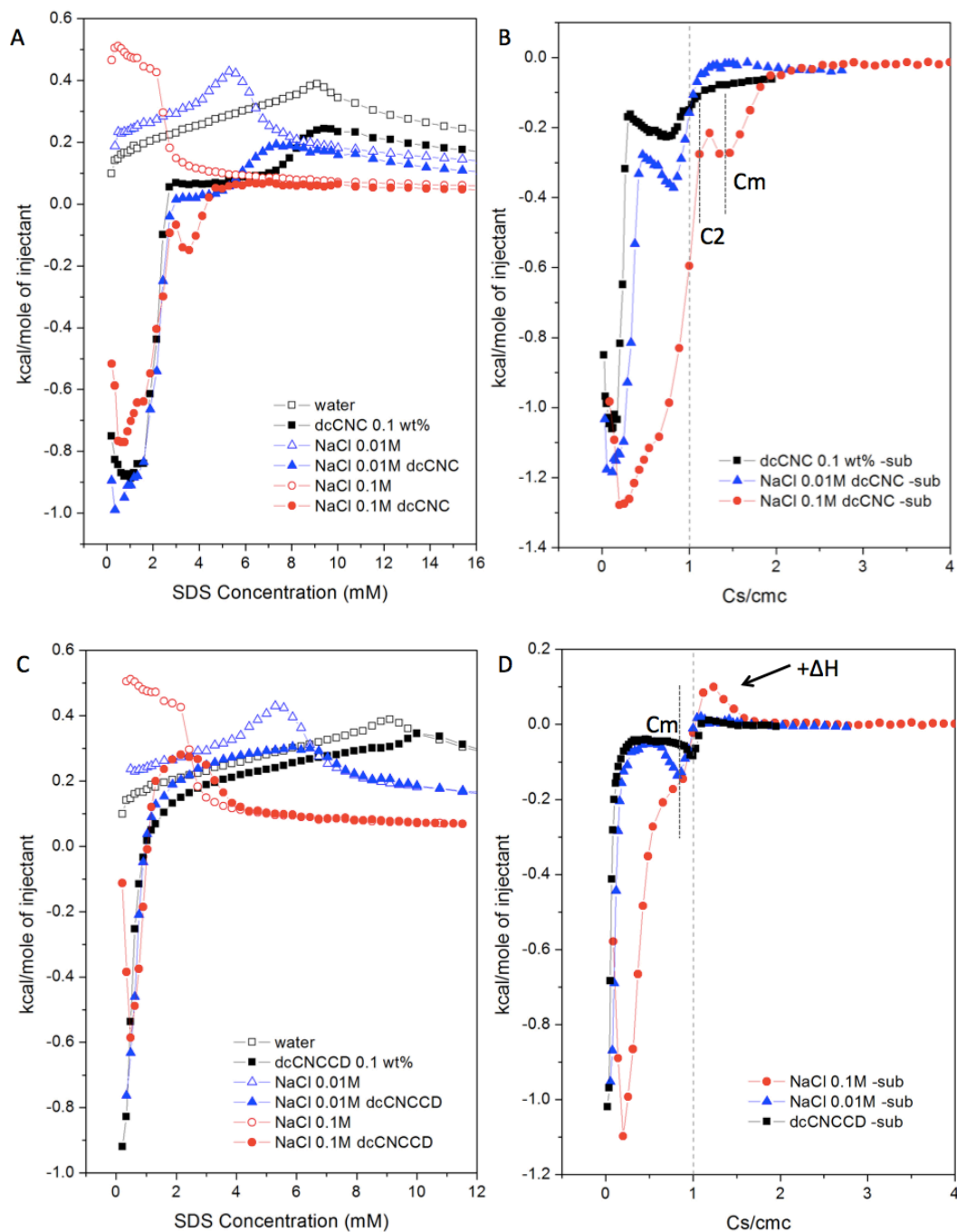


Figure 4.15 Thermogram SDS titration to (A) dcCNC 0.1 wt% and (C) dcCNC-CD 0.1 wt% with 0, 0.01 M and 0.1 M of NaCl in solution. (B) and (D) are enthalpy curves in (A) and (C) corrected by subtracting corresponding SDS dilution curves respectively.

4.4 Conclusions

In this chapter, desulfation, cationization of CNC and the synthesis of dcCNC-CD were performed and characterized. The grafting ratio of β -CD was determined by PHTH method and found to be higher in CNC-CD system. Measurements of surface tension, binding isotherm, transmittance, phase separation, zeta potential and conductivity showed different behavior in the cationic CNC nanoparticles upon grafting with β -CD. The formation of inclusion complex between β -CD and surfactants can induce surfactant aggregation on the surface of cationic CNC that dissociate the nanoparticle aggregates at concentrations below and above cmc, respectively. The impacts of temperature on CTAB binding as well as ionic strength on SDS binding were also studied and discussed. It was found that aside from the influence of host-guest interactions, structures of surfactant/polymer aggregates was also affected by changes in the charge density and hydrophobicity due to the crystallinity and rigidity of dcCNC and dcCNC-CD nanoparticles. The formation and structure of mixed layer co-adsorbed at the air-water interface, and the conformational rearrangement of dcCNC, dcCNC-CD induced aggregates at increasing surfactant concentration. This phenomenon can be further elucidated using ellipsometry, X-ray and neutron reflectivity to provide further evidence on the different mechanisms in their interactions with ionic surfactants. In view of the vast applications of surfactant/polymer solutions, studies on wetting, drop breakage, two-phase flow, emulsification and emulsion stability, as well as surface dynamic behaviors such as adsorption kinetics and surface rheology would provide critical information for the practical use of dcCNC-CD in personal care products.

5 Influence of 1-dodecanol on the Adsorption and Thermodynamic Properties of Sodium Dodecyl Sulfate Micellar Solution

5.1 Introduction

Sodium alkyl sulfates have attracted wide spread interests due to their wide-ranged scientific and technological applications.^{197,198} The most common, sodium dodecyl sulfate (SDS) has been extensively used as a model surfactant in the surface and colloidal science researches.¹⁹⁹ However, due to the synthesis or hydrolysis of SDS, n-dodecanol was frequently observed as a major contaminant in SDS and can be very difficult to remove.^{200,201} Different process has been achieved in developing surfactant purification procedures and criteria.²⁰²⁻²⁰⁴ Theoretical and experimental studies on the dominant effect of trace amounts of n-dodecanol on the co-adsorption of SDS/n-dodecanol systems from aqueous solutions and the comparison to single surfactant solutions have attracted special interests and corroborated in many studies.²⁰⁵⁻²⁰⁸ Techniques such as surface tensiometry^{200,201}, radiotracer technique²⁰⁹, foam fractionation²¹⁰, Brewster angle microscopy (BAM)²¹¹, and neutron reflection²¹² have been used to study the SDS/dodecanol system at the air-water interface. The co-adsorption of SDS/dodecanol at solid-water interface has also been characterized using sum-frequency spectroscopy.^{206,207} It was well accepted that adsorbed pure SDS monolayers do not show phase transition even at bulk concentration higher than the cmc and at low temperature. Whereas, even with trace amounts of n-dodecanol, condensed domains in the adsorbed n-dodecanol monolayer was detected, and a first-order phase transition and subsequent growth of condensed phase domains were observed by Fainerman et al.²¹³ They studied two-dimensional phase behavior during the kinetics and the features of the condensed phase by performing BAM investigations. Similar adsorption and phase behavior of SDS/n-dodecanol system were also analyzed by Vollhardt et al.²⁰⁸ using equilibrium surface pressure measurements, surface pressure transients and BAM. They concluded that depending on the mixing ratio and system conditions, such as bulk concentration and temperature, a phase transition may or may not occur. Comparable surface concentration could be determined under the conditions that phase transition was absent.²⁰⁸

The pronounced effects of n-dodecanol on the co-adsorption of SDS/dodecanol mixtures are attributed to the considerable higher surface activity of n-dodecanol compared with SDS, which results in phase transition and condensed phase domains at air-water interface even when n-dodecanol is present in trace amounts. The effects of the presence of aliphatic alcohols on the micellar solution have also been widely studied. The role of alcohols was considered to be crucial in the formation of microemulsions.²¹⁴ From a practical point of view, addition of alcohols induces large reduction in the viscosity of micellar

systems, which is especially useful in tertiary oil recovery. Moreover, they are able to strongly accelerate the equilibrium and decrease the adsorption of co-surfactants in the pores of the rock in the oil field due to their stronger activity. Thus, addition of alcohols to surfactant systems can be used to increase the efficiency and decrease the cost of tertiary oil recovery process.²¹⁵ Researchers have also reported from a fundamental point view that the effects on dynamic character of microemulsions by the presence of alcohol can enhance their formation and stability. These facts explained the importance of characterizing the effects of alcohols on the dynamics of micellar solutions. It is possible to consider alcohols as non-ionic surfactants and theories of mixed-micelle formation can be used in such systems to analyze the effect of hydrophobic interactions on the micellar structure, composition and thermodynamic properties.²¹⁶ Moya et al.²¹⁷ used regular solution theory to obtain information on micelle formation and composition when interacting with long-chain alcohol n-octanol and cetylpyridinium chloride (CPC). Similar method was also used by Treiner et al.²¹⁸ to study mixed micelles of 1-pentanol-binary system. But they considered the alcohol as solubilize instead of a third surfactant component due to the fact that solubilized alcohols oriented in a way similar to surfactant molecules in micelles.²¹⁹ More studies on the effect of alcohols were used to evaluate the theory of micellar solubilization. The techniques used to study this phenomenon include vapour pressure²²⁰, overall solubility²²¹, decrease of cmc^{222,223}, fluorescence²²⁴, Krafft point depression and calorimetry²²³.

The trace amounts of lauryl alcohol-induced formation of aggregates below the cmc was reported by Phillips et al. using light scattering.²²⁵ They found that above the cmc, alcohols were completely solubilized in the micelles of SDS without contributing to any light scattering intensity increase. Also the micelle structure was not significantly affected in the presence of alcohols. While, a new and finely defined phase was formed below the cmc even in SDS solution with trace amount of alcohol, which is represented by a strong peak of scattering intensity in the region of cmc. This peak was initially assigned to be associated to the released impurities as micelle deconstructed below the cmc, however it was later reported to be associated with the adduct LOH/2SDS aggregates that was induced by the presence of LOH.²²⁶ The lower concentration of the appearance of the peak was associated to the solubility of the alcohol in the surfactant solution. This concentration representing the water-solubility was considered to largely depend on the concentration of surfactant rather than alcohol and the minor variation was easily masked within the experimental error due to lack of sensitivity.²²⁶ Recently, Zhu et al.²²⁷ used automatic continuous mixing on a programmable Shimadzu HPLC pump equipped with a light scattering detector to monitor this phenomenon. Due to the high resolution of this technique, they observed considerable change in the water-solubility of dodecanol in SDS solutions with different loading ratio. Corti et al.²²⁸

used the light scattering technique to determine the size of these aggregates in SDS/dodecanol systems with different molar ratio. They reported that the radius of aggregates was approximately 500Å, which is about twenty times larger than SDS micelles, and it was not affected by SDS or dodecanol concentration, but only by the type of solubilizates. Thereafter, they concluded that the change of intensity in the light scattering peak was due to a variation in the aggregate number.

Studies on the effects of n-dodecanol solubilization on the surfactant's thermodynamic properties are limited, and most of the studies were conducted decades ago.²²⁹ The heat of solubilization and micellization were calculated using a two-phase theory and Gibbs-Helmholtz equation by measuring the amount of solubilization and cmc of the mixture, but thermodynamic parameters were hardly measured directly. Masahiko et al.²³⁰ reported a direct measurement of the heat involved in dodecanol solubilization using a twin differential conduction-type micro-calorimeter by adding various amounts of dodecanol into SDS micellar solution. The solubilization process was an exothermic process in which the heat of mixing increased with increasing amounts of dodecanol in SDS solution. Then an abrupt decrease in the heat was observed that was attributed to phase transformation: solubilization phase to emulsification phase, when the endothermic interaction between alcoholic and water molecules took place outside the SDS micelles.

In this study, the adsorption behavior and thermodynamic properties of 1-dodecanol/SDS (DDC/SDS) systems at different molar ratios were studied using surface tensiometry, light scattering and isothermal titration calorimetry (ITC) by keeping the molar ratio constant while increasing the total concentration. Adsorption of 1-dodecanol/SDS at water-air interface was described by surface concentration and explained by the change of surface activity of dodecanol as well as the mixture under various molar ratios. The influence of temperature on the adsorption was also discussed. Thermodynamic parameters of 1-dodecanol solubilization and SDS micellization were calculated and used to explain the solution behavior of DDC and SDS micelles. Distribution of 1-dodecanol in the system at various concentrations was determined, which can be used to predict the solution composition of systems with different DDC/SDS molar ratio.

5.2 Experimental section

5.2.1 Materials

Sodium dodecyl sulfate (SDS) (>99.0%), 1-dodecanol (DDC) (>99.0%), toluene (>99.9%) were purchased from Sigma-Aldrich and used without further purification. DDC was selected because it is the main source of the impurities in SDS as by-product of the synthesis or from hydrolysis of SDS in aqueous

solutions. The DDC and SDS mixture solutions with DDC/SDS molar ratio (R) 1:99, 2:98, 3:97, 4:96 and 5:95 were prepared by measuring the weight of chemicals then dissolved in deionized water. The SDS concentration in the mixtures was at least 4 times higher than the critical micelle concentration (cmc) of SDS (8 mM). All the solutions were prepared at least 24 hours before characterization in order to obtain the equilibrium of DDC solubilization in SDS micelles. The DDC/SDS molar ratio of the mixtures were kept constant in all the characterizations where quantities were measured with respect to the total concentration of the mixture and plotted against the SDS concentration. Deionized Millipore water was used in all the tests and measurements.

5.2.2 Surface tension

All the stock solutions of SDS and DDC/SDS mixtures (with R of 1:99 and 3:97) used for surface tension measurements were prepared by keeping the SDS concentration at 30 mM. Surface tension of DDC/SDS mixtures in aqueous solutions were measured on a DCAT 11(Dataphysics) tensiometer equipped with a water bath and an automatic dosing device, which is controlled by the software DCAT. The program used for titration was CMC increasing measurement with 30s of stirring and 30s of equilibrium after each titration. The dynamic surface tension at the air-water interface upon the titration of stock solution to 40 mL water was measured using Wilhelmy plate method at 15°C, 25°C and 35°C and plotted against SDS concentration in mM.

5.2.3 Light scattering

Light scattering measurements were performed on a Brookhaven BI-200SM goniometer and BI-9000AT digital correlator equipped with an argon-ion laser. An 800 nm filter was used to remove dust prior to all the measurements and the experimental temperature was controlled by a PolyScience water-bath at 25°C. The DDC/SDS stock solutions of R=1:99, 2:98, 3:97, 4:96 and 5:95 with SDS concentration of 100 mM were used for light scattering measurements. All the samples with various mixture concentrations were stock solutions diluted in water and equilibrated for 5 min. The counts per second of light scattering was measured at 90° for 3 min and the average was taken (designated as average counting rate, ACR). Then the excess Rayleigh scattering ratio at 90° (I_R) was determined via calibration of the known scattering of a standard solvent, toluene ($ACR_{std}=388.5$ cps). The excess Rayleigh ratio of toluene a good wavelength dependence described by equation:

$$I_{R, std} = (2.038 \times 10^6) \left(\frac{1}{\lambda^4} \right) - 6.893 \times 10^{-8} \quad \text{Equation 5.1}$$

where λ is the wavelength of the incoming light, which is 636 nm in this study. The $I_{R,std}$ was calculated to be $1.2387E-5 \text{ cm}^{-1}$. The calibration equation of ACR and I_R was:

$$I_R = I_{R,std} \times \frac{ACR_s - ACR_{slv}}{ACR_{std}} \quad \text{Equation 5.2}$$

where ACR_s , ACR_{slv} and ACR_{std} are the average counting rate of the sample, solvent (water) and toluene respectively. From the light scattering intensity correlation function, we obtained the approximation of $I_R = KM_w C$, and the M_w can be extracted from the equation²²⁷:

$$\frac{\partial I_R}{\partial C} = -KM_w \quad \text{Equation 5.3}$$

where $\partial I_R / \partial C$ is the slope in the I_R vs. SDS concentration plot.

5.2.4 Isothermal titration calorimetry

Isothermal titration calorimetry (ITC) was used to study the thermodynamic properties of DDC/SDS systems in aqueous solution. The instrument used was Microcal VP-ITC programmed to titrate DDC/SDS stock solutions of R=1:99, 2:98, 3:97, 4:96 and 5:95 loaded in a 282 μL syringe. SDS stock solutions with concentrations of 30 mM and 100 mM were used for the highest SDS concentration of 4.5 mM and 18 mM respectively. 1-10 μL of titrants were injected to a sample cell loaded with 1.455 mL of deionized water by a pre-programmed procedure. The titrations were conducted under 25°C for all the samples. Enthalpy change of each injection was measured, integrated and plotted against overall SDS concentration. The data used for analysis was corrected by subtracting the isotherm of SDS dilution in water.

5.2.5 Conductivity titration

SDS stock solution of 200 mM and DDC/SDS stock solutions of R=1:99, 2:98, 3:97, 4:96 and 5:95 with SDS concentration of 200 mM were used for conductivity measurements conducted on a Metrhm 809 Titando automatic titrator controlled by Tiamo software. Stock solutions were titrated to 20 mL of deionized water at the rate of 0.5 mL/min with a volume of 20 μL per injectant. All the measurements were conducted in a jacketed vessel under a stirring speed of 4, and the temperature was controlled at 25°C. Finally, the conductivity values were plotted against SDS concentration in mM converted from volume of stock solutions consumed.

5.3 Results and discussion

5.3.1 Surface co-adsorption of 1-dodecanol/SDS (DDC/SDS) before micellization

Surface tensions of water upon titration of SDS and DDC/SDS mixtures with molar ratio (R) of 1:99 and 3:97 (designated as $R=1:99$, $R=3:97$) were measured to investigate the co-adsorption of DDC/SDS on the air-water interface. (Figure 5.1) In the plot of surface tension vs. logarithm of SDS concentration at 25°C, a curvature was observed near the cmc of SDS in pure water (8 mM), which suggested that even trace amount of impurities in SDS has considerable effect on the adsorption behavior of SDS as previously reported.²³¹ The impurities are usually surface-active molecules from synthesis or hydrolysis of SDS that makes the purification very complicated. It was reported that with the increase of alkyl chain length, the surface activity of alcoholic impurities increased and was considerably higher than that of pure SDS.

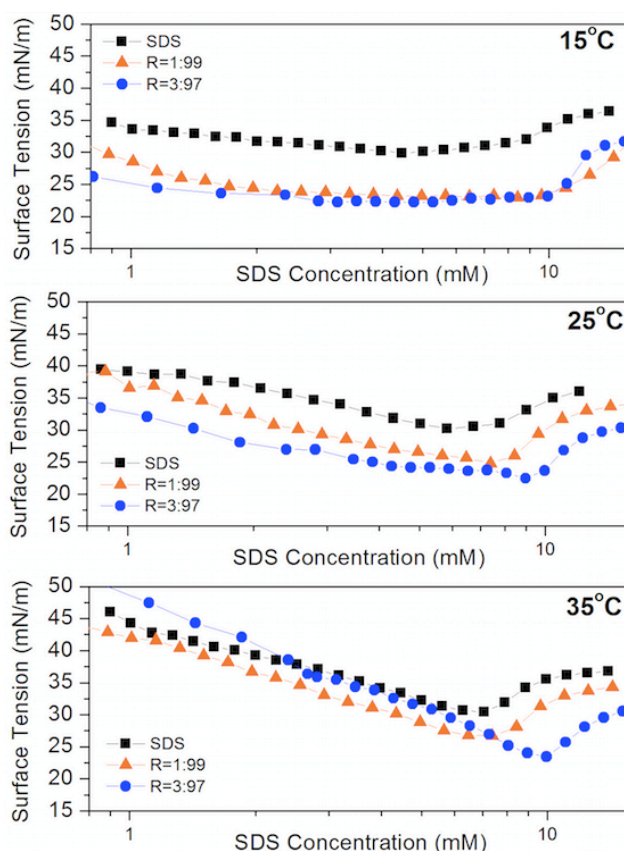


Figure 5.1 Surface tension of water upon titration of SDS, DDC/SDS of $R=1:99$ and $3:97$ were plotted against logarithm of SDS concentration in mM at 15°C, 25°C and 35°C.

As we can observe from the surface tension isotherms at 25°C, the surface tension values in the range of SDS concentration below the cmc decreased with increasing DDC/SDS molar ratio and tended

to level off at lower surface tension value at concentrations above the cmc. Similar effects of DDC addition were also observed at 15°C and 35°C. The minimum surface tension values of DDC/SDS mixtures are summarized in Table 5.1. The results show the positive effects of increasing R and negative effect of increasing temperature on DDC's ability to reduce the surface tension of solution. Furthermore, the adsorption was also affected by varying the temperature. The smaller slope at 15°C and larger slope at 35°C indicated an enhanced surface activity of DDC and stronger co-adsorption possibly due to stronger hydrophobic interactions between alkyl chains of SDS and DDC when the temperature was decreased, and vice versa at higher temperature. In order to investigate the adsorption process of DDC/SDS mixture quantitatively, determination of the surface concentration of the solution is one of the most applied methods.

Table 5.1 Minimum surface tension in the isotherms of SDS, R=1:99 and R=3:97 at 15, 25 and 35°C.

Surfactant Mixtures	Minimum surface tension (mN/m)		
	15°C	25°C	35°C
SDS	30.1	30.2	30.4
R=1:99	23.2	24.8	26.7
R=3:97	22.3	22.5	23.0

The characterization of multi-component surfactant systems is rather complicated. However, it can be realized for two-component surfactant systems with assumptions of ideality: one is the absence of surface interactions, another is the maximum surface concentration of both components are approximately the same.²⁰⁰ Thereafter, the surface tension of the two-component solution can be expressed by the generalized Von-Szyszkowski equation:

$$\pi = RT\Gamma_m \ln \left(1 + \frac{c_1}{a_1} + \frac{c_2}{a_2} \right) \quad \text{Equation 5.4}$$

where $\pi = \gamma_0 - \gamma$ is the surface pressure (γ_0 and γ are the surface tension of pure water and the mixture solution, respectively), R is the gas constant, T is the absolute temperature, Γ_m is the maximum surface concentration, c_1 and c_2 are monomer concentrations of two surfactants, a_1 and a_2 are surface activity parameters of each surfactant. By fitting this equation with surface tension data, the adsorption parameters Γ_m , a_1 and a_2 were obtained and summarized in Table 5.2. The calculated results of a_1 and a_2 of R=1:99 at 25°C were comparable with the reported results of $a_1=3.67 \times 10^{-6}$ mol/cm³ and

$a_2=3.7\times 10^{-9}$ mol/cm³.²⁰⁸ The ratio of a_1/a_2 being significantly large demonstrated the considerably higher surface activity of DDC in comparison to SDS. Furthermore, the increasing surface activity was reflected by a decreased a_2 at low temperature, as well as the fact that the a_1/a_2 ratio increased dramatically when temperature was decreased to 15°C and the reverse was true when temperature was increased to 35°C (Figure 5.2), indicated the negative impact of temperature on the hydrophobic interaction between alkyl chains of SDS and DDC as interpreted by directly observing surface tension isotherm. (Figure 5.1) The temperature effects on the adsorption activity corresponded with the conclusion drawn by Vollhardt et al.²³² They calculated the standard free energy for the adsorption using the equation proposed by Rosen et al.²³³, which led to an almost zero value of the standard enthalpy of adsorption calculated from Gibbs-Helmholtz equation. The results were used to explain the decrease in the n-dodecanol adsorption activity with increasing temperature. The decrease in the standard entropy in adsorption was explained as the disordering that occurred in the bulk solution.²³⁴

Table 5.2 Characteristic adsorption parameters calculated by fitting experimental data to Equation 5.4.

	Component	a_1 (mol/cm ³)	a_2 (mol/cm ³)	Γ_m (mol/m ²)
15°C	SDS	2.19×10^{-11}	--	9.73×10^{-7}
	R=1:99		1.81×10^{-17}	7.60×10^{-7}
	R=3:97		3.75×10^{-20}	6.15×10^{-7}
25°C	SDS	7.18×10^{-6}	--	2.54×10^{-6}
	R=1:99		5.60×10^{-9}	2.05×10^{-6}
	R=3:97		1.39×10^{-11}	1.22×10^{-6}
35°C	SDS	3.12×10^{-5}	--	2.97×10^{-6}
	R=1:99		6.23×10^{-7}	3.03×10^{-6}
	R=3:97		1.84×10^{-6}	4.84×10^{-6}

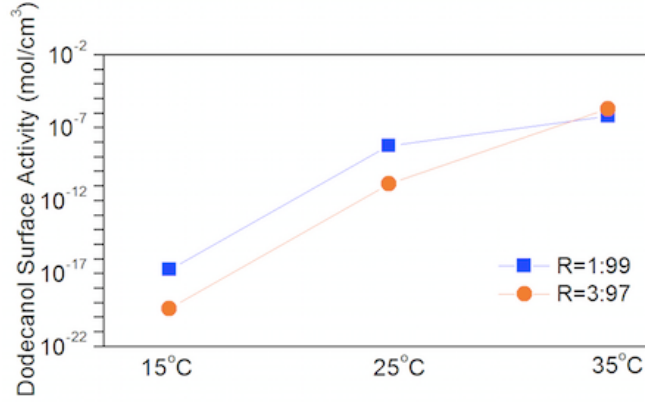


Figure 5.2 Surface activity of DDC at different temperature and DDC/SDS molar ratio.

Using the procedure described above to determine the surface activity parameter a_2 of highly surface-active substances with poor water-solubility, such as dodecanol, is highly desirable, due to the difficulty in using other methods. With the surface activity parameters of SDS and DDC determined, we can further obtain the overall surface activity parameter a^0 using Equation 5.5:

$$\frac{1}{a^0} = \frac{1}{a_1} + \frac{c_2}{c_1 a_2} \quad \text{Equation 5.5}$$

The calculated a^0 values of R=1:99, R=3:97 with increasing temperature were plotted in Figure 5.3. The y-axis is in logarithm scale for the ease of comparison. The overall surface activity parameters increased with R, indicating a positive effect of DDC addition on the surface activity of SDS, which was significant at low temperature due to the co-adsorption process, while it diminished when temperature was increased. Furthermore, the surface coverage per molecule, A^0 (nm²), at equilibrium could be determined from the maximum surface concentration Γ_m values using Equation 5.6, where N_A is the Avogadro constant (6.02×10^{23}), and summarized in Table 5.3. The A^0 values of SDS and R=1:99 at 25°C agreed with the literature values⁴⁰. The larger A^0 values indicated stronger co-adsorption due to the increase in the overall surface activity by the synergistic effects of DDC.

$$A^0 = \frac{1}{\Gamma_m \times N_A} \quad \text{Equation 5.6}$$

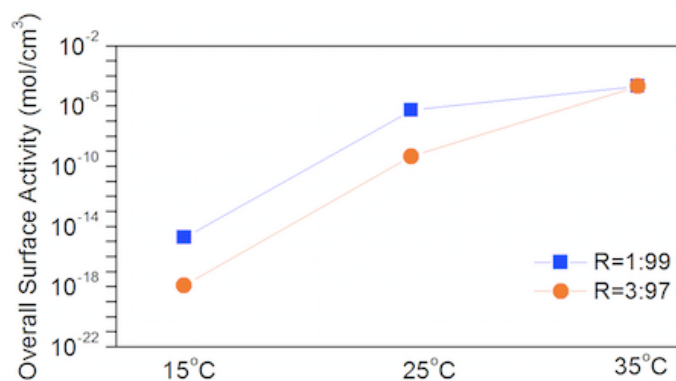


Figure 5.3 Overall surface activity parameters of DDC/SDS with R=1:99 and 3:97 at 15°C, 25°C and 35°C.

Table 5.3 Surface coverage area per molecule A⁰ of SDS, R=1:99, R=3:97 at 15°C, 25°C and 35°C.

A ⁰ (nm ²)	15°C	25°C	35°C
SDS	170	65.5	55.9
R=1:99	218	80.9	54.9
R=3:97	270	136	34.3

It should be pointed out that the maximum surface concentration of surfactant systems can be calculated from the surface tension isotherm using the Gibbs equation:

$$\Gamma_m = -\frac{\partial\gamma/\partial(\ln c)}{RT} \quad \text{Equation 5.7}$$

where R is the gas constant, T is absolute temperature and $\partial\gamma/\partial(\ln c)$ is the slope of the linear region of surface tension isotherm. The Gibbs equation was applied with the assumption that the Γ is a constant in the linear region since the interface is saturated within the region.⁴⁰ Nevertheless, Menger et al.²³⁵ directly measured the surface concentration Γ of SDS solution upon the titration and the interfacial adsorption was monitored by a flow-proportional counter. They discovered that the air-water interface was far from saturated at the beginning of the linear region and the percentage of coverage was determined to be only 67%. (Figure 5.4) The steep drop in the plot reflected the progressive occupancy of the interface in the pre-micellization region. Thus, this region is by no means reflecting saturation and does not demand a constant surface concentration. However, since the interfacial packing in this region is relatively high

(>80%), the Gibbs equation-based surface concentration results were found to depart from ideality by a factor of only 2 or less when compared with direct area measurements such as radioisotope methods. Furthermore, the increased surface activity of DDC/SDS mixtures with higher R and at low temperature led to surface tension isotherms that were quite different from the empirical ones for single surfactant solutions. Therefore, the determination of the linear region was difficult under certain experimental conditions and it was preferable to use the fitting of generalized Von-Szyszkowski equation to calculate the maximum surface concentration.

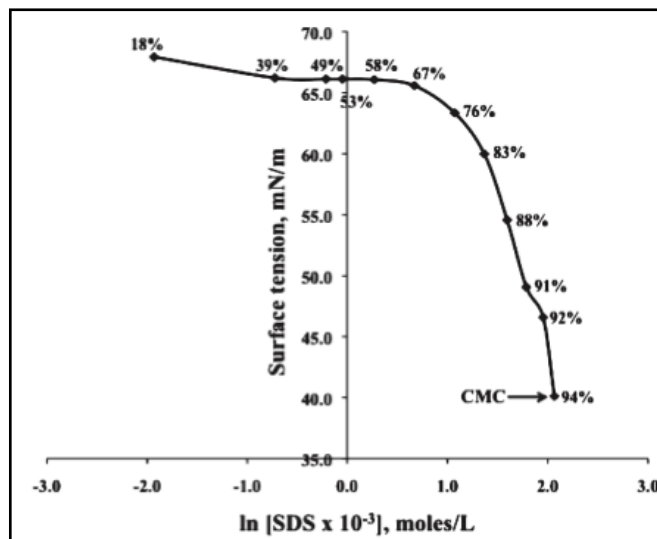


Figure 5.4 Plot of surface tension vs. ln(SDS concentration) for pre-cmc concentrations with the percent surface coverage written above the points.²³⁵

Based on the above theory, it will be useful to analyze the surface concentration profile of our systems to gain a better understanding on the effects of R and temperature on the DDC/SDS co-adsorption behavior with increasing mixture concentration. The surface concentration Γ was calculated using the extended Langmuir equation:

$$\Gamma = \Gamma_m \times \frac{c}{a_2 \left(1 + \frac{c_1}{a_1}\right) + c} \quad \text{Equation 5.8}$$

where, c is the SDS concentration, c_1 is the cmc of the mixture measured by conductivity titration, a_1 and a_2 are surface activity parameters obtained previously. This analysis provided information on the adsorption process and degree of surface saturation at pre-micelle region by comparing the effects of R and temperature. In the plot of normalized Γ vs. SDS concentration of DDC/SDS with R=1:99 and

R=3:97 at increasing temperatures (Figure 5.5), the curves overlapped as expected for R=3:97 at 35°C. The Γ curves collapsed onto a master curve indicated that the degree of saturation was not dependent on temperature when R was small, while in the mixture with larger R, increasing the temperature resulted in a delayed saturation concentration that was possibly due to a larger amount of DDC partitioning to the air-water interface, as reflected in the value of Γ_m .

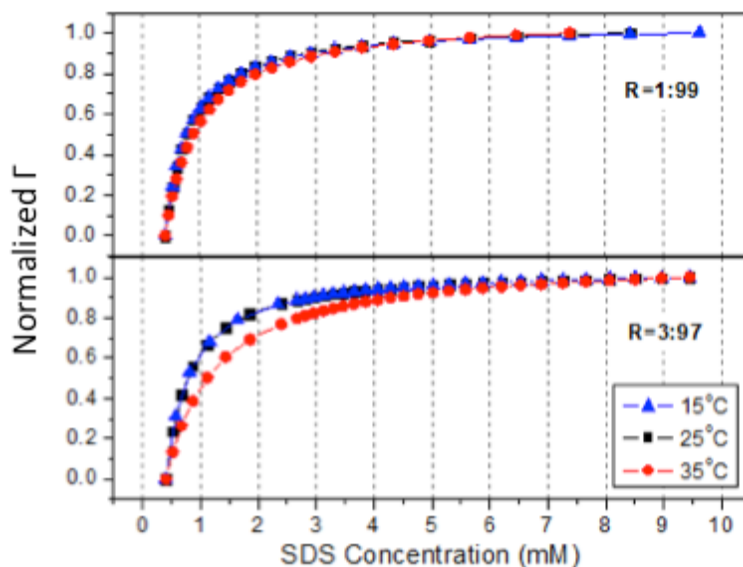


Figure 5.5 Plots of normalized Γ vs. SDS concentration showing the effects of temperature (at 15°C, 25°C and 35°C) on the surface concentration of R=1:99 and R=3:97.

In addition, the Γ values were divided by Γ_m to compare the degree of adsorption in DDC/SDS with increasing R. (Figure 5.6) At 15°C and 25°C, the degree of adsorption of R=3:97 was approximately 10^3 times higher than R=1:99, indicating higher overall surface activity. This also explained the fact that due to the saturation of the air-water interface by highly surface-active DDC, their surface tension became insensitive to concentration increase and micellization at such conditions. Whereas, the two Γ/Γ_m curves were in the same order of magnitude at 35°C, they possessed similar a^0 values. Furthermore, Γ was significantly close to saturation at 15°C even at very low SDS concentration, and with increasing temperature, the degree of saturation decreased for both R=1:99 and R=3:97 due to the reduced surface activity of DDC with increasing temperature. This corresponded to the extended minimum surface tension region of surface isotherms at concentration below the cmc when measured at low temperature.

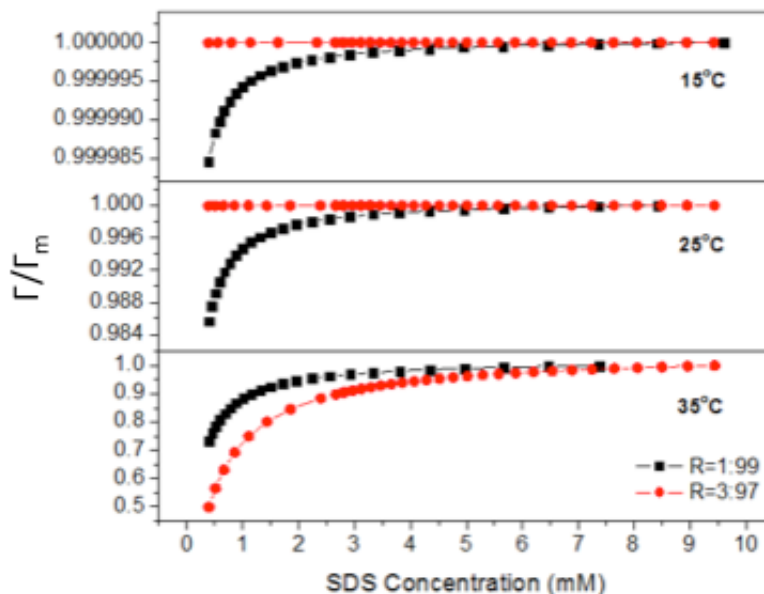


Figure 5.6 Plots of Γ/Γ_m vs. SDS concentration. The effects of DDC/SDS molar ratio on degree of saturation at 15°C, 25°C and 35°C.

Except for the DDC/SDS molar ratio and temperature, the adsorption properties of SDS were affected by other factors such as alkyl chain length and chain branching of the alcohol. It was found that at constant molar ratio of alcohol molecules, surface tension of SDS continuously decreased with increasing chain length of alcohols from C₈ to C₁₃, and the effect was enhanced with increasing alcohol content.²⁰⁸

5.3.2 Light scattering and isothermal titration calorimetry (ITC)

Excess Rayleigh scattering ratios (I_R) of DDC/SDS mixtures of different R were plotted against SDS concentration in Figure 5.7. Large scattering peaks can be observed in the samples in the presence of DDC and the peak amplitude increased with increasing molar ratio of DDC, while the overall shape of the peak remained the same. All the I_R curves approached the maximum value at a concentration above the cmc of the mixture (cmc*), which were determined using conductivity titrations. This peak was assigned to the light scattered by the large aggregates of DDC/SDS formed only at concentration near cmc*. Once the concentration increased beyond cmc*, a sharp drop corresponded to the disappearance of DDC/SDS aggregates, indicating that upon the formation of SDS micelles the aggregates dissociated due to the solubilization of DDC in the micelles. The negative slope of the I_R for mixture with different DDC ratio had similar slopes, which agreed with the observation reported by Zhu et al.²²⁷ Using the

intensity correlation function, they correlated the similarity of the slope to the molecular weight of DDC/SDS aggregates and drew the conclusion that the molecular weight of aggregates was virtually constant in all cases (1.95×10^7 g/mol), which was independent of DDC/SDS molar ratio (R). Due to the low resolution of the titration, the concentration of DDC solubilization in water was not detected as previously obtained using continuous mixing device in another study, whereas the strong dependence of the DDC water-solubilization concentration was not observed in our data. In order to precisely determine the critical concentrations of the solubilization process, techniques with higher resolution in the studied concentration range are necessary.

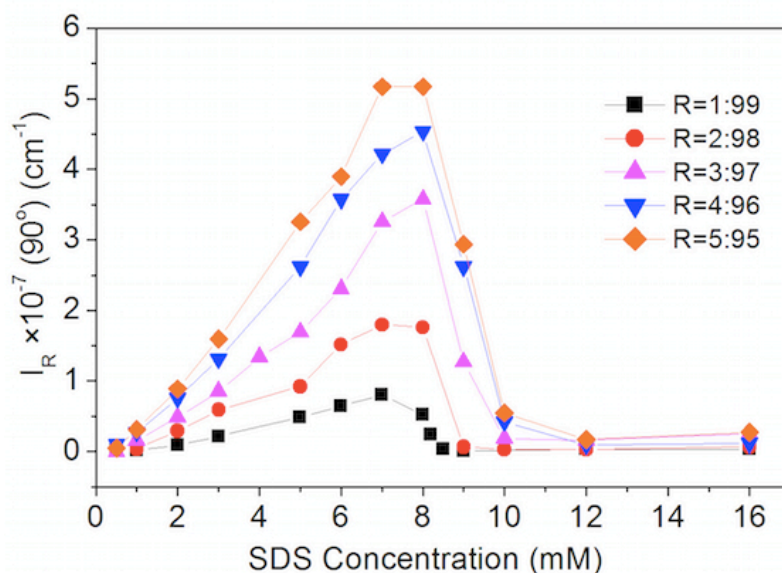


Figure 5.7 Light scattering of DDC/SDS mixture of various molar ratios at increasing SDS concentration.

Isothermal titration calorimetry (ITC) is a technique with high sensitivity that has been widely used to study the thermodynamic properties of mixed surfactant systems.²³⁶ Since ITC can titrate volume as small as 1 μ L, we were able to obtain a smaller concentration increment that led to plots with higher resolution. (Figure 5.8) The initial decrease at low concentration was due to the solubilization of trace amounts of DDC in water²³⁰. Thus, the first inflection point was assigned as the DDC water-solubilization concentration (C_i), which was not discernable in light scattering measurements (Figure 5.8B). There was no strong dependence of C_i on R, leading to different slopes for the aggregation process. This observation was different from previous study by Zhu et al., indicating that the size of DDC/SDS aggregates was not constant below cmc^* . Two peaks were evident in all the DDC/SDS curves and the $|\Delta H|$ increased with increasing R. The corrected ITC isotherm and I_R were plotted together in Figure 5.9 for each R, aiming

at designating critical concentrations regarding the changes of both scattering ratio and heat. For different R values, the positive slope of I_R and the slow decreasing ΔH were in the same concentration range and was assigned as Region I, where the formation of DDC/SDS aggregates contributed to the heat release possibly due to the water cage formed around the excess amount of DDC and $\text{LOH} \cdot 2\text{SDS}$.²²⁸ The second inflection point in ITC isotherm was at the same concentration (cmc^*) as the peak of I_R . This concentration was designated as C_p , which represented the micellization of SDS and the beginning of the solubilization of DDC into SDS micelles. The amount of DDC/SDS aggregates gradually decreased in Region II upon solubilization while the molecular weight remained constant.²²⁷ At the end of Region II, I_R returned to the baseline and corrected ΔH also returned to 0 kJ/mol at C' , which represented the formation of free DDC loaded SDS micelles.

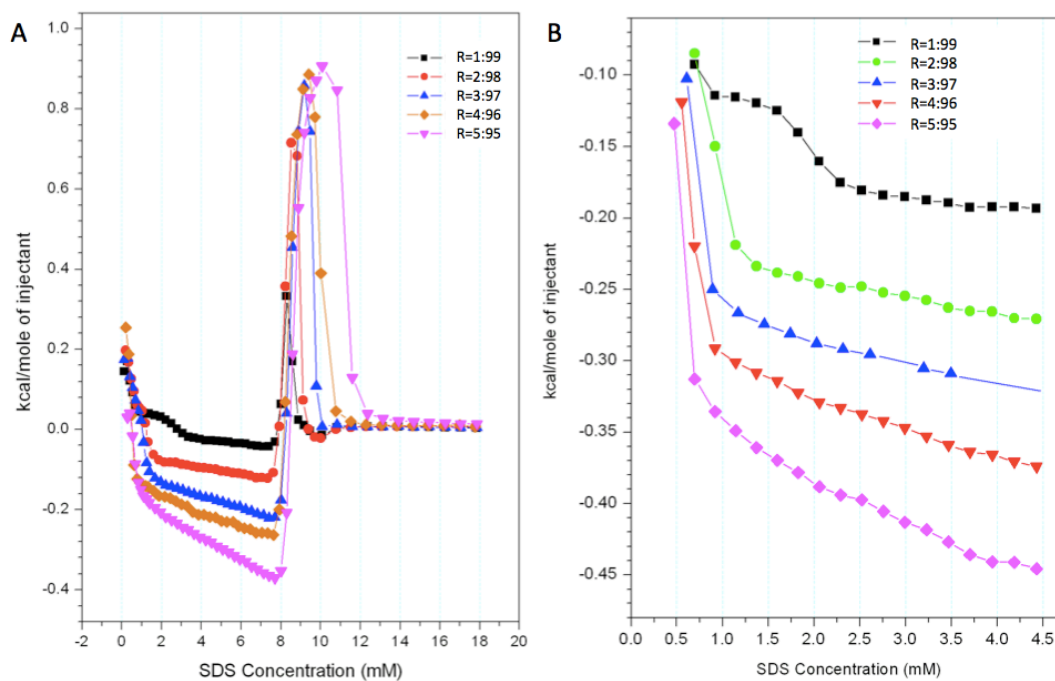


Figure 5.8 (A) ITC isotherm of DDC/SDS mixture of various molar ratios at increasing SDS concentration at 25°C. The curves were corrected by subtracting the SDS dilution curve. (B) is the isotherm at lower SDS concentration, showing the minor change in DDC water-solubilization concentration.

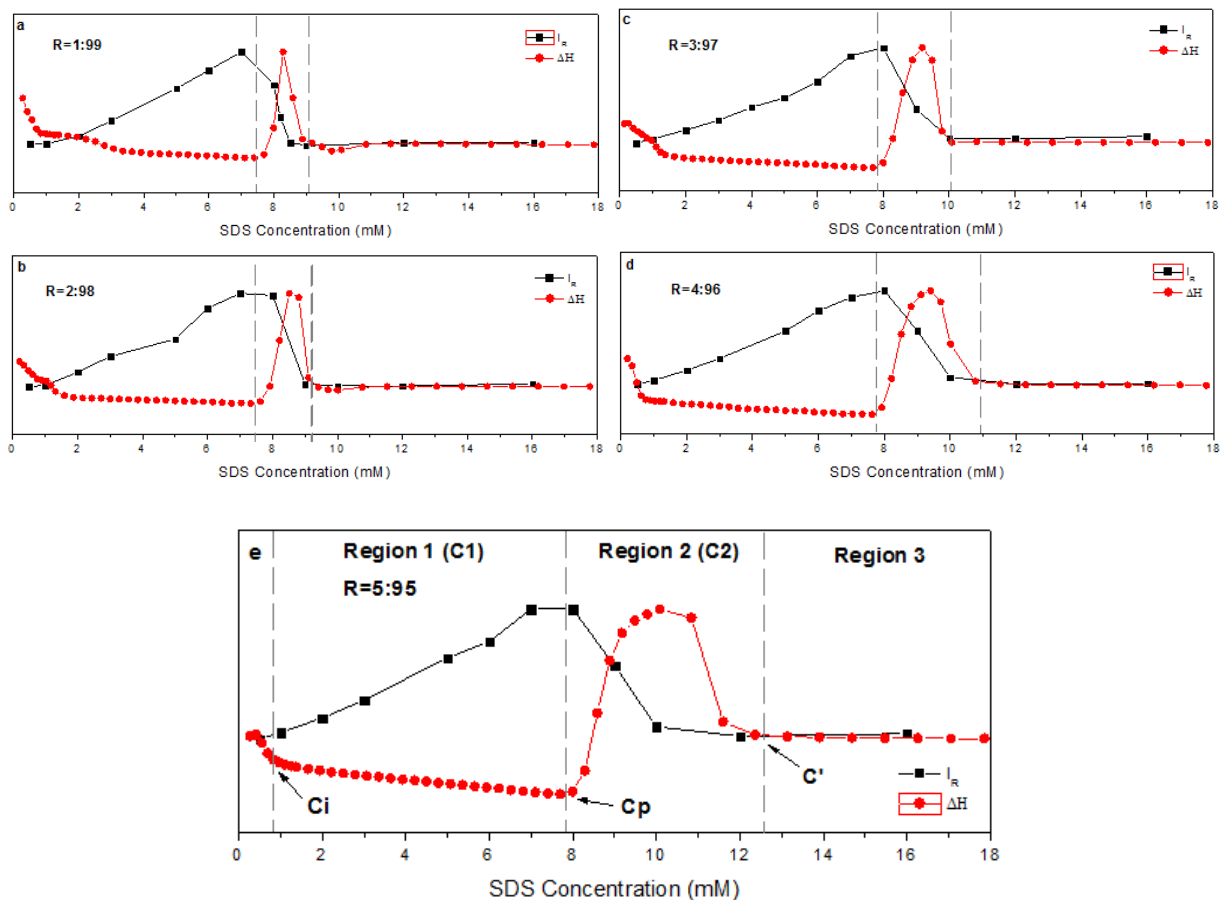


Figure 5.9 Plots of I_R and ΔH vs. SDS concentration for DDC/SDS with various R . (e) shows the critical concentration and regions assigned in DDC/SDS with R of 5:95.

As discussed above, the formation of aggregates proceeded until SDS concentration approached C_p , where the aggregates had the maximum DDC loading ratio q . Since the molecular weight did not vary according to the light scattering slopes in Region II, it is justifiable to assume that the loading ratio kept constant as q , while the number of aggregates was reduced upon solubilization in a growing number of SDS micelles. The loading ratio of DDC per SDS molecule in the micelle, r , was also considered a constant throughout Region II and Region III due to the fact that micelle composition was not affected by DDC concentration but DDC/SDS molar ratio and length of the aliphatic chain.²²¹ Thereafter, when all the DDC/SDS aggregates disappeared at C' , we were able to calculate the value of r using equation:

$$r = \frac{C_{D,m}}{C_m} = \frac{C \cdot R - C_i \cdot R}{C - cmc^*} \quad \text{Equation 5.9}$$

where $C_{D,m}$ is the concentration of DDC solubilized in micelles, C_m is the concentration of SDS in micelles, C is the concentration of SDS. The value of q and r were determined and summarized in Table 5.4. Comparing the values of q and r , it can be concluded that the DDC loading capability of SDS was higher in the form of micelles than aggregates, and was enhanced with increasing amount of DDC presenting in the solution.

Table 5.4 DDC loading ratio of aggregate (q) and micelle (r) in DDC/SDS mixtures with increasing R .

DDC/SDS molar ratio (R)	q	r
1:99	0.008	0.072
2:98	0.017	0.096
3:97	0.027	0.090
4:96	0.037	0.095
5:95	0.048	0.100

5.3.3 Pre-micellar aggregation and micellization of SDS/1-dodecanol

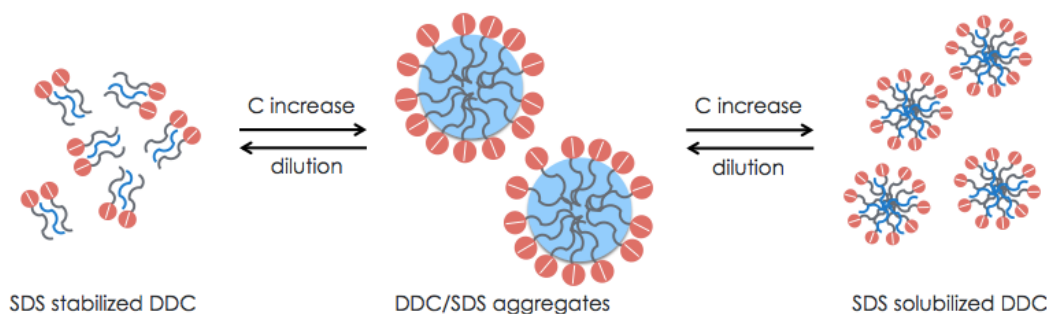
To study the effects of alcohols on the properties of surfactant micellar solutions, there are three experimental procedures adopted as evident from the literatures. One is keeping the alcohol concentration constant and progressively increasing the surfactant concentration. This method is mostly used for short chain alcohols, which is considered as a co-solvent of the surfactant and can dissolve slightly into micelles.^{222,237,238} Whereas, alcohols with longer chain partitioned partially into micelles that leads to the formation of mixed micelles of various compositions. The second way is keeping the surfactant concentration constant and increasing the alcohol concentration. The last procedure is to keep the ratio of surfactant and alcohol constant and changing the concentration of both. This procedure is similar to the method used for studying mixed surfactant systems. In our study, the 1-dodecanol can be considered as a non-ionic surfactant added to SDS solution, for it has the same chain length as SDS and was reported to incorporate into the micelles with its long axes lying approximately parallel to adjacent SDS monomers, while the interaction with the surrounding was negligible. Furthermore, considering that the solubility of DDC is significantly enhanced even in SDS solutions below the cmc, the last approach of keeping the alcohol/surfactant ratio constant is the most suitable technique for used in this study.

Table 5.5 Summarization of counterion binding % and cmc* measured by conductivity titration of DDC/SDS mixtures with increasing R.

DDC/SDS molar ratio (R)	Counterion binding % (f %)	cmc* (mM)
0.00	0.358	8.27
1:99	0.405	7.82
2:98	0.409	7.56
3:97	0.419	7.47
4:96	0.421	7.46
5:95	0.423	7.39

The participation of alcohols into SDS micelles changes the surface charge density of the micelle resulting in a decrease of counterion binding (f), which was measured by conductivity titration of DDC/SDS mixtures with various R. The results are summarized in Table 5.5. The DDC molecules were reported to insert between two SDS molecules with its alkyl chain solubilized in the hydrophobic core of SDS micelle and hydroxyl group located between two negatively charged sulfate groups. The static effect of solubilized DDC increased the average distance between the ionic head groups and the surface area per head group at micelle surface increased, that is, the surface charge density decreased, which led to an increase of counterion binding upon the addition of DDC. This effect was reported to be minor unless more than one DDC was solubilized per micellized surfactant in the case of pentanol-tetradecyltrimethylammonium bromide (TTAB) system²³⁹, which was possibly due to a much larger dimension of the ionic group. Whereas, for smaller head groups such as that of SDS, the effect of DDC addition was more dramatic, even when only one DDC molecule was solubilized by 11~13 micellized SDS molecules. In addition, at large molar ratio of DDC, more DDC molecules participated in the SDS mixed micelles, resulting in an increasing f with higher molar ratio of DDC. Furthermore, the inflection point in the conductivity titration curves represented the micellization of SDS in the presence of DDC. We observed that the cmc* value decreased with increasing R, and the values were corresponding with the C_p obtained from ITC isotherm. The decrease in the micellization concentration was also attributed to the lower charge density, which reduced the electrostatic repulsion between SDS head groups thus the association of surfactant ions together with alcohol molecules appeared at lower concentration than that

of DDC free solutions. To the best of our knowledge, no determination of cmc and f of DDC/SDS systems using this procedure have been reported.



Scheme 5.1 Partitioning of DDC into aggregates and SDS micelles with the increasing mixture concentration.

To further elucidate the driving force of SDS micellization in the presence of DDC, thermodynamic parameters can be calculated based on the ITC and conductivity titration measurements. Similar to the mixed micelle systems that are generally described by phase-separation model as well as chemical equilibrium of surfactant monomers and micelles, the DDC/SDS micellization obeyed the closed association process due to the fact that the size of micelles were found to be independent of concentration as determined from light scattering data.²⁴⁰ The Gibbs free energy of micellization (ΔG_m^0) of DDC/SDS system can therefore be calculated based on equation:

$$\Delta G_m^0 = (1 + f)RT \ln X_{\text{cmc}^*} \quad \text{Equation 5.10}$$

where R is the gas law constant, T is the absolute temperature, X_{cmc^*} and f are the critical micellization concentration expressed in mole fraction units and counterion bound%, respectively, obtained from conductivity measurements. The standard enthalpy of micellization, ΔH_m^0 , was directly extracted from the amplitude of the ITC binding isotherm corrected for the heat effect of dilution, and the entropy of micellization, ΔS_m^0 , can be subsequently estimated from the previously determined ΔG_m^0 and ΔH_m^0 using an existing fundamental expression described in equation:

$$\Delta S_m^0 = -(\Delta G_m^0 - \Delta H_m^0)/T \quad \text{Equation 5.11}$$

The calculated thermodynamic parameters are summarized in Table 5.6. In addition, the Gibbs free energy of DDC solubilization in aqueous solution of SDS can be calculated based on the partition constant, K_s , defined as the fraction of DDC in the micelle divided by the fraction of DDC in the non-micelle phase. Under the present experimental conditions, Equation 5.12-5.13 can be used to determine

the thermodynamic parameters of DDC solubilization and the values are summarized in Table 5.6. ΔH_s^0 was also obtained from the ITC binding isotherm.

Table 5.6 Thermodynamic parameters of SDS micellization and DDC solubilization in DDC/SDS systems with increasing R.

DDC/SDS molar ratio (R)	ΔG_m^0 (kJ/mol)	ΔH_m^0 (kJ/mol)	ΔS_m^0 (kJ/mol.T)	ΔG_s^0 (kJ/mol)	ΔH_s^0 (kJ/mol)	ΔS_s^0 (kJ/mol.T)
0.00	-37.40	1.504	0.131	--	--	--
1:99	-38.85	-1.390	0.126	-3.72	0.182	0.013
2:98	-39.02	-3.192	0.120	-4.20	0.509	0.016
3:97	-39.30	-3.587	0.120	-5.96	0.925	0.023
4:96	-39.36	-3.703	0.120	-6.80	1.101	0.026
5:95	-39.43	-3.788	0.120	-7.67	1.548	0.031

The negative Gibbs free energy of both micellization and solubilization were attributed to the hydrophobic interaction between alkyl chains of both SDS and DDC, while the negative ΔG_m^0 indicated a preference of SDS micellization in the system. The Gibbs free energy decreased with DDC/SDS molar ratio due to the increasing hydrophobic interaction between hydrophobic core of SDS micelles and alkyl chain of DDC. SDS micellization is an exothermic process driven by entropy gain. In conventional surfactant systems, the hydrophobic tail of surfactant is usually surrounded by structured water clusters known as “iceberg” or “flickering clusters”.²³⁰ The positive ΔS_m^0 is attributed to the expelled water molecules from disrupted hydrogen bonds in solvent cage due to micellization. It was observed that the entropy change rarely varied with R, since it was largely dependent on the majority of SDS in the system rather than the amount of DDC. DDC solubilization is an endothermic process observed from ITC isotherm, which was compensated by the positive entropy gain. Whereas, the ΔS_s^0 of DDC solubilization increased with increasing R value in the system. This can be explained by the theory proposed by Abe and Ogino²³⁰ that the loss of mobility of DDC molecules upon solubilization was counteracted by enhanced randomness or increased configurational entropy of the solubilized DDC molecules.

$$\Delta G_s^0 = RT \ln K_s \quad \text{Equation 5.12}$$

$$\Delta S_s^0 = -(\Delta G_s^0 - \Delta H_s^0)/T \quad \text{Equation 5.13}$$

The composition of DDC/SDS mixture with fixed R with increasing concentration can be calculated for each of the three regions assigned in ITC isotherm using the designated critical concentrations and micelle loading ratio. In Region 1, the SDS concentration was below cmc, thus all the DDC was either slightly solubilized in water or partitioned in DDC/SDS aggregates. Thus, the aggregate composition, given by $C_{d,agg}/C_d$, can be obtained using the equation:

$$\frac{C_{d,agg}}{C_d} = \frac{(C_1 - C_i) \times R}{C_d} \quad \text{Equation 5.14}$$

where $C_{d,agg}$ is the concentration of DDC in DDC/SDS aggregates, C_d is the total concentration of DDC titrated in water, C_1 is the SDS concentration in Region 1. In Region 3, all of the DDC in aggregates were solubilized in SDS metastable micellar structure and the amounts of DDC solubilized in water can be neglected due to its low water-solubility, therefore the micelle composition was considered as 1. Whereas, DDC/SDS aggregates and SDS micelles containing solubilized DDC coexisted in Region 2, and upon the formation of micelles and solubilization of DDC in the aggregates the composition of the solution kept changing through out this region. With the assumptions that the micelle composition did not vary with concentration, viz, r was constant in Region 2, we can calculate the composition of aggregates and micelles using the following equations:

$$\frac{C_{d,agg}}{C_d} = \frac{C_d - (C_2 - cmc^*) \times R}{C_d} \quad \text{Equation 5.15}$$

$$\frac{C_{d,m}}{C_d} = \frac{(C_2 - cmc^*) \times R}{C_d} \quad \text{Equation 5.16}$$

where $C_{d,m}$ is the concentration of DDC solubilized in micelles, C_2 is the SDS concentration in Region 2. The results of calculation were plotted in Figure 5.10, from which we can see that at the beginning of Region 1 the formation of DDC/SDS aggregates was very rapid, and it slowed down, approaching the maximum at concentration close to the cmc^* . Also, the higher the DDC/SDS molar ratio, the more rapid was the formation of aggregates as we can observe from the slopes in Region 1. When the micellization of SDS took place, DDC/SDS aggregates dissociated and the DDC was solubilized in the hydrophobic core of micelles, thus the aggregate composition continued to decrease while the micelle composition increased until all the DDC were partitioned to the micelles.

By comparing the curve of different R, we observed prolonged solubilization process in the system

with higher R cause it took more SDS micelles to incorporate DDC molecules in the aggregates. Interestingly, if we took the concentration of the intersection of $C_{d,agg}/C_d$ and $C_{d,m}/C_d$ (C_s) and compared with the concentration of the endothermic peak in ITC isotherm (C_{p2}) of the same R, we saw that the values were almost identical. (Table 5.7) This can be explained by the thermodynamic property of the solubilization process. Since below C_s , the majority of DDC molecules were in the aggregates and the solubilization process dominated, which was endothermic as calculated. However, when most of DDC were solubilized in micelles at concentration above C_s , the heat release from solubilization started to decrease and eventually vanished at concentration beyond C' , where only the dilution of micelles existed upon titration. This approach enabled us to gain a better understanding on the system composition and locate DDC and SDS at a particular concentration. With a good correspondence with ITC data, this method can also be used to predict the thermodynamic behavior of DDC/SDS systems with different R values.

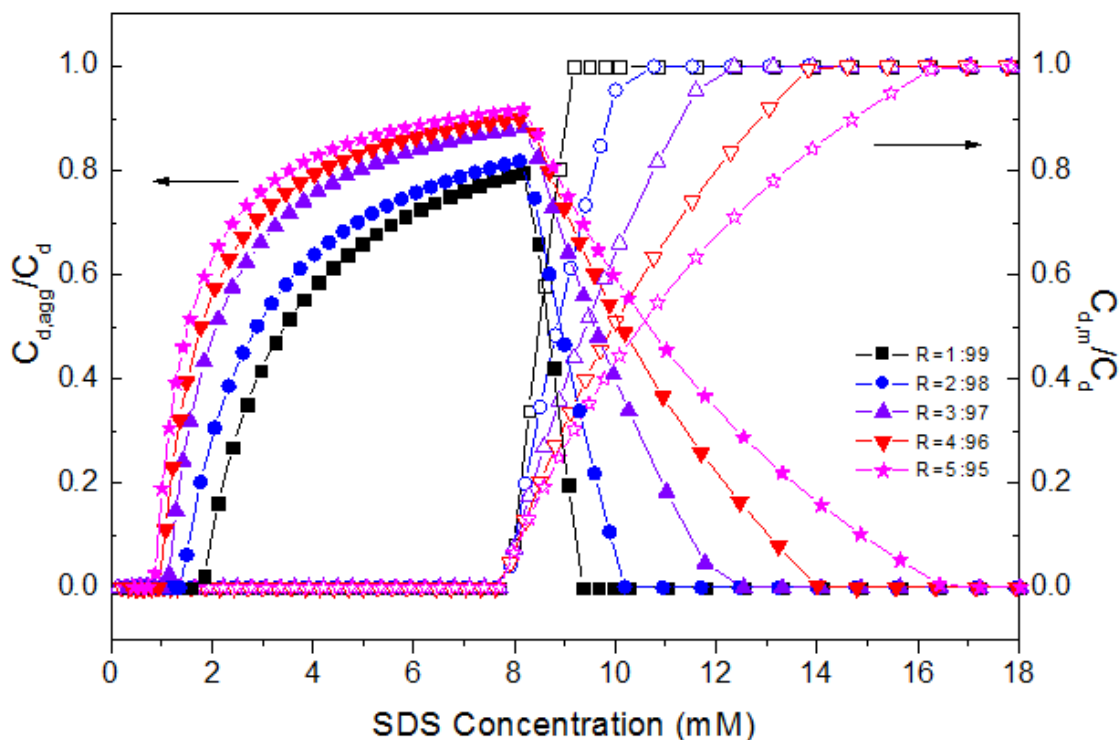


Figure 5.10 Aggregation composition (left axis) and micelle composition (right axis) of DDC with different R vs. SDS concentration.

Table 5.7 Summarization of concentrations extracted from Figure 5.10 and ITC isotherm of DDC/SDS with various R (Figure 5.8A).

DDC/SDS molar ratio (R)	Cs (mM)	Cp2 (mM)
1:99	8.385	8.336
2:98	8.594	8.590
3:97	9.119	9.164
4:96	9.559	9.477
5:95	9.977	10.06

5.4 Conclusions

In this chapter, the adsorption of SDS/1-dodecanol mixtures at air-water interface was characterized under varied dodecanol molar ratio and temperature to systematically investigate their impacts on the surface activity of the surfactant mixtures. Surface activity parameters, surface concentration were determined by applying the generalized Von-Szyszkowski equation and extended Langmuir equation to the surface tension isotherms. Discussions on the overall surface activity and coverage percent of the interface were made based on the calculated quantities. Further investigated using light scattering technique and isothermal titration calorimetry to obtain information of the solution behavior and thermodynamic properties were conducted. Aggregation of DDC/SDS at SDS concentration below cmc^* and solubilization of DDC into SDS micelles were observed and characterized. Thermodynamic parameters of DDC solubilization and SDS micellization were calculated. It was found that both of the processes were entropy driven, while that of DDC partitioning into micelles increased with increasing R. The distribution of DDC at different total concentration was studied and compared with ITC isotherm, which can be used to predict the solution composition of systems of different DDC/SDS molar ratio. The molecular weight of DDC/SDS aggregate with increasing concentration can be determined using static light scattering to resolve the question whether the increase of I_R was due to the increasing amount or the growing size of the aggregates.

6 Contributions and Recommendations

6.1 General Contributions

As two types of the most important components used in the formulation of personal care products, polymers and surfactants have attracted intensive interests with regard to their physicochemical properties, interfacial and solution behaviors as well as the interactions in polymer/surfactant and mixed surfactant systems in aqueous solution. This thesis aims at developing a novel functional nanomaterial based on biodegradable and sustainable CNC and β -CD for personal care applications. Three main objectives were fulfilled: β -CD-functionalized CNC was synthesized and characterized. Interactions between CNC-CD and three model surfactants were studied (Chapter 3); desulfation and cationization of CNC were performed and the product was characterized. The interactions with the same model surfactants were investigated and compared with that of CNC-CD (Chapter 4); investigations on the interfacial and solution behaviors of 1-dodecanol/surfactant mixture system (Chapter 5). The main findings of each section are summarized in the following:

6.1.1 Synthesis, optimization and characterization of CNC-CD and its interaction with surfactants

β -CD was successfully grafted on the surface of pristine negatively charged CNC using cyanuric chloride as cross-linker. Under the optimized synthetic condition, the grafting ratio of β -CD was calculated to be 3.32 wt% on average using phenolphthalein inclusion method, which was much higher than previously reported using the same grafting approach. The micellization process of surfactants, surface activity and flocculation behaviors of CNC were changed by the host-guest interaction between grafted β -CD and selected surfactants, which is an exothermic interaction as examined by ITC. Surface activity of CNC-CD was enhanced in the presence of CTAB below their critical micelle concentration due to the dominant electrostatic interaction. On the contrary, a reduced surface activity of CNC-CD was observed due to the shielded hydrophobic tail of TX-100 by β -CD. The minor difference for SDS was the fast recovery of surface tension at cmc by removing impurities from air-water interface into cavity of β -CD. The aggregates of SDS/CNC-CD complex at concentration below cmc and SDS aggregates on the surface of re-dispersed CNC were observed despite the electrostatic repulsion between negatively charged CNC and anionic SDS. β -CD-induced aggregation of CTAB induced fast flocculation of CNC-CD at a lower CTAB concentration compared to CNC. The rearrangement of the structure from compact precipitates to loose and floating clusters was also observed.

6.1.2 Synthesis and characterization of β -CD-functionalized cationic CNC and its interaction with surfactants

Cationic polymers are widely used in personal care products for moisturizing and conditioning purposes. Their flocculation and deposition can be affected by the existence of surfactants in solution. In this thesis, pristine CNC was firstly desulfated to remove the negatively charged sulfonic acid groups, then cationized by modification of GTMAC to reverse the surface charge of CNC. Cationic CNC was functionalized with β -CD using the optimized reaction procedure in Chapter 3 and the grafting ratio was determined to be 7.05 wt% on average. Interactions with cationic surfactant CTAB and anionic surfactant SDS were investigated. The host-guest interactions between β -CD-grafted dcCNC reduced the amount of free molecules in the solution. The inclusion complex further induced aggregation of dcCNC-CD at concentration below cmc, which was not seen in the suspension of CNC. The aggregation effect was found to be more exothermic when solution temperature was increased since less energy was required for disrupting the water cage surrounding CTAB hydrophobic tails. dcCNC also interacted with CTAB at concentration above cmc, however, due to the weak hydrophobicity of backbone, the interaction was not energetic enough to form large aggregates. Electrostatic interaction dominated in solutions of SDS in the presence of dcCNC-CD. Precipitations of multi-chain aggregates and conformational transition were observed below the cmc in both the dcCNC and dcCNC-CD. However, only the transmittance of dcCNC-CD solution with SDS concentration above cmc was restored, which was due to the β -CD inclusion complex-induced SDS aggregation and resulting electrostatic repulsion between dcCNC-CD.

6.1.3 Influence of 1-dodecanol on the adsorption and thermodynamic properties of sodium dodecyl sulfate micellar solution

The adsorption behaviors of DDC-solubilized SDS micellar solutions with different molar ratio at air-water interface were studied. The surface activity parameters for each component and overall mixture were determined by fitting the generalized Von-Szyszkowski equation and extended Langmuir equation to surface tension data. An enhancement of overall surface activity at 15°C and higher DDC molar ratio was observed due to the enhanced hydrophobicity of alkyl chains. Light scattering measurements showed aggregation of DDC/SDS mixture below the cmc and disaggregation above the cmc with DDC solubilization into SDS micelles. The enthalpy change of aggregation, micellization and solubilization were measured using ITC and compared to LS results. Regions with only aggregates, micelles and mixture of both at increasing mixture concentration were distinguished from the isotherms. Micelle loading ratio of DDC was calculated from the cmc*, which increased with DDC/SDS molar ratio. From

the conductivity measurements, percent counterion binding increased with increasing DDC molar ratio due to the reduced surface charge density of DDC inserting between SDS molecules in micelles. Due to same effect, cmc^* also decreased as more DDC was present in the solution mixtures. Thermodynamic parameters of SDS micellization and DDC solubilization were calculated on the basis of certain assumptions. Both processes were entropy driven and the increasing entropy change was explained by the breakdown of the surrounding water cage. Finally, the composition of DDC in aggregates and micelles was determined with respect to the increasing concentration in each region. Compared with the ITC results we can explain the endothermic peak of enthalpy change by the decreasing solubilization of DDC and saturation of SDS micelles.

6.2 Recommendation for Future Studies

On the basis of the results from this research project and from the practical application perspective, the following recommendations are proposed for future studies. A higher grafting ratio of β -CD is desirable for the purpose of guest molecule-delivery. However, due to the limitation of cyanuric chloride activities towards reactive groups on pristine CNC, it will be useful to consider the modification of hydroxyl groups to amine groups²⁴¹ or using other grafting approaches, e.g. peptide coupling²⁴² and click chemistry²⁴³. A better characterization of β -CD grafting can be performed using solid-state carbon NMR. The aggregation behavior and aggregate structure of CNC-CD/surfactant can be further investigated using fluorescence, small-angle X-ray, as well as neutron reflectivity techniques to provide further information on the binding mechanisms. The self-assembling behavior of β -CD consisting polymers was widely studied for drug delivery²⁴⁴ and viscosity modification²⁴⁵, which are also applicable for CNC-CD. The rod-like structure of CNC has a greater capacity to increase the solution viscosity, and together with the host-guest property of β -CD towards hydrophobic segment of amphiphilic polymers, studies on CNC-CD/polymer interaction will also be useful for the purpose of rheology modification. Furthermore, the adsorption of CNC-CD to the air-water interface in the presence of surfactant can be extended to liquid-liquid interface or solid-liquid interface adsorptions for further applications in deposition, emulsification or Pickering emulsion¹²⁹. Lastly, due to the inclusion property of cyclodextrin and its well-recognized applications in personal care products, β -CD-grafting to the surface of CNC has great potential in imparting novel functionalities to this promising material, such as delivering active reagents for nourishing, perfuming or UV protection, facilitating pre-micellar aggregation of surfactants to reduce free monomers, caption of malodor molecules from human body, and construction of polymer network for viscosity modification.¹³¹ More researches need to be conducted using model guest molecules/polymers to explore the potential applications of (dc)CNC-CD in personal care products.

Adsorption of alcohol/SDS mixture to the air-water interface has been widely studied. It was reported that the DDC aggregates at interface would undergo a first-order phase transition to form a crystalline structure before its solubilization in micelles. In addition, the possibility of sequencing adsorption of SDS and DDC was also proposed²⁴⁶. However, in these studies either the concentration of DDC or SDS was kept constant while changing the other parameters. Thus, it is desirable to conduct measurements with constant DDC/SDS molar ratio and study the effects of molar ratio and temperature on the adsorption kinetics and surface rheology of such mixtures, for this is the most commonly encountered issue for alcohol impurities of SDS in practical applications. Furthermore, studies on the effects of temperature and ionic strength on the thermodynamic properties of such systems will provide valuable information on the co-adsorption and solubilization process for the applications of emulsion formation and stabilization.

References

- (1) Mark, H. **1946**.
- (2) De Souza Lima, M. M.; Borsali, R. *Macromol. Rapid Commun.* **2004**, *25*, 771–787.
- (3) Samir, A.; Alloin, F.; Sanchez, J.; Kissi, N. El; Dufresne, A. *Macromolecules* **2004**, 1386–1393.
- (4) Mwaikambo, L. Y.; Ansell, M. P.; Dufresne, A.; Hughes, M.; Hill, C.; Wild, P. M. *J. Mater. Sci.* **2001**, *6*, 2107–2131.
- (5) Barse, B.; Kaul, P.; Banerjee, A.; Kaul, C. L.; Banerjee, U. C. *Chem. Today* **2003**, 48–53.
- (6) Martin Del Valle, E. M. *Process Biochem.* **2004**, *39*, 1033–1046.
- (7) Pan, J.; Hamad, W.; Straus, S. K. *Macromolecules* **2010**, *43*, 3851–3858.
- (8) Yao, Z. L.; Grishkewich, N.; Tam, K. C. *Soft Matter* **2013**, *9*, 5319.
- (9) Huldcn, M. *Colloids Surfaces A Physicochem. Eng. Asp.* **1994**, *82*, 263–277.
- (10) Xu, B.; Yekta, A.; Li, L.; Masoumi, Z.; Winnik, M. a. *Colloids Surfaces A Physicochem. Eng. Asp.* **1996**, *112*, 239–250.
- (11) Thuresson, K.; Nystrom, B.; Lindmant, B. *Langmuir* **1995**, 3730–3736.
- (12) Kfistner, U.; Hoffmann, H.; Dnges, R.; Ehrler, R. *Colloids Surfaces A Physicochem. Eng. Asp.* **1996**, *112*, 209–225.
- (13) Tirtaatmadja, V.; Tam, K. C.; Jenkins, R. D. *Macromolecules* **1997**, *9297*, 3271–3282.
- (14) Kumacheva, E.; Rharbi, Y.; Winnik, M. A.; Guo, L.; Tam, K. C.; Jenkins, R. D.; Carolina, N. *Langmuir* **1997**, *13*, 182–186.
- (15) Tam, K. C.; Farmer, M. L.; Jenkins, R. D.; Bassett, D. R. *J. Polym. Sci. Part B Polym. Phys.* **1998**, *36*, 2275–2290.

- (16) Seng, W. P.; Tam, K. C.; Jenkins, R. D. *Colloids Surfaces A Physicochem. Eng. Asp.* **1999**, *154*, 365–382.
- (17) Gebelein, C. G.; Yang, V. C. *Cosmetic and Pharmaceutical Applications of Polymers Cosmetic and Pharmaceutical Applications of Polymers*; 1st ed.; Plenum Press, New York, 1991; p. 9.
- (18) Carbone-Howell, A. L.; Ouimet, M. A.; Uhrich, K. E. In *Polymers for Personal Care and Cosmetics*; American Chemical Society, 2013; Vol. 1148, pp. 145–155.
- (19) Simonnet, J.; Fanchon, C.; Ribier, A.; Segot, E. Anti-acne composition for the simultaneous treatment of the surface layers and deep layers of the skin, and use thereof, 1997.
- (20) Kalyon, B. D.; Olgun, U. *Am. J. Infect. Control* **2001**, *29*, 124–125.
- (21) Carbone, A. L.; Uhrich, K. E. *Macromol. Rapid Commun.* **2009**, *30*, 1021–1026.
- (22) Prado, A. G. S.; Santos, A. L. F.; Pedroso, C. P.; Carvalho, T. O.; Braga, L. R.; Evangelista, S. M. *J. Therm. Anal. Calorim.* **2011**, *106*, 415–420.
- (23) Trüeb, R. M. *J. Dtsch. Dermatol. Ges.* **2007**, *5*, 356–365.
- (24) Nazir, H.; Wang, L.; Lian, G.; Zhu, S.; Zhang, Y.; Liu, Y.; Ma, G. *Colloids Surf. B. Biointerfaces* **2012**, *100*, 42–49.
- (25) Nazir, H.; Lv, P.; Wang, L.; Lian, G.; Zhu, S.; Ma, G. *J. Colloid Interface Sci.* **2011**, *364*, 56–64.
- (26) Li, W.; Jordan, S. L. P. *Cationic cellulosic polymers with multifunctional and outstanding performance for personal care*; 2003; pp. 1–4.
- (27) Bouillon, C. Shampoos. *Clinics in dermatology*, 1996, *14*, 113–121.
- (28) Mehta, S. K.; Bhasin, K. K.; Dham, S.; Singla, M. L. *J. Colloid Interface Sci.* **2008**, *321*, 442–451.
- (29) Holmberg, K.; Bo, J.; Kronberg, B. *SOLUTION AND POLYMERS IN AQUEOUS*; 2002; pp. 0–471.
- (30) Zhang, W.; Li, G.; Mu, J.; Shen, Q.; Zheng, L.; Liang, H.; Wu, C. *Chinese Sci. Bull.* **2000**, *45*,

1854–1857.

- (31) Danov, K. D.; Kralchevsky, P. a.; Ananthapadmanabhan, K. P. *Adv. Colloid Interface Sci.* **2014**, *206*, 17–45.
- (32) Swisher, R. D. In *Solution Behavior of Surfactants SE - 7*; Mittal, K. L.; Fendler, E. J., Eds.; Springer US, 1982; pp. 149–159.
- (33) Federle, T. W.; Pastwa, G. M. *Ground Water* **1988**, *16*, 761–770.
- (34) Cserhádi, T.; Forgács, E.; Oros, G. *Environ. Int.* **2002**, *28*, 337–348.
- (35) Dorn, P. B.; Salanitro, J. P.; Evans, S. H.; Kravetz, L. *Environ. Toxicol. Chem.* **1993**, *12*, 1751–1762.
- (36) Somasundaran, P.; Fu, E.; Xu, Q. *Langmuir* **1992**, 1065–1069.
- (37) Huang, L.; Somasundaran, P. *Langmuir* **1996**, *7463*, 5790–5795.
- (38) Crosslinking:hydrophobic domain for loading-Surfactants polymers and their nanoparticles for personal care applications.pdf.
- (39) Paria, S.; Khilar, K. C. *Adv. Colloid Interface Sci.* **2004**, *110*, 75–95.
- (40) Rosen, M. J. *Surfactants and Interfacial Phenomena*; 3rd ed.; Wiley: Chichester, U.K., 2004; pp. 65–80.
- (41) Jones, M. N. *J. Colloid Interface Sci.* **1967**, *23*, 36–42.
- (42) Dai, S.; Tam, K. C. *J. Phys. Chem. B* **2001**, *105*, 10759–10763.
- (43) Kaler, E. W.; Billman, J. F.; Fulton, J. L.; Smith, R. D. *J. Phys. Chem.* **1991**, *95*, 458–462.
- (44) Olofsson, G.; Wang, G. *Pure Appl. Chem.* **1994**, *66*, 527–532.
- (45) Saito, S.; Yukawa, M. *J. Colloid Interface Sci.* **1969**, *30*, 211–218.
- (46) Mezei, A.; Mészáros, R. *Langmuir* **2006**, *22*, 7148–7151.

- (47) Ritacco, H. A.; Kurlat, D.; G. Rubio, R.; Ortega, F.; Langevin, D. *Macromolecules* **2009**, *42*, 5843–5850.
- (48) Sullivan, A. C. O. *Cellulose* **1997**, 173–207.
- (49) Azizi Samir, M. A. S.; Alloin, F.; Dufresne, A. *Biomacromolecules* **2005**, *6*, 612–626.
- (50) Nishiyama, Y. *J. Wood Sci.* **2009**, *55*, 241–249.
- (51) Moon, R. J.; Martini, A.; Nairn, J.; Simonsen, J.; Youngblood, J. *Cellulose nanomaterials review: structure, properties and nanocomposites.*; 2011; Vol. 40, pp. 3941–3994.
- (52) Revol, J.-F.; Goring, D. a. I. *J. Appl. Polym. Sci.* **1981**, *26*, 1275–1282.
- (53) Klemm, D.; Heublein, B.; Fink, H.-P.; Bohn, A. *Angew. Chem. Int. Ed. Engl.* **2005**, *44*, 3358–3393.
- (54) Nogi, M.; Iwamoto, S.; Nakagaito, A. N.; Yano, H. *Adv. Mater.* **2009**, *21*, 1595–1598.
- (55) Tanner, S. F.; Cartier, N.; Chanzy, H. **1989**, *1617*, 1615–1617.
- (56) Nishiyama, Y.; Sugiyama, J.; Chanzy, H.; Langan, P. *J. Am. Chem. Soc.* **2003**, *125*, 14300–14306.
- (57) Debzi, E. M.; Chanzy, H.; Sugiyama, J.; Tekely, P.; Excoffier, G. *Macromolecules* **1991**, *24*, 6816–6822.
- (58) Yamamoto, H.; Horii, F. *Macromolecules* **1993**, 1313–1317.
- (59) Watanabe, A.; Morita, S.; Ozaki, Y. *Biomacromolecules* **2007**, *8*, 2969–2975.
- (60) Horikawa, Y.; Sugiyama, J. *Biomacromolecules* **2009**, *10*, 2235–2239.
- (61) Nishiyama, Y.; Johnson, G. P.; French, A. D.; Forsyth, V. T.; Langan, P. *Biomacromolecules* **2008**, *9*, 3133–3140.
- (62) Tashiro, K.; Kobayashi, M. *Polymer (Guildf)*. **1991**, *32*, 1516–1526.

- (63) Eichhorn, S. J.; Davies, G. R. *Cellulose* **2006**, *13*, 291–307.
- (64) Cousins, S. K.; Brown, R. M. *Polymer (Guildf)*. **1995**, *36*, 3885–3888.
- (65) Garcia de Rodriguez, N. L.; Thielemans, W.; Dufresne, A. *Cellulose* **2006**, *13*, 261–270.
- (66) Wang, B.; Sain, M. *Compos. Sci. Technol.* **2007**, *67*, 2521–2527.
- (67) Bai, W.; Holbery, J.; Li, K. *Cellulose* **2009**, *16*, 455–465.
- (68) Filson, P. B.; Dawson-Andoh, B. E. *Bioresour. Technol.* **2009**, *100*, 2259–2264.
- (69) Wang, N.; Ding, E.; Cheng, R. *Langmuir* **2008**, *24*, 5–8.
- (70) Petersson, L.; Kvien, I.; Oksman, K. *Compos. Sci. Technol.* **2007**, *67*, 2535–2544.
- (71) Fukuzumi, H.; Saito, T.; Iwata, T.; Kumamoto, Y.; Isogai, A. *Biomacromolecules* **2009**, *10*, 162–165.
- (72) Angle, M. N.; Dufresne, A. *Macromolecules* **2001**, *15*, 2921–2931.
- (73) Peng, B. L.; Dhar, N.; Liu, H. L.; Tam, K. C. *Can. J. Chem. Eng.* **2011**, *89*, 1191–1206.
- (74) Elazzouzi-Hafraoui, S.; Nishiyama, Y.; Putaux, J.-L.; Heux, L.; Dubreuil, F.; Rochas, C. *Biomacromolecules* **2008**, *9*, 57–65.
- (75) Roman, M.; Winter, W. T. *Biomacromolecules* **2004**, *5*, 1671–1677.
- (76) Habibi, Y.; Goffin, A.-L.; Schiltz, N.; Duquesne, E.; Dubois, P.; Dufresne, A. *J. Mater. Chem.* **2008**, *18*, 5002.
- (77) Heux, L.; Chauve, G.; Bonini, C. *Langmuir* **2000**, *16*, 8210–8212.
- (78) Habibi, Y.; Lucia, L. a; Rojas, O. J. *Chem. Rev.* **2010**, *110*, 3479–3500.
- (79) Hamad, W. *Front. Chem. Eng. Res.* **2006**, *84*, 513–519.

- (80) Beck-Candanedo, S.; Roman, M.; Gray, D. G. *Biomacromolecules* **2005**, *6*, 1048–1054.
- (81) Lu, P.; Hsieh, Y.-L. *Carbohydr. Polym.* **2010**, *82*, 329–336.
- (82) Araki, J.; Wada, M.; Kuga, S.; Okano, T. *Colloids Surfaces A Physicochem. Eng. Asp.* **1998**, *142*, 75–82.
- (83) Jun Araki, Masahisa Wada, S. K. T. O. *J. wood Sci.* **1999**, *45*, 258–261.
- (84) Araki, J.; Wada, M.; Kuga, S.; Okano, T. *Langmuir* **2000**, *16*, 2413–2415.
- (85) Wang, N.; Ding, E.; Cheng, R. *Polymer (Guildf)*. **2007**, *48*, 3486–3493.
- (86) Filpponon, I. The Synthetic Strategies for Unique Properties in Cellulose Nanocrystal Materials, North Carolina State University, 2009.
- (87) Revol, J.-F.; Bradford, H.; Giasson, J.; Marchessault, R. H.; Gray, D. G. *Int. J. Biol. Macromol.* **1992**, *14*, 170–172.
- (88) Bordel, D.; Putaux, J.-L.; Heux, L. *Langmuir* **2006**, *22*, 4899–4901.
- (89) Fleming, K.; Gray, D.; Prasannan, S.; Matthews, S. *J. Am. Chem. Soc.* **2000**, *122*, 5224–5225.
- (90) Habibi, Y.; Heim, T.; Douillard, R. *J. Polym. Sci. Part B Polym. Phys.* **2008**, *46*, 1430–1436.
- (91) Dong, X. M.; Kimura, T.; Revol, J.-F.; Gray, D. G. *Langmuir* **1996**, *12*, 2076–2082.
- (92) Beck-Candanedo, S.; Viet, D.; Gray, D. G. *Macromolecules* **2007**, *40*, 3429–3436.
- (93) Dong, X. M.; Gray, D. G. *Langmuir* **1997**, *13*, 2404–2409.
- (94) Elazzouzi-Hafraoui, S.; Putaux, J.-L.; Heux, L. *J. Phys. Chem. B* **2009**, *113*, 11069–11075.
- (95) Li, Q.; Zhou, J.; Zhang, L. *J. Polym. Sci. Part B Polym. Phys.* **2009**, *47*, 1069–1077.
- (96) Junior de Menezes, A.; Siqueira, G.; Curvelo, A. a. S.; Dufresne, A. *Polymer (Guildf)*. **2009**, *50*, 4552–4563.

- (97) Kimura, F.; Kimura, T.; Tamura, M.; Hirai, A.; Ikuno, M.; Horii, F. *Langmuir* **2005**, *21*, 2034–2037.
- (98) Heux, L.; D'Uriage, S.-M.; Bonini, C. Microfibrillated and/or microcrystalline dispersion, in particular of cellulose, in an organic solvent. US006967027B1, 2005.
- (99) Bondeson, D.; Oksman, K. *Compos. Interfaces* **2007**, *14*, 617–630.
- (100) Kim, J.; Montero, G.; Habibi, Y.; Hinestroza, J. P.; Genzer, J.; Argyropoulos, D. S.; Rojas, O. J. *Polym. Engineering Sci.* **2009**, *49*, 2054–2061.
- (101) Rojas, O. J.; Montero, G. A.; Habibi, Y.; Carolina, N. *J. Appl. Polym. Sci.* **2009**, *113*, 927–935.
- (102) Hasani, M.; Cranston, E. D.; Westman, G.; Gray, D. G. *Soft Matter* **2008**, *4*, 2238.
- (103) Jiang, X.; Gu, J.; Tian, X.; Li, Y.; Huang, D. *Bioresour. Technol.* **2012**, *104*, 473–479.
- (104) A.G., L.; Dodgson, K. S. *Biochim Biophys Acta* **1961**, *46*, 116–120.
- (105) Viana, a; Nosedá, M.; Duarte, M.; Cerezo, a. *Carbohydr. Polym.* **2004**, *58*, 455–460.
- (106) Pomin, V. H.; Valente, A. P.; Pereira, M. S.; Mourão, P. a S. *Glycobiology* **2005**, *15*, 1376–1385.
- (107) Nagasawa, K.; Inoue, Y.; Kamata, T. *Carbohydr. Res.* **1977**, *58*, 47–55.
- (108) Navarro, D. a.; Flores, M. L.; Stortz, C. a. *Carbohydr. Polym.* **2007**, *69*, 742–747.
- (109) Habibi, Y.; Chanzy, H.; Vignon, M. R. *Cellulose* **2006**, *13*, 679–687.
- (110) Zaman, M.; Xiao, H.; Chibante, F.; Ni, Y. *Carbohydr. Polym.* **2012**, *89*, 163–170.
- (111) Habibi, Y.; Heim, T.; Douillard, R. *J. Polym. Sci. Part B* **2008**, 1430–1436.
- (112) Cao, X.; Habibi, Y.; Lucia, L. a. *J. Mater. Chem.* **2009**, *19*, 7137.
- (113) Araki, J.; Wada, M.; Kuga, S. *Langmuir* **2001**, *17*, 21–27.

- (114) Mangalam, A. P.; Simonsen, J.; Benight, A. S. *Biomacromolecules* **2009**, *10*, 497–504.
- (115) Azzam, F.; Heux, L.; Putaux, J.-L.; Jean, B. *Biomacromolecules* **2010**, *11*, 3652–3659.
- (116) Wang, J.; Matyjaszewski, K. *J. Am. Chem. Soc.* **1995**, 5614–5615.
- (117) Chen, G.; Dufresne, A.; Huang, J.; Chang, P. R. *Macromol. Mater. Eng.* **2009**, *294*, 59–67.
- (118) Lin, N.; Chen, G.; Huang, J.; Dufresne, A.; Chang, P. R. *J. Appl. Polym. Sci.* **2009**, *113*, 3417–3425.
- (119) Siqueira, G.; Bras, J.; Dufresne, A. *Langmuir* **2010**, *26*, 402–411.
- (120) Ridell, A.; Evertsson, H.; Nilsson, S. *J. Colloid Interface Sci.* **2002**, *247*, 381–388.
- (121) Bloor, D. M.; Mwakibete, H. K. O.; Wyn-Jones, E. *J. Colloid Interface Sci.* **1996**, *178*, 334–338.
- (122) Zana, R.; Binana-Limbele, W. *J. Phys. Chem.* **1992**, *96*, 5461–5465.
- (123) Wang, G.; Olofsson, G. *J. Phys. Chem.* **1995**, *99*, 5588–5596.
- (124) Trabelsi, S.; Raspaud, E.; Langevin, D. *Langmuir* **2007**, *23*, 10053–10062.
- (125) Chakraborty, T.; Chakraborty, I.; Ghosh, S. *Langmuir* **2006**, *22*, 9905–9913.
- (126) Wang, C.; Tam, K. C. *Langmuir* **2002**, *18*, 6484–6490.
- (127) Mata, J.; Patel, J.; Jain, N.; Ghosh, G.; Bahadur, P. *J. Colloid Interface Sci.* **2006**, *297*, 797–804.
- (128) Dhar, N.; Au, D.; Berry, R. C.; Tam, K. C. *Colloids Surfaces A Physicochem. Eng. Asp.* **2012**, *415*, 310–319.
- (129) Peng, B.; Han, X.; Liu, H.; Berry, R. C.; Tam, K. C. *Colloids Surfaces A Physicochem. Eng. Asp.* **2013**, *421*, 142–149.
- (130) Szejtli, J. *Chem. Rev.* **1998**, *98*, 1743–1754.

- (131) Eastburn, S. D.; Tao, B. Y. *Biotechnol. Adv.* **1994**, *12*, 325–339.
- (132) Schollmeyer, E. *J. Cosmet. Sci.* **2002**, *191*, 185–191.
- (133) Szejtli, J. *Trends Biotechnol.* **1989**, *7*, 170–174.
- (134) Dass, C. R.; Jessup, W. *J. Pharm. Pharmacol.* **2000**, *52*, 731–761.
- (135) Sin, K.; Nakamura, A.; Kobayashi, K.; Masaki, H.; Uozumi, T. *Appl. Microbiol. Biotechnol.* **1991**, *35*, 600–605.
- (136) Loftsson, T. *Cosmet Toilet* **2000**, *115*, 59–66.
- (137) Schneiderman, E.; Stalcup, a M. *J. Chromatogr. B. Biomed. Sci. Appl.* **2000**, *745*, 83–102.
- (138) Kacso, I.; Borodi, G.; Fărcaș, S. I.; Bratu, I. *J. Phys. Conf. Ser.* **2009**, *182*, 012009.
- (139) Jadhav, G. S.; Vavia, P. R. *Int. J. Pharm.* **2008**, *352*, 5–16.
- (140) Bencini, M.; Ranucci, E.; Ferruti, P.; Trotta, F.; Donalisio, M.; Cornaglia, M.; Lembo, D.; Cavalli, R. *J. Control. Release* **2008**, *126*, 17–25.
- (141) Chow, D.; Karara, H. *Int. J. Pharm.* **1986**, *28*, 95–101.
- (142) Ammar, H. O.; Salama, H. a; Ghorab, M.; Mahmoud, a a. *Int. J. Pharm.* **2006**, *309*, 129–138.
- (143) Nasr-Esfahani, M.; Khakifiroz, A.; Tavakoli, N.; Soleimani, M. H. *Desalin. Water Treat.* **2010**, *21*, 202–209.
- (144) Mura, P.; Furlanetto, S.; Cirri, M.; Maestrelli, F.; Corti, G.; Pinzauti, S. *J. Pharm. Biomed. Anal.* **2005**, *37*, 987–994.
- (145) Al-Marzouqi, A. H.; Shehatta, I.; Jobe, B.; Dowaidar, A. *J. Pharm. Sci.* **2006**, *95*, 292–304.
- (146) Wang, L.; Jiang, X.; Xu, W.; Li, C. *Int. J. Pharm.* **2007**, *341*, 58–67.

- (147) Lin, S.; Wouessidjewe, D.; Poelman, M.; Duchcne, D. *Int. J. Pharm.* **1991**, *69*, 211–219.
- (148) Erden, N.; Celebi, N. *Int. J. Pharm.* **1988**, *48*, 83–89.
- (149) Jobe, D. J.; Reinsborough, V. C.; Wetmore, S. D. *Langmuir* **1995**, 2476–2479.
- (150) Tucker, E. E.; Taylor, R. W.; Scamehord, J. F. **1993**, 2258–2263.
- (151) Rafati, A. A.; Bagheri, A. *Bull. Chem. Soc. Jpn.* **2004**, *77*, 485–490.
- (152) Brocos, P.; Banquy, X.; Díaz-Vergara, N.; Pérez-Casas, S.; Piñeiro, A.; Costas, M. *J. Phys. Chem. B* **2011**, *115*, 14381–14396.
- (153) Jiang, Y.; Wang, X. *Appl. Spectrosc.* **1994**, *48*, 1428–1431.
- (154) Jiang, L.; Deng, M.; Wang, Y.; Liang, D.; Yan, Y.; Huang, J. *J. Phys. Chem. B* **2009**, *113*, 7498–7504.
- (155) Mwakibete, H.; Cristantino, R.; Bloor, D.; Wyn-Jones, E.; Holzwarth, J. *Langmuir* **1996**, 57–60.
- (156) Szeman, J.; Fenyvesi, E.; Szejtli, J.; Ueda, H.; Machida, Y.; Nagai, T. *J. Inclusion Phenom.* **1987**, *5*, 427–431.
- (157) Works, C. *J. Inclusion Phenom.* **1988**, *6*, 537–545.
- (158) Rodriguez-Tenreiro, C.; Alvarez-Lorenzo, C.; Rodriguez-Perez, a; Concheiro, a; Torres-Labandeira, J. J. *Eur. J. Pharm. Biopharm.* **2007**, *66*, 55–62.
- (159) Leprêtre, S.; Chai, F.; Hornez, J.-C.; Vermet, G.; Neut, C.; Descamps, M.; Hildebrand, H. F.; Martel, B. *Biomaterials* **2009**, *30*, 6086–6093.
- (160) Mura, P.; Faucci, M. T.; Maestrelli, F.; Furlanetto, S.; Pinzauti, S. *J. Pharm. Biomed. Anal.* **2002**, *29*, 1015–1024.
- (161) Liu, Y.-Y.; Fan, X.-D.; Kang, T.; Sun, L. *Macromol. Rapid Commun.* **2004**, *25*, 1912–1916.

- (162) Zhang, X.; Zhang, X.; Wu, Z.; Gao, X.; Shu, S.; Wang, Z.; Li, C. *Carbohydr. Polym.* **2011**, *84*, 1419–1425.
- (163) Schipper, N. G.; Olsson, S.; Hoogstraate, J.; DeBoer, G.; Vårum, K. M.; Artursson, P. Chitosans as absorption enhancers for poorly absorbable drugs 2: mechanism of absorption enhancement. *Pharmaceutical research*, 1997, *14*, 923–929.
- (164) Merkus, F.; Verhoef, J.; Martin, E.; Romeijn, S.; van der Kuy PH; Hermens, W.; Schipper, N. *Adv. Drug Deliv. Rev.* **1999**, *36*, 41–57.
- (165) Hu, Q.; Fan, H.; Lou, W.; Wang, Q.; Tang, G. *J. Zhejiang Univ. Sci. B* **2011**, *12*, 720–729.
- (166) Siemoneit, U.; Schmitt, C.; Alvarez-Lorenzo, C.; Luzardo, A.; Otero-Espinar, F.; Concheiro, A.; Blanco-Méndez, J. *Int. J. Pharm.* **2006**, *312*, 66–74.
- (167) Nanoparticles, A.; Bartlett, D. W.; Davis, M. E. **2007**, 456–468.
- (168) Bellocq, N. C.; Pun, S. H.; Jensen, G. S.; Davis, M. E. *Bioconjug. Chem.* **2003**, *14*, 1122–1132.
- (169) Pltha, J. Water Soluble Forms of Retinoids. 4371673, 1983.
- (170) Weisse, S.; Perly, B.; Dalbiez, J.; Archambault, J.; Rollin, P.; Andr, P. E. *J. Incl. Phenom. Macrocycl. Chem.* **2002**, *44*, 87–91.
- (171) Murthy, C. N.; Geckeler, K. E. *Chem. Commun.* **2001**, *60*, 1194–1195.
- (172) Peresin, M. S.; Habibi, Y.; Zoppe, J. O.; Pawlak, J. J.; Rojas, O. J. *Biomacromolecules* **2010**, *11*, 674–681.
- (173) Shopsowitz, K. E.; Qi, H.; Hamad, W. Y.; Maclachlan, M. J. *Nature* **2010**, *468*, 422–425.
- (174) Goddard, E. D. *J. Am. Oil Chem. Soc.* **1994**, *71*, 1–16.
- (175) Tam, K. C.; Wyn-Jones, E. *Chem. Soc. Rev.* **2006**, *35*, 693–709.
- (176) Da Silva, R. C.; Loh, W.; Olofsson, G. *Thermochim. Acta* **2004**, *417*, 295–300.

- (177) Chakraborty, T.; Chakraborty, I.; Ghosh, S. *Langmuir* **2006**, *22*, 9905–9913.
- (178) Liu, Y.; Guo, R. *Biomacromolecules* **2007**, *8*, 2902–2908.
- (179) Bain, C. D.; Claesson, P. M.; Langevin, D.; Meszaros, R.; Nylander, T.; Stubenrauch, C.; Titmuss, S.; von Klitzing, R. *Adv. Colloid Interface Sci.* **2010**, *155*, 32–49.
- (180) Cal, K.; Centkowska, K. *Eur. J. Pharm. Biopharm.* **2008**, *68*, 467–478.
- (181) Helena, M.; Marques, C. *Flavour Fragr. J.* **2010**, *25*, 313–326.
- (182) Dharmawardana, U. R.; Christian, S. D.; Tucker, E. E.; Taylor, R. W.; Scamehorn, J. F. *Langmuir* **1993**, *9*, 2258–2263.
- (183) Liu, J. H.; Xu, H. C.; Shen, L.; Chen, R. Y.; Yu, Z. C. *Adv. Mater. Res.* **2012**, *441*, 431–435.
- (184) Ibrahim, N. a; Abdalla, W. a; El-Zairy, E. M. R.; Khalil, H. M. *Carbohydr. Polym.* **2013**, *92*, 1520–1529.
- (185) Kamiński, Z. *J. Biopolymers* **2000**, *55*, 140–164.
- (186) Abitbol, T.; Palermo, A.; Moran-Mirabal, J. M.; Cranston, E. D. *Biomacromolecules* **2013**, *14*, 3278–3284.
- (187) Wang, H.; Wang, Y.; Yan, H.; Zhang, J.; Thomas, R. K. *Langmuir* **2006**, *22*, 1526–1533.
- (188) Draelos, Z.; Hornby, S.; Walters, R. M.; Appa, Y. *J. Cosmet. Dermatol.* **2013**, *12*, 314–321.
- (189) Faucher, J. A.; Goddard, E. D. *J. Soc. Cosmet. Chem* **1976**, *27*, 543.
- (190) Zaman, M.; Xiao, H.; Chibante, F.; Ni, Y. *Carbohydr. Polym.* **2012**, *89*, 163–170.
- (191) Bajpai, M.; Gupta, P.; Bajpai, S. K. *Fibers Polym.* **2010**, *11*, 8–13.
- (192) Liu, Z.; Fatehi, P.; Sadeghi, S.; Ni, Y. *Bioresour. Technol.* **2011**, *102*, 9613–9618.

- (193) Ren, J. L.; Sun, R. C.; Liu, C. F.; Chao, Z. Y.; Luo, W. *Polym. Degrad. Stab.* **2006**, *91*, 2579–2587.
- (194) Jahan, M. S.; Saeed, A.; He, Z.; Ni, Y. *Cellulose* **2011**, *18*, 451–459.
- (195) Sun, R.; Sun, X. F.; Liu, G. Q.; Fowler, P.; Tomkinson, J. *Polym. Int.* **2002**, *51*, 117–124.
- (196) Wang, H.; Wang, Y.; Yan, H.; Zhang, J.; Thomas, R. K. *Langmuir* **2006**, *22*, 1526–1533.
- (197) Baumann, H. *Lipid / Fett* **1990**, *92*, 49–56.
- (198) Baumann, H.; Bühler, M.; Fochem, H.; Hirsinger, F.; Zoebelin, H.; Falbe, J. *Angew. Chemie* **1988**, *100*, 41–62.
- (199) Vollhardt, D.; Czichocki, G.; Rudert, R. *Colloids Surfaces A Physicochem. Eng. Asp.* **1993**, *76*, 217–225.
- (200) Vollhardt, D.; Czichocki, G. *Colloids and Surfaces* **1984**, *11*, 209–217.
- (201) Vollhardt, D.; Czichocki, G. *Langmuir* **1990**, *6*, 317–322.
- (202) Lunkenheimer, K.; Czichocki, G. *J. Colloid Interface Sci.* **1993**, *160*, 509–510.
- (203) Hines, J. D. *J. Colloid Interface Sci.* **1996**, *180*, 488–492.
- (204) Lunkenheimer, K.; Fruhner, H.; Theil, F. *Colloids Surfaces A Physicochem. Eng. Asp.* **1993**, *76*, 289–294.
- (205) Vinaraphong, P.; Krisdhasima, V.; McGuire, J. *J. Colloid Interface Sci.* **1995**, *174*, 351–360.
- (206) Bain, C. D.; Davies, P. B.; Ward, R. N. *Langmuir* **1994**, *10*, 2060–2063.
- (207) Ward, R. N.; Davies, P. B.; Bain, C. D. *J. Phys. Chem. B* **1997**, *101*, 1594–1601.
- (208) Vollhardt, D.; Emrich, G. *Colloids Surfaces A Physicochem. Eng. Asp.* **2000**, *161*, 173–182.
- (209) Nakamura, A.; Muramatsu, M. *J. Colloid Interface Sci.* **1977**, *62*, 165–171.

- (210) Wilson, A.; Epstein, M. B.; Ross, J. *J. Colloid Sci.* **1957**, *12*, 345–355.
- (211) Vollhardt, D.; Melzer, V. *J. Phys. Chem. B* **1997**, *101*, 3370–3375.
- (212) Purcell, I. P.; Lu, J. R.; Thomas, R. K.; Howe, A. M.; Penfold, J. *Langmuir* **1998**, *14*, 1637–1645.
- (213) Fainerman, V. B.; Vollhardt, D.; Emrich, G. *J. Phys. Chem. B* **2001**, *105*, 4324–4330.
- (214) Schulman, J. H.; Montagne, J. B. *Ann. N. Y. Acad. Sci.* **1961**, *92*, 366–371.
- (215) Martel, R.; Gelinas, P. J.; Desnoyers, J. E.; Masson, A. *Ground Water* **1993**, *31*, 789–800.
- (216) Hayase, K.; Hayano, S. *J. Colloid Interface Sci.* **1978**, *63*, 446–451.
- (217) Moya, S. E.; Schulz, P. C. *Colloid Polym. Sci.* **1999**, *742*, 735–742.
- (218) Treiner, C.; Khodja, A. A.; Fromon, M. *Langmuir* **1987**, *3*, 729–735.
- (219) Cardinal, J. R.; Mukerjee, P. *J. Phys. Chem.* **1978**, *82*, 1614–1620.
- (220) Wan-Badhi, W.; Bloor, D. M.; Wyn-Jones, E. *Langmuir* **1994**, *10*, 2219–2222.
- (221) Ttab, I.; All, E.; The, R. *J. Colloid Interface Sci.* **1984**, *101*, 587.
- (222) Shirahama, K.; Kashiwabara, T. *J. Colloid Interface Sci.* **1971**, *36*, 65–70.
- (223) Rao, I. V.; Introduction, I. *J. Colloid Interface Sci.* **1986**, *113*, 375–387.
- (224) Buin, E. A.; Issi, E. L. *J. Colloid Interface Sci.* **1996**, *233*, 229–233.
- (225) Phillips, J. N.; Mysels, K. J. *J. Phys. Chem.* **1955**, *59*, 325–329.
- (226) Princen, J. N.; Mysels, K. D. *J. Phys. Chem.* **1959**, *63*, 1781–1782.
- (227) Zhu, Z.; Reed, W. F. *Langmuir* **2013**, *29*, 10376–10382.
- (228) Corti, M.; Degiorgio, V. *Chem. Phys. Lett.* **1977**, *49*, 141–144.

- (229) Mukerjee, P. *Solution Chemistry of Surfactants*; K. L. Mitt.; Plenum, New York, 1979; pp. 153–175.
- (230) Abe, M.; Ogino, K. *J. Colloid Interface Sci.* **1981**, *80*, 146–152.
- (231) Miles, G. D.; Shedlovsky, L. *J. Phys. Chem.* **1944**, *48*, 57–62.
- (232) Vollhardt, D.; Fainerman, V. B.; Emrich, G. *J. Phys. Chem. B* **2000**, *104*, 8536–8543.
- (233) Rosen, M. J.; Cohen, A. W.; Dahanayake, M.; Hua, X. Y. *J. Phys. Chem.* **1982**, *86*, 541–545.
- (234) Markina, Z. N.; Zadymova, N. M.; Bovkun, O. P. *Colloids and Surfaces* **1987**, *22*, 9–20.
- (235) Menger, F. M.; Rizvi, S. a. a. *Langmuir* **2011**, *27*, 13975–13977.
- (236) Li, X.; Wettig, S. D.; Verrall, R. E. *J. Colloid Interface Sci.* **2005**, *282*, 466–477.
- (237) Larsen, J. W.; Tepley, L. B. *J. Colloid Interface Sci.* **1974**, *49*, 113–118.
- (238) Birdi, K. S.; Backlund, S.; Sorensen, K.; Krag, T.; Dalsager, S. *J. Colloid Interface Sci.* **1978**, *66*, 118–123.
- (239) Zana, R.; Yiv, S.; Strazielle, C.; Lianos, P. *J. Colloid Interface Sci.* **1981**, *80*, 208–223.
- (240) Sinaga, A.; Hatton, T. A.; Tam, K. C. *J. Phys. Chem. B* **2008**, *112*, 11542–11550.
- (241) Chen, L.; Berry, R. M.; Tam, K. C. *ACS Sustain. Chem. Eng.* **2014**, *2*, 951–958.
- (242) Van de Manakker, F.; Vermonden, T.; van Nostrum, C. F.; Hennink, W. E. *Biomacromolecules* **2009**, *10*, 3157–3175.
- (243) Nielsen, T. T.; Wintgens, V.; Amiel, C.; Wimmer, R.; Larsen, K. L. *Biomacromolecules* **2010**, *11*, 1710–1715.
- (244) Zhou, J.; Ritter, H. *Polym. Chem.* **2010**, *1*, 1552.
- (245) Liao, D.; Dai, S.; Tam, K. C. *Polymer (Guildf)*. **2004**, *45*, 8339–8348.

(246) Fang, J. P.; Joos, P. *Colloids and Surfaces* **1992**, *65*, 113–120.